NUMERICAL STUDIES OF THE FOKKER-PLANCK EQUATION

Alastair David McGowan

A Thesis Submitted for the Degree of PhD
at the
University of St Andrews

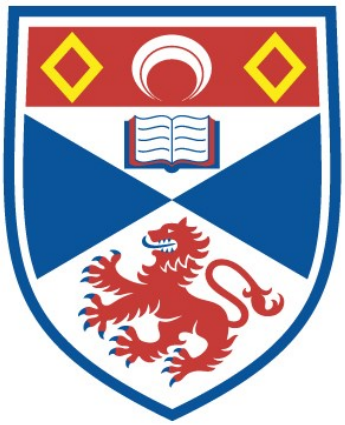

1992

Full metadata for this item is available in
St Andrews Research Repository
at:
http://research-repository.st-andrews.ac.uk/

Please use this identifier to cite or link to this item:
http://hdl.handle.net/10023/13995

This item is protected by original copyright

NUMERICAL STUDIES OF THE FOKKER - PLANCK EQUATION

by

ALASTAIR DAVID MCGOWAN

THESIS SUBMITTED IN SEPTEMBER 1990 TO THE FACULTY OF SCIENCES OF ST ANDREWS UNIVERSITY FOR THE DEGREE OF DOCTOR OF PHILOSOPHY

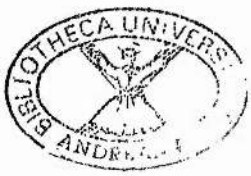

ProQuest Number: 10167142

All rights reserved

INFORMATION TO ALL USERS
The quality of this reproduction is dependent upon the quality of the copy submitted.

In the unlikely event that the author did not send a complete manuscript
and there are missing pages, these will be noted. Also, if material had to be removed,
a note will indicate the deletion.

ProQuest 10167142

Published by ProQuest LLC (2017). Copyright of the Dissertation is held by the Author.

All rights reserved.
This work is protected against unauthorized copying under Title 17, United States Code
Microform Edition © ProQuest LLC.

ProQuest LLC.
789 East Eisenhower Parkway
P.O. Box 1346
Ann Arbor, MI 48106 – 1346

TH B155

Certificate

I certify that Alastair David McGowan has satisfied the conditions of the Ordinance and Regulations and is thus qualified to submit the accompanying application for the Degree of Doctor of Philosophy .

Postgraduate Career

I was admitted into the University of St Andrews as research student under Ordinance General No. 12 in October 1986 to work on Laser Plasma Transport under the supervision of Prof. J. J. Sanderson . I was admitted under the above resolution as a candidate for the Degree of Doctor of Philosophy in October 1987 .

Declaration

I declare that the following thesis is a record of research work carried out by me , that the thesis is my own composition , and that it has not previously been submitted in application for a higher degree .

In submitting this thesis to the University of St Andrews I understand that I am giving permission for it to be made available for use in accordance with the regulations of the University Library for the time being in force , subject to any copyright vested in the work not being affected thereby . I also understand that the title and abstract will be published , and that a copy of the work may be made and supplied to any bona fide library or research worker .

To my parents

Abstract

Jorna and Wood recently developed a program that numerically solved the Fokker - Planck equation in spherical geometry . In this thesis , we describe how the original program has been redeveloped to produce a program that is an order of magnitude quicker and that has superior energy and density conservation .

The revised version of the program has been used to extend the work of Jorna and Wood on thermal conduction in laser produced plasmas . It has been shown that the effect of curvature on heat flow can be described from a purely geometrical argument and that for aspect ratios similar to those found in targets , the heat flow is reduced by approximately 10 % . Also , it has been shown , in contradiction with Jorna and Wood , that the inclusion of the anisotropic portion of the Rosenbluth potentials does not have a significant effect on the heat flow . Even for highly anisotropic plasmas , the inclusion of the anisotropic portion only increases the heat flow by 10 % .

In addition , the revised version of the program has been used to study the energy relaxation of model distributions . It has been shown that the relaxation time of most non - thermal distributions depends on the detailed structure of the distribution and that the normal Spitzer collision time can under-estimate or over-estimate the time required for energy relaxation .

Contents

Acknowledgements

I would like to thank my supervisor Professor Jeffrey Sanderson for his supervision during my period as a research student . His advice , encouragement and patience has been a source of strength to me .

I would also like to thank Drs Alan Cairns , Sebe Jorna and Lindsay Wood for many useful discussions on my project . My thanks also go to the other members of the Plasma Physics Group , namely , Allan Taylor , Morag McMinn , Ruhul Amin , Andrew Miller , Brian Harvey and Ashley Buckner for their helpful support .

Special thanks must go to Dr Victoria Barrow who had to suffer me during the long gestation period of this thesis. Without Vicky's love and support, this thesis would not have been possible.

I am grateful to the Science and Engineering Council for their financial support .

Finally I would like to thank my friends in St. Andrews for helping to make my stay such an enjoyable one .

A D McGowan

CHAPTER 1: INTRODUCTION

1.1 Introduction

Throughout the universe, the most common state of matter is the plasma. The plasma state of matter occurs in a wide variety of natural phenomena. Amongst astrophysical sources, it is known that stellar interiors and atmospheres, gaseous nebulae and much of the inter-stellar medium are in the plasma state. Within the solar system, the plasma state is found in the solar wind and the radiation belts around planets. On Earth, the plasma state is naturally produced within a lightning bolt, a neon sign and the Aurora Borealis. However, in the last forty years, the main interest in the plasma state has been dué to the drive for controlled thermonuclear fusion.

What is a plasma? A plasma can be considered as a quasineutral ensemble of free charged ions and electrons. By quasineutral, it is meant that the overall charge of the plasma is neutral but locally the plasma can deviate enough from neutrality to support electromagnetic fields. Also, a plasma generally has a large enough density that the Coulomb force between the particles is a dominant force, yet a low enough density that nearest neighbour interactions are dominated by multiple-particle Coulomb interactions.

The properties of a plasma can be analysed using two separate, though not independent, methods. When considering large scale phenomenon in a plasma, it is possible to assume that the plasma is a highly conducting fluid. This approach is called magnetohydrodynamics and deals with the thermodynamic properties of a plasma such as temperature and density.

Chapter 1

Magnetohydrodynamics has been used to determine the overall stability of a plasma and also to study how energy is transported through the plasma.

When studying microscopic phenomena, it is necessary to use a statistical model when analysing a plasma. Plasma kinetic theory deals with the distribution function of particle velocities in a plasma from which thermodynamic properties can be obtained. It is the only method that can be used when studying phenomena that are critically dependent on particle energy such as collisions. It is also able to supply the transport coefficients that are required by magnetohydrodynamics and to put magnetohydrodynamics on a sound theoretical footing; magnetohydrodynamics is a derivative of plasma kinetic theory obtained when one reduces the complexity by "averaging" over velocity space.

1.2 Plasma Kinetic Theory

In plasma kinetic theory, we are generally concerned with the evolution of the single particle distribution function. This distribution function, $f(\underline{x}, \underline{v}, t)$, obeys the collisional kinetic equation which is

$$\frac{\partial f}{\partial t} + \underline{v}.\nabla_x f + q(\underline{E} + \underline{v}\times\underline{B}) .\nabla_v f = \frac{\partial f}{\partial t}\Big|_{coll}$$

- eqn (1.2.1)

where t is time, $\underline{x}$ is the position vector, $\underline{v}$ is the velocity vector, q is the charge of the particle, $\underline{E}$ is the electric field and $\underline{B}$ is the magnetic field. The right hand side of equation (1.2.1) describes how collisions affect the distribution. If the frequencies of the phenomena of interest (e.g the response to the fields) are faster than the time for the collisions to drive the plasma towards thermal equilibrium, then it is possible to ignore the right hand side of equation (1.2.1) - this is called the collisionless or Vlasov regime. However, if the frequencies of the phenomena of interest are less than or the order of the collision frequency, then we must find an expression for the right hand side of equation (1.2.1) that describes the effect of collisions on the distribution function.

In the most general theory of plasma kinetics, it is possible to obtain an equation of the form of equation (1.2.1) with an expression for the collision term from first principles. However, the derivation of the collision term from the general theory is well known (see Nicholson, 1987) so it shall not be repeated here. Instead, we shall outline a less rigorous but

physically more clear method of deriving the collision term for equation (1.2.1).

In a plasma, the collision between particles is governed by the Coulomb force. Unlike collisions in a neutral gas, the range of the force is long and weak. As the range of the force is long, a particle in a plasma will feel the effect of many weak distant interactions at once. Although these encounters are weak, the sum of these small perturbations outweigh the effect of the rare large perturbations to the particle's path caused by strong binary interactions with nearest neighbours. Hence, the trajectory of a particle in a plasma, due to collisions, is essentially a random-walk process.

From the theory of Brownian motion, which is also a random-walk process, it is known that the equation best suited to describe the random-walk process is the Fokker-Planck equation. In the derivation of the Fokker-Planck equation it is assumed that deflections are small, the collisions are elastic and that Coulomb scattering is a Markovian process. The Fokker-Planck equation resembles a Taylor expansion in velocity space and is given by (Shkarofsky, 1966)

$$\frac{\partial f}{\partial t}\Big|_{coll} = -\sum_{\mu} \frac{\partial}{\partial v_\mu} f\langle \Delta v_\mu \rangle + \frac{1}{2} \sum_{\mu\omega} \frac{\partial^2}{\partial v_\mu \partial v_\omega} f\langle \Delta v_\mu \Delta v_\omega \rangle$$

- eqn (1.2.2)

where $\langle \Delta v_\mu \rangle$ represents the coefficient of dynamical friction and $\langle \Delta v_\mu \Delta v_\omega \rangle$ represents the diffusion coefficient. The coefficient of dynamical friction reduces the speed of particles travelling faster than the average velocity and

increases the speeds of those which are travelling slower than the average velocity. The diffusion coefficient spreads out the particles in velocity space until the thermal equilibrium is achieved.

However to determine the friction and diffusion coefficients, $\langle \Delta v_\mu \rangle$ and $\langle \Delta v_\mu \Delta v_\omega \rangle$, it is necessary to examine the physics of the collision process. When this is done (Rosenbluth et al, 1957), the Fokker-Planck equation for a plasma is given by

$$\frac{1}{\Gamma}\frac{\partial f}{\partial t}\Big|_{coll} = \sum_{\mu} \frac{\partial}{\partial v_\mu} f \frac{\partial h}{\partial v_\mu} + \frac{1}{2}\sum_{\mu\omega} \frac{\partial^2}{\partial v_\mu \partial v_\omega} f \frac{\partial^2 g}{\partial v_\mu \partial v_\omega}$$

- eqn (1.2.3)

where the functions h and g are the Rosenbluth potentials and (defined later in Chapter 4). The Rosenbluth potentials are integral functions that are dependent on the distribution function. This makes the Fokker-Planck equation for a plasma a non-linear, partial, integro-differential equation. The complexity of this equation makes it difficult to solve mathematically. It is normally necessary to solve the equation numerically.

1.3 Numerical Studies of the Fokker-Planck Equation

Over the last 30 years, the numerical solutions of the Fokker-Planck equation have evolved with the increasing power of the computer. To solve the Fokker-Planck equation numerically for all of its seven independent variables is beyond the scope of even today's most powerful supercomputers. Therefore, it has been necessary to reduce the number of independent variables until the reduced equation is tractable. This has been done, for example, by assuming that the plasma is spatially homogeneous or only varies in one direction. In addition, it has been assumed that the distribution function is isotropic or that it has azimuthal symmetry in velocity space. By making these assumptions, the numerical solution of the Fokker-Planck equation has been made tractable.

Numerical studies of the Fokker-Planck equation have produced interesting results in a wide variety of problems. To give an exhaustive review of all cases where the equation has been used would be too great a diversion, so we shall give only a flavour of what can be achieved by the numerical solution of the Fokker-Planck equation.

The earliest work done with the Fokker-Planck equation was carried out by Rosenbluth et al (1957a) where they investigated the relaxation of non-thermal distributions. They solved the Fokker-Planck equation assuming that the plasma was homogeneous and that it was isotropic in velocity space. Their results showed that it is not possible to have a single self-collision time for a plasma but that it is strongly dependent on velocity. We shall have more to say on this topic in Chapter 6 when we consider the relaxation of model distribution functions.

Chapter 1

In the early 1960's, Roberts and Carr (1960) and Bing and Roberts (1961) used the Fokker-Planck equation to determine how particles were lost in mirror machines. The Fokker-Planck equation was solved using only one species of ion, neglecting the effect of electrons and ignoring the spatial inhomogeneities except for the magnetic loss cone. Soon after, Killeen et al (1962,1968) studied the transfer of energy from ions to electrons in mirror machines. Their code was time-dependent and followed the evolution of the electrons and the ions while assuming that both distributions were isotropic. During the 1970's, Killeen and Marx (1970) developed codes that solved the Fokker-Planck equation in two velocity dimensions for a multi-species plasma including the anisotropic portion of the Rosenbluth potentials and differencing the equation in a form that ensured that particle number was conserved. The result of these studies is that Fokker-Planck codes can now accurately predict the confinement times of different species in a mirror machine.

The Fokker-Planck equation has also been used to model runaway electrons in tokamaks. The first study was by Dreicer (1960) who solved the Fokker-Planck equation assuming that the collision coefficients were Maxwellian and that the distribution was only weakly anisotropic. From the numerical solution, it was possible to determine the runaway rate for a given electric field. Since then, a number of authors (eg Wiley et al, 1980; Fuchs et al, 1986) have calculated the runaway rate using a number of different two dimensional models. These two dimensional models have given a more accurate picture of how the distribution has been distorted by the electric field.

A number of authors (eg O'Brien et al, 1986; Harvey et al, 1981) have used the Fokker-Planck equation to study the deposition of energy in tokamaks by radio-frequency heating and neutral beam injection. These codes have used approximations similar to those mentioned above and they have produced useful scaling laws between input power and the power absorbed by a plasma.

Most recently, the Fokker-Planck equation has been used to simulate thermal conduction in laser-produced plasmas. However, as this is the topic of Chapter 3, discussion of this problem will be left until then.

1.4 Outline of Thesis

In Chapter 2, we review how the Fokker-Planck equation has been used to simulate thermal conduction in a uniform laser-produced plasma. In particular, we describe the code developed by Jorna and Wood and discuss the results of their work.

Chapter 3 describes how we attempted to extend the original code to simulate thermal conduction in a non-uniform laser-produced plasma. The problems discovered with the original code and the reasons for redeveloping the original code are discussed.

The redeveloped version of the Fokker-Planck code is described in Chapter 4. This chapter also includes calibration tests for the new Fokker-Planck code.

In Chapter 5, we apply the new version of the Fokker-Planck code to the same problem as Jorna and Wood. It is found that the new version of the code gives results significantly different to those presented by Jorna and Wood.

In Chapter 6, the code is used to study the relaxation of model distributions where distributions are far from equilibrium.

Finally, in Chapter 7, we present the main conclusions of the thesis and present several ideas for future work.

CHAPTER 2: THERMAL ELECTRON TRANSPORT IN DIRECT DRIVE LASER FUSION

2.1 Introduction

In direct drive laser fusion, the thermal conduction of energy by electrons plays an important role. The energy in a sub-micron laser is absorbed in the low density corona, up to the critical surface, by inverse bremsstrahlung. The energy that is not absorbed is reflected out of the plasma. The energy absorbed by the plasma is transported by thermal conduction from the critical surface to the ablation surface. This inward flow of hot material is countered by the flow of cool material from the ablation surface into the expanding corona. Since the hot material at the ablation surface forces the target to ablate away material, there must be an inward pressure on the target to conserve momentum. It is this inward pressure that compresses the core. Figure 2.1 shows schematically the processes in direct-drive laser fusion.

Thermal electron transport can reduce the efficiency of direct drive laser fusion in two ways. If there is a reduction in the heat flow between the critical surface and the ablation surface, then the inward pressure will not be as high and the core compression will suffer. Secondly, thermal electron transport can affect how much energy the plasma absorbs from the laser. If the heat flow is reduced, then more of the energy that is absorbed will end up in the corona. This results in the coronal temperature increasing which in turn reduces the opacity. A fall in the opacity will reduce the amount of energy absorbed.

The two reasons given above show that it is important to obtain a proper understanding of thermal electron

transport. A brief review of thermal conduction is now presented.

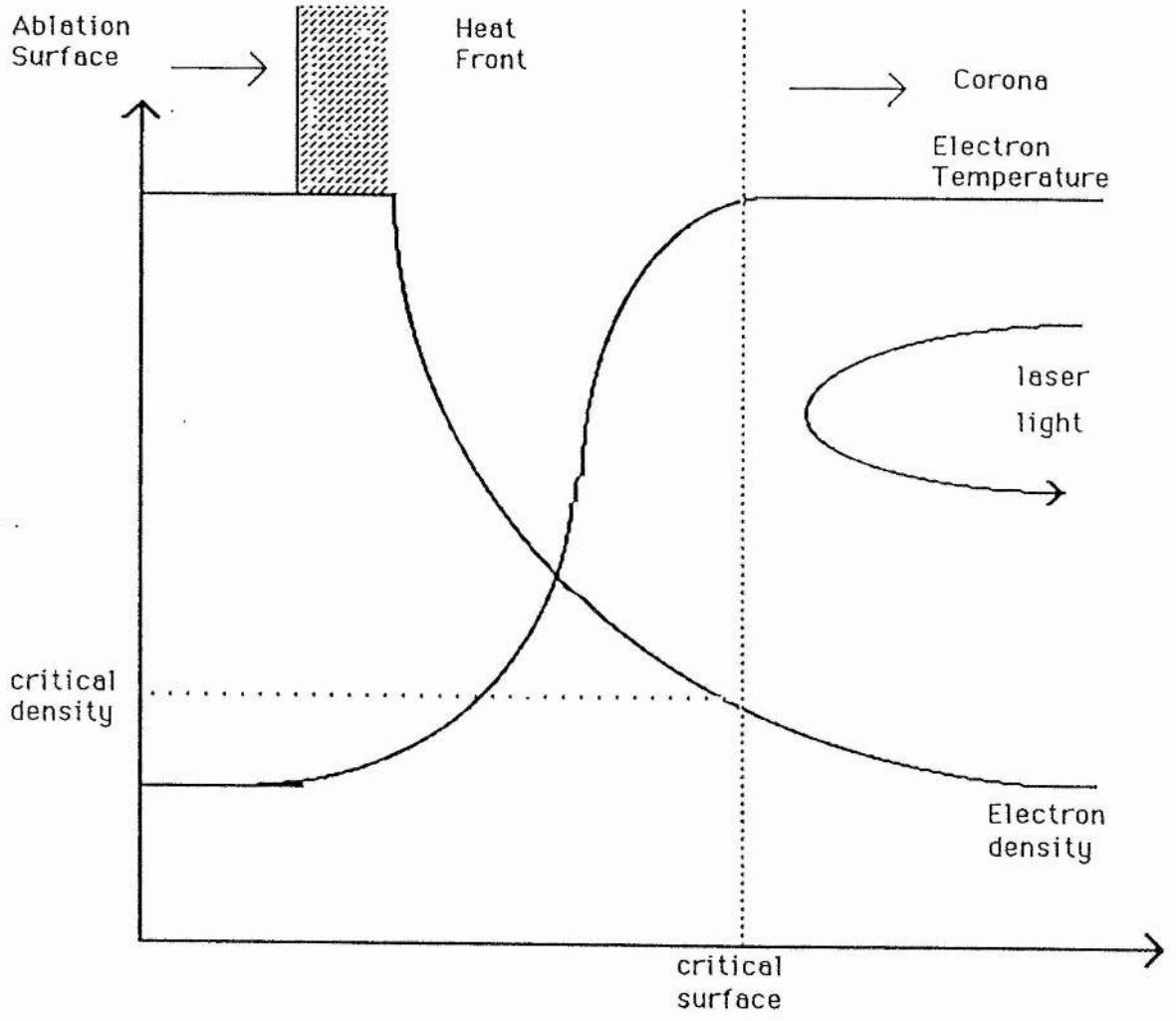

Figure 2.1: **SCHEMATIC OF DIRECT DRIVE LASER FUSION**

2.2 Review of Thermal Electron Transport

If a plasma has only small temperature gradients, then it is valid to assume that thermal conduction is a local, diffusive process which can be described by (Delletrez, 1983)

$$N_e C_v \frac{\delta T_e}{\delta t} = -\underline{\nabla}.\mathrm{K}\nabla T_e$$

- eqn (2.2.1)

where N_e is the number of electrons, C_v is the heat opacity, T_e is the electron temperature and K is the coefficient of thermal conductivity. The most commonly used coefficient of thermal conductivity was derived by Spitzer and Harm (1957).

Spitzer and Harm solved the Fokker-Planck equation for small gradients under the assumption that the distribution function has only a weak angular dependence which can be prescribed by

$$f(x, v, \mu, t) = f_0(x, v, t) + \mu f_1(x, v, t)$$

- eqn (2.2.2)

where f_0 is assumed to be the local Maxwellian. By assuming that the plasma is quasi-neutral and in a steady state situation, it is possible to numerically calculate the conductivity.

The Spitzer-Harm conductivity is given by

$$K = \frac{20\epsilon\left(\frac{2}{\pi}\right)^{3/2}(\kappa T)^{5/2}\kappa\delta}{m_e^{1/2}e^4 Z \ln\Lambda}$$

- eqn (2.2.3)

where ϵ is a reduction factor due to the neutralising electric field, K is Boltzmann's constant, m_e the electron mass, e the electric charge, Z the atomic number, In Λ the Coulomb logarithm and δ a constant which is calculated numerically and depends on Z.

However, the Spitzer-Harm theory is only valid for small temperature and density gradients and in a laser produced plasma this assumption breaks down. When there are large temperature gradients, the heat flow predicted by the Spitzer-Harm theory, Q_{SH}, can be larger than the free streaming heat flux, which is defined as

$$Q_{FS} = f n_e v_{th} \kappa T$$

- eqn (2.2.4)

where v_{th} is the velocity of a thermal electron and f is called the flux limiter which is of order unity. Physically, the free-streaming heat flux is the heat flux carried by the thermal electrons flowing uninhibited into vacuum. However, in laser fusion, the flux limiter is used as a free parameter to obtain agreement between experiments and hydrocodes. It has been found that the "best" value of f is between 0.03 and 0.1.

Chapter 2

Many different anomalous processes have been suggested to explain why the heat flux in experiments is much less than the free-streaming value. However, it has been shown that when a correct treatment of thermal conduction has been carried out, the heat flux is predicted to be much smaller than the value predicted by Spitzer-Harm theory without the need to invoke other physical processes.

The first correct treatment of anomalous heat transport, based on Coulomb collisions, was completed by Bell, Evans and Nicholas (1981). The Fokker-Planck equation was solved for the case of a heat front propagating through a plasma. The equation was solved for uniform density by expressing the angular dependence in the form of a Legendre decomposition of f in μ. It was shown that, in the presence of steep temperature gradients, the heat flow is not a unique function of the local plasma parameters but that it depends on the temperature gradient over a region of the plasma that is a few mean free paths thick. The heat flux at the steepest point of the temperature gradient is found to be much less than the local Spitzer-Harm value while at the foot of the heat front, the heat flux is larger than the local Spitzer-Harm value. Both of these effects are due to the non-local nature of heat transport. Electrons contributing to the heat flux at the foot of the heat front have originated in the hot part of the plasma but have not yet lost their energy through collisions. The heat flux reached a maximum value of about 15% of the free streaming limit.

Matte and Virmont (1982) showed similar results to Bell et al by studying the transport of energy from a hot cathode to a cold one. The method used to solve the Fokker-Planck equation was similar to that used by Bell except that the boundary conditions were slightly different. In this case, the heat flux reached a maximum of about $0.3Q_{FS}$. It was shown that the isotropic part of the electron velocity distribution evolves to become a two temperature Maxwellian with the main part at the background cold temperature, and a hot tail which is at the same temperature as the hot cathode.

Since these two pieces of work, there have been several other codes written that solve the Fokker-Planck equation which have included more physics than the two considered above. Bell (1985) considered thermal electron transport in a steadily ablating plasma and showed that whilst Spitzer conductivity correctly predicts the density and temperature profiles in planar geometry, it breaks down in spherical geometry. Matte at al (1984) included inverse bremmstrahlung, using the Langdon operator, and ion motion into their simulations. Their results, which were compared with a hydrocode which used a simple flux limited conductivity, showed that the "best" value of f lay between 0.08 and 0.15. Recently, Epperlein, Rickard and Bell (1989) have solved the Fokker-Planck equation in two spatial dimensions. Epperlein has shown that Spitzer conductivity smooths out perturbations faster than their more complete treatment predicts.

2.3 Review of Jorna and Wood's Fokker-Planck code

In the previous section, the results of several Fokker-Planck simulations have been discussed. In all of these simulations the numerical techniques employed were alike, the underlying assumption being that the electron distribution function could be represented by a truncated expansion of Legendre polynomials in the angular variable. Indeed, in several of the simulations the expansion was limited to representation of the electron distribution by just the zeroth and first Legendre polynomials. Hence the anisotropic component was assumed to be linear in μ, where μ is the cosine of the angle between the velocity and radial vector.

Another important assumption adopted in these simulations is that it is possible to neglect the anisotropic component of the collision coefficients. Hence when the Rosenbluth potentials are calculated, it is possible to use an angular average of the background distribution function.

The advantage in using these assumptions, is that it significantly reduces the complexity of the Fokker-Planck equation. Rather than having to solve a two-dimensional partial differential equation, the problem is reduced to solving a series of coupled ordinary equations.

However, it is difficult to know where to truncate the Legendre polynomial expansion before performing the simulation. Furthermore, by neglecting the effect of the anisotropic components of the Rosenbluth potentials on the evolution of the anisotropic components of the electron distribution function, the solution does not remain self-consistent.

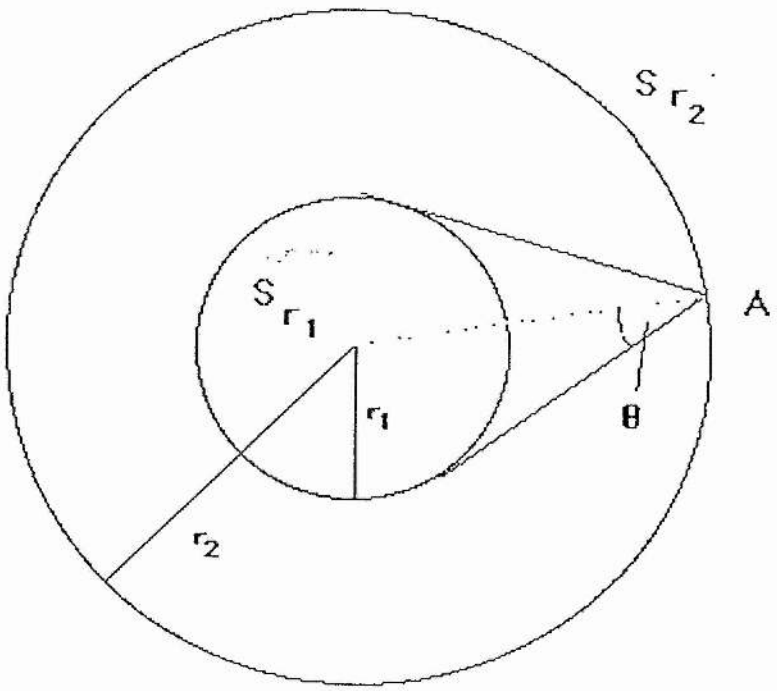

Figure 2.2

Jorna and Wood developed a Fokker-Planck code to assess the validity of these two assumptions and to study the importance of sphericity on heat flow. The code solved the Fokker-Planck equation in one spatial dimension and two velocity dimensions (azimuthal symmetry was assumed) but no other assumptions were made about the angular dependence of the electron distribution function and the Rosenbluth potentials. For aid of comparison, a version of the code was developed that calculated the Rosenbluth potentials from the angular average of the background distribution function. The radial electric field was calculated using Gauss' s law and then decreased by 10^3 so that the effective plasma frequency would be comparable with the collision time. The Fokker-Planck equation was solved by the method of fractional steps. Unusually for recent Fokker-Planck codes, the equations were not solved in such a way that guaranteed particle conservation. Therefore, to guarantee particle conservation, a facility was built into the code which tests for particle loss and adds a Maxwellian distribution at the current density and prevailing temperature if more than a certain percentage of particles are lost.

Jorna and Wood initially developed their code to investigate the effect of sphericity on heat flow. Figure 2.2 shows the two boundary problems considered. The outer boundary is heated from an initial temperature T_e linearly in time to a temperature T_2 and held there. The hotter particles are added at the outer boundary in such a way that no net current is added to the plasma (see section 5.2 for a fuller description). These hot particles create a temperature gradient at the outer boundary which transports through the cooler plasma.

From their simulations, Jorna and Wood concluded that the effect of sphericity inhibits the heat flow as the degree of sphericity increases. However, they were unable to quantify the amount of inhibition as the degree of sphericityincreases. Indeed, it is unclear from their simulations whether the reduction in heat flow is due to a purely geometric effect or from a stronger return current as a result of the stronger electric fields near the inner boundary. Jorna and Wood also presented results which were broadly in agreement with other workers. It was shown that the heat flux is not a simple, local or unique function of the mean free path. The distribution function is highly anisotropic and it develops a hot Maxwellian tail at the temperature of the hot injected Maxwellian. Finally, it was shown that as the plasma approached steady-state, the heat flow and the temperature of the plasma could be well represented by two counter-streaming half-Maxwellians.

All of the results discussed above were obtained using the isotropic version of the code. Jorna and Wood repeated the simulations using the anisotropic code and discovered that the heat flow could be significantly affected. The ratio of the heat flows obtained using the anisotropic and isotropic codes showed that as the plasma approached steady state, the heat flow was 10% larger when calculated using the anisotropic code. Earlier in the simulation, it was shown that the heat flow could be 50% larger when calculated using the anisotropic code.

Jorna and Wood also examined the situation where the plasma is heated by an anisotropic distribution rather than by a hot Maxwellian. The plasma was heated by a bi-Maxwellian distribution with the hotter component parallel to the radial vector. Once again, it was discovered that the anisotropic code predicted a larger heat flow than the isotropic code. As the plasma approached steady state, the anisotropic code predicted a heat flow almost double that of the isotropic code.

From these results, Jorna and Wood suggested that although it is sufficient to ignore the anisotropic component of the Rosenbluth potentials when calculating the temperature, it is not sufficient to ignore it when calculating the heat flow. They also postulated that the anisotropic code gives a larger value for the heat flow because the more anisotropic, less collisional electrons are not averaged over angles and reach the inner boundary without colliding.

Jorna and Wood's findings were significant in that it called into question the validity of other Fokker-Planck codes. All other codes had ignored the anisotropic portion of the Rosenbluth potentials and Jorna and Wood had found that the neglect of it could under-estimate the heat flow by a factor of 2.

Jorna and Wood had only investigated the importance of the anisotropic component of the Rosenbluth potentials for the case of a weakly collisional uniform plasma and it was important to investigate this effect for a wider range of plasmas.

CHAPTER 3: THERMAL ELECTRON TRANSPORT IN A NON-UNIFORM PLASMA

3.1 Introduction

The cathode model adopted by Jorna and Wood, described in the previous chapter, enables the study of the basic physics of electron transport. However, the conditions of the cathode model are far from those found in a laser produced plasma. The model assumed that the background ion density and temperature are uniform but they may vary by a factor of 10^3 between the critical surface (the hot cathode) and the ablation surface (the cold cathode). In fact the precise form of the density profile is dependent on the intensity, polarization and profile of the laser pulse.

To model thermal conduction accurately, it is necessary to couple a Fokker-Planck code to a hydrocode. The Fokker-Planck code simulates the conduction of the electrons while the hydrocode simulates the evolution of the ions. At present, it is not possible to model thermal conduction in a laser produced plasma with gradients comparable with experiment because of the high density and low temperature at the ablation front. Never the less, several codes have been developed that do model thermal conduction in moderate density gradients with a Fokker-Planck code.

Albritton (1983) solved a simplified Fokker-Planck equation in which the diffusion approximation was used and the effect of the electron-electron collisions on the evolution of the anisotropic portion of the distribution function was neglected. This reduced the Fokker-Planck equation from a non-linear integro-partial differential

equation to a single ordinary differential equation. Albritton added some complexity by adding inverse bremsstrahlung and an exponential density profile. Simulations were performed for a 1 micron laser of intensity 10^{14} W/cm^2 and 10^{15} W/cm^2 with an electron density scale length of 100 microns. It was found that for 10^{14} W/cm^2 laser, the peak flux predicted a flux limiter of 0.14. The distribution function near the critical surface was flattened near zero velocity due to the laser absorption and a hot tail appeared near the bottom of the heat front.

Matte (1984) extended his code, described in section 2.2, to include ion-motion and inverse-bremsstrahlung. The initial density profile, which consisted of two plateaus of density of $4 * 10^{19}$ cm^{-3} and $2 * 10^{22}$ cm^{-3} connected by an exponential density profile with a gradient length of 45 microns, was illuminated by a 1 micron laser pulse of $3 * 10^{14}$ W/cm^2. The results of the Fokker-Planck code were compared with those of a hydrodynamic code that used the harmonic method of computing the effective conductivity. After 600 ps, it was found that the heat front predicted by the Fokker-Planck code was best modelled by the hydrocode with a flux limiter of 0.08. However, with this value for the flux limiter, the hydrocode over-estimated the coronal temperature. For the hydrocode to give a similar coronal temperature as predicted by the Fokker-Planck code required a flux limiter of 0.15.

Several other authors (Bell (1984),Kho (1983) for example) have modelled thermal conduction in moderate density gradients. In summary, they have reduced the flux limiter from 0.25 to 0.3 for uniform plasmas, to between 0.08 and 0.15 for non-uniform plasmas. They have

showed that it is important when modelling thermal conduction in a laser-produced plasma to solve the transport equation coupled with hydrodynamic motion.

Nevertheless, all these simulations were subject to the assumptions discussed in section 2.3. As Jorna and Wood had shown that these assumptions were not always valid in a spatially uniform plasma, it was decided that it would be useful to extend Jorna and Wood's code to include density gradients. By including density gradients, it was hoped that it would be possible to determine the importance of sphericity and anisotropy in a more realistic model of a laser produced plasma. No attempt was made at this stage to couple the Fokker-Planck code to a hydrocode. It was not our objective to model a more realistic plasma than those used in other models, but to determine if the assumptions adopted in other models were valid.

In Section 3.2, we describe the results and problems discovered when density gradients are introduced to the simulations. The origin of these problems is discussed in Section 3.3 and possible solutions are presented. Finally, in Section 3.4, we summarise the results of the chapter and discuss the effect on the development of the thesis.

3.2 Results of Density Gradient Simulations

To simulate thermal conduction in a spatially non-uniform plasma required several alterations to the original code. The initialization of the simulation was modified to include a linear ion density gradient that obeyed the relation

$$n(r) = n_e + \frac{(n_s - n_e)\, r}{d}$$

-eqn (3.1.1)

where d = plasma width, n_e = electron density at outer boundary, n_s = electron density at inner boundary. The radial electric field calculation was altered to include the varying ion density. To test the above changes, several simulations were performed with the isotropic code with $n_e = n_s$. The result of these simulations were in agreement with Jorna and Wood,

The following simulations were carried out for three different plasma conditions. In the first we were essentially modelling thermal conduction through a small density gradient. In the second situation we modelled thermal conduction through a small density gradient but without forcing particle conservation. Finally, we simulated how the electron density profile would evolve when no heat was added. Let us now examine what happened for each of these simulations.

Chapter 3

The first simulations were performed with only small density gradients and initial conditions similar to those adopted by Jorna and Wood. In figures 3.1 and 3.2, we see the evolution of the temperature profiles for n_s / n_e = 2 and n_s / n_e = 4, respectively. For both simulations n_e = 10^{21} cm^{-3}, d = 12 μm, T_e = 02.keV and the temperature at the outer boundary was increased from 0.2 keV to 04.keV over 0.3 t_o where t_o is the electron self collision time. It can be seen in both simulations, that the temperature profiles have developed feet that precede the main temperature fronts. The main temperature profile of the n_s / n_e = 2 simulation has travelled further than the n_s / n_e = 4 simulation. This is to be expected as both plasmas have been injected with the same quantity of energy and the n_s / n_e = 2 simulation has fewer particles to heat. However, in both simulations, the heat flow profiles developed an instability as the simulation progressed. In figure 3.3, we schematically show how the heat profiles evolved for both simulations. As this instability was not seen in the temperature profiles, it can be surmised that the distribution is being distorted at high velocities.

In the simulations described above, the particles were conserved by calculating the particle loss for each radial mesh point and adding a Maxwellian at the current density and prevailing temperature. If this source of particles is not added, then the heat and temperature profiles look quite different. In figure 3.4, we see the temperature profiles for a simulation with the same parameters as before, except that n_s / n_e = 5 and T_e = 1 keV and without a background Maxwellian distribution being added. In figure 3.4, we see that there is considerable cooling near the inner boundary. Once again the heat flow profiles were found to be highly unstable.

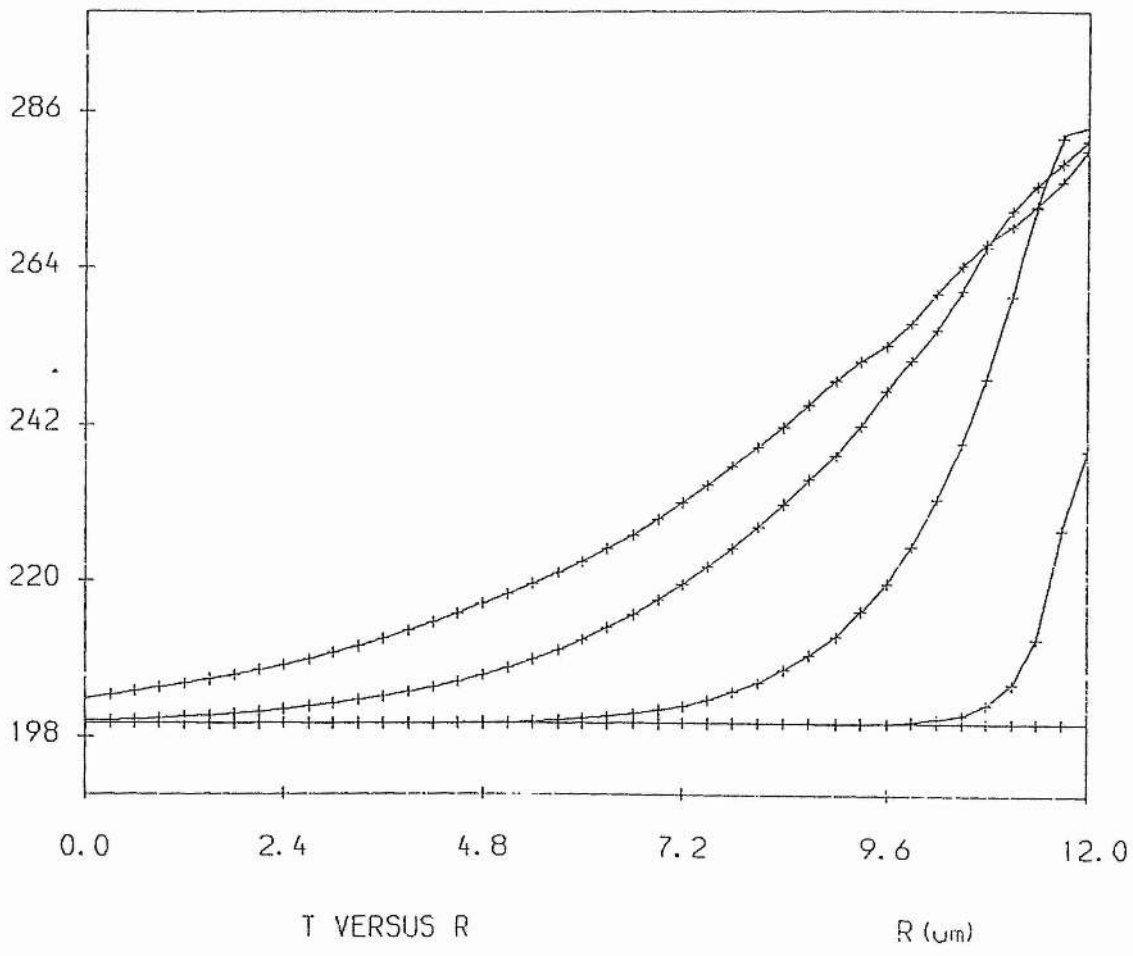

Figure 3.1 **TEMPERATURE PROFILES FOR A NON-UNIFORM PLASMA WITH N_S/N_E = 2, T_H/T_C = 2 AND N_E = 10^{21} CM^{-3} AND T_E = 0.2KEV**

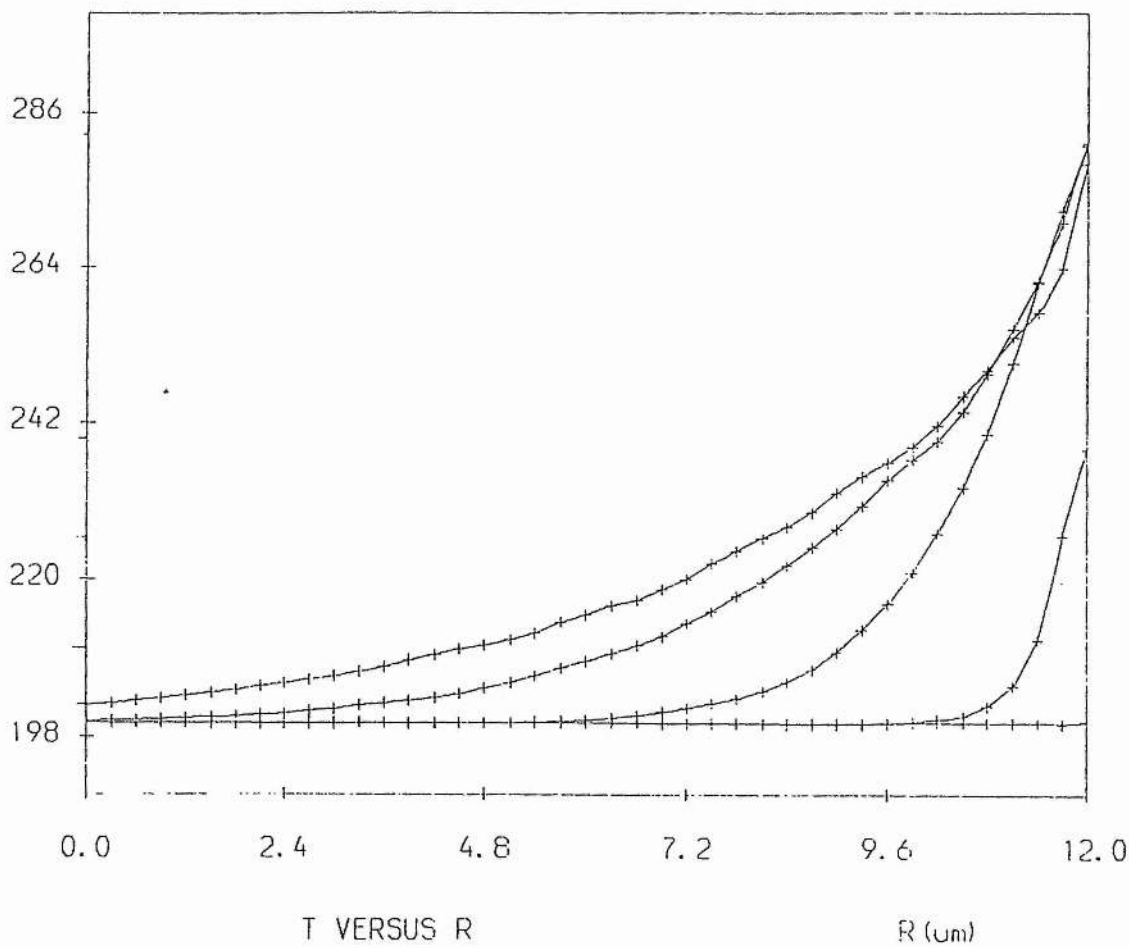

Figure 3.2 **TEMPERATURE PROFILES FOR A NON-UNIFORM PLASMA WITH $N_S/N_E = 2$, $T_H/T_C = 2$ AND $N_E = 10^{21}$ CM^{-3} AND $T_E = 0.2$KEV**

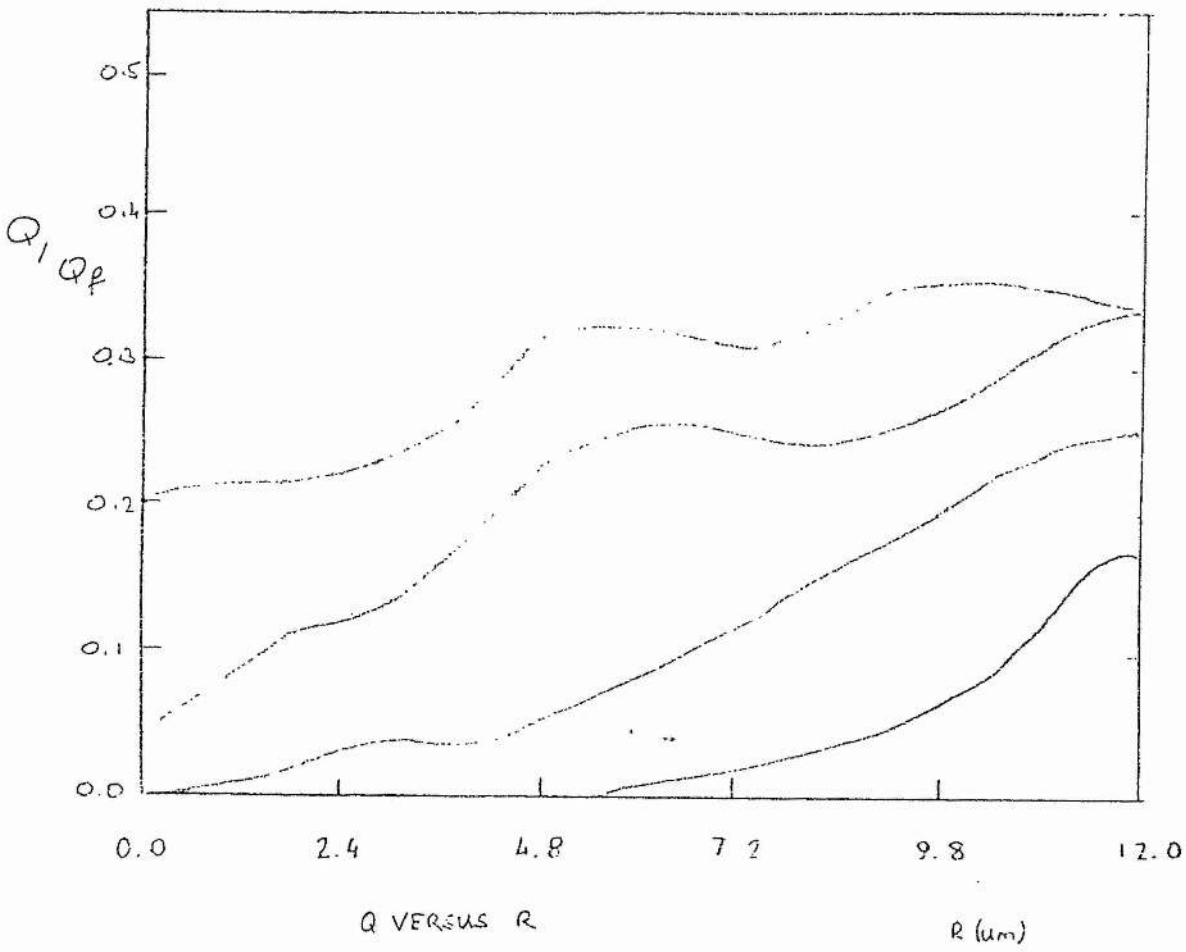

Figure 3.3 **TYPICAL HEAT FLOW PROFILES FOR A NON-UNIFORM.**

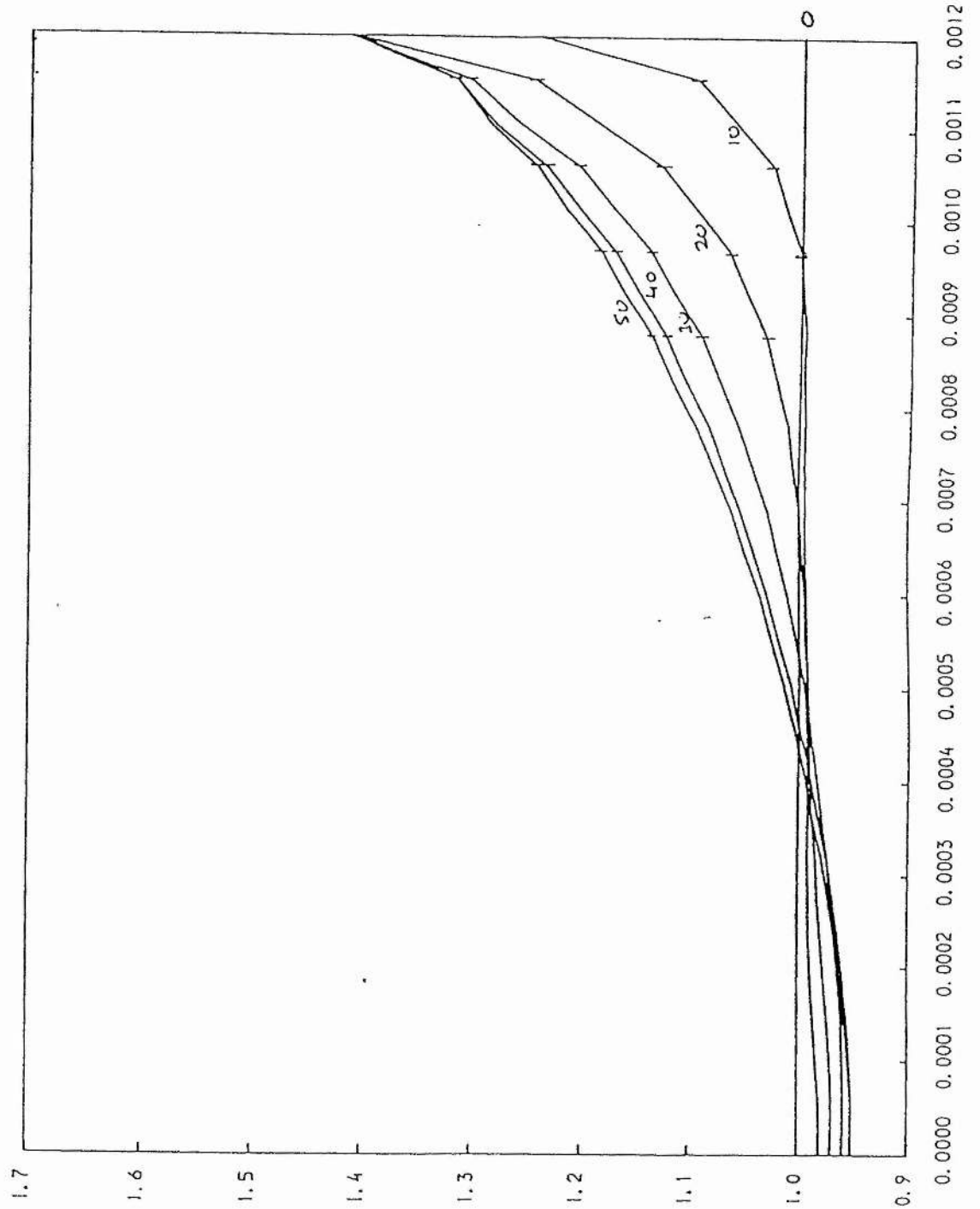

Figure 3.4 TEMPERATURE PROFILES FOR A NON-UNIFORM PLASMA WITH $N_S/N_E = 5$, $T_B/T_C = 2$ AND $N_E = 10^{21}$ CM^{-3} AND $T_E = 1.0$KEV

Finally we consider how the plasma evolves when $n_s / n_e = 2$, $T_e = 1$ kev, $n_e = 10^{21}$ cm^{-3}, $\Delta t = t_o /1000$, particle conservation is switched on and no heat is added to the plasma. We would expect that the electron density would start to decrease near the inner boundary until the charge separation forced the electric field to arrest its descent. Figures 3.5 and figure 3.6 show what we would expect the electron density and electric field to relax to. In figures 3.7 to 3.11, the heat flow is plotted at different timesteps. It can be seen that a travelling wave is set up. As the simulation progresses, the magnitude of the heat flow reduces near the inner boundary but increases near the outer boundary. By the 500th timestep the heat flow is effectively zero from the inner boundary to approximately half-way across the plasma. Near the outer boundary the heat flow has increased to approximately 0.1 Q_f. Figure 3.12 measures the deviation from neutrality of the electron distribution. This deviation is small near the inner boundary but appears to deviate substantially near the outer boundary.

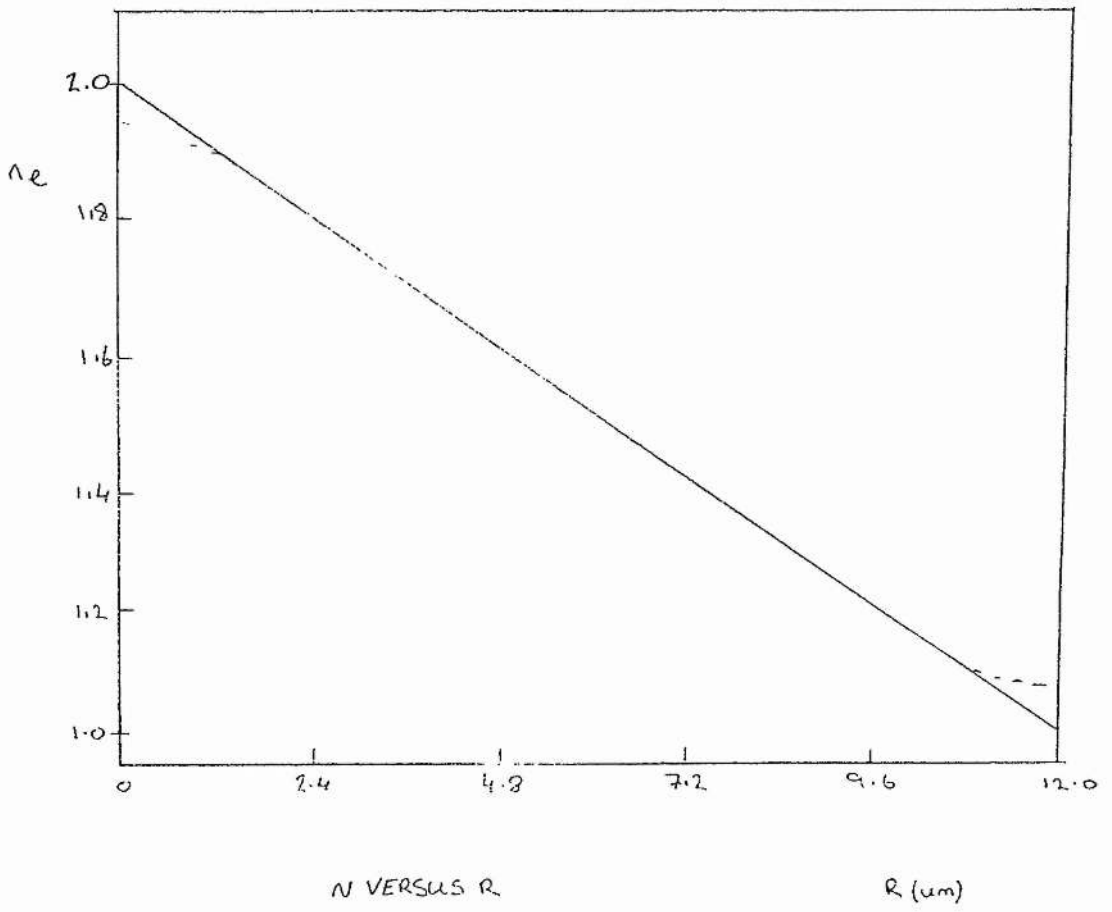

Figure 3.5 SCHEMATIC DIAGRAM OF PREDICTED ELECTRON DENSITY AS PLASMA APPROACHES EQUILIBRIUM.

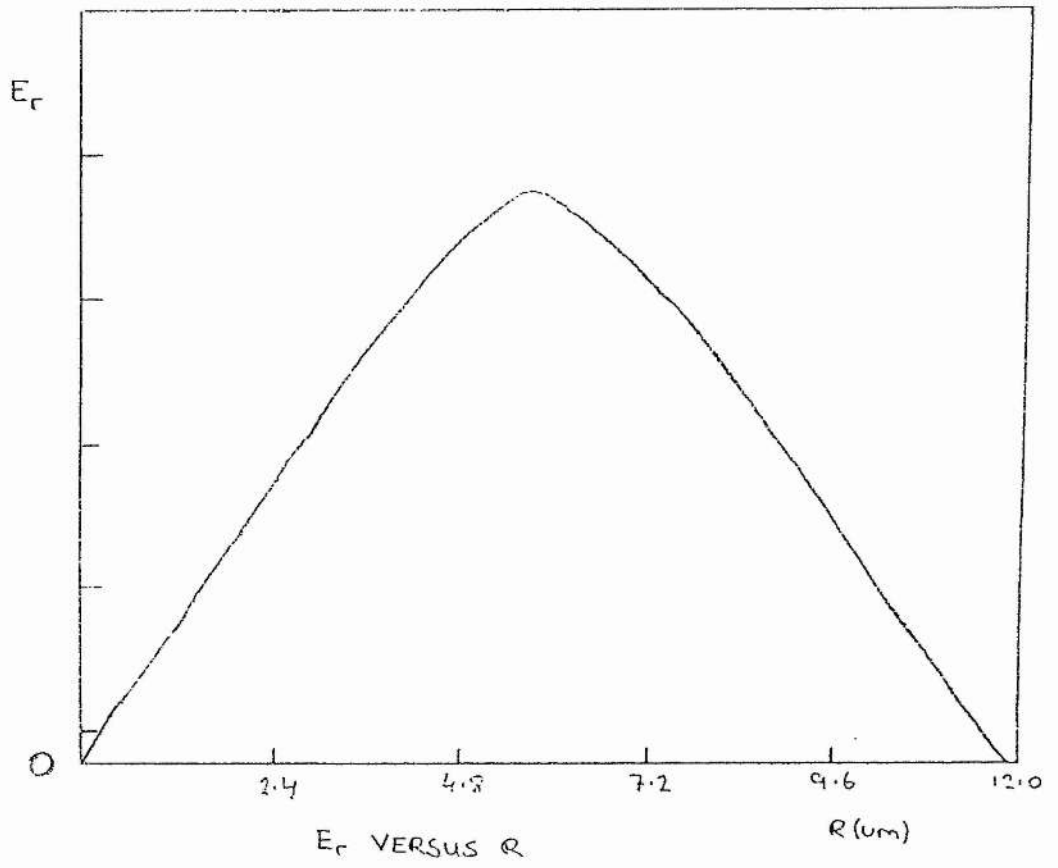

Figure 3.6 SCHEMATIC DIAGRAM OF PREDICTED ELECTRIC FIELD AS PLASMA APPROACHES EQUILIBRIUM.

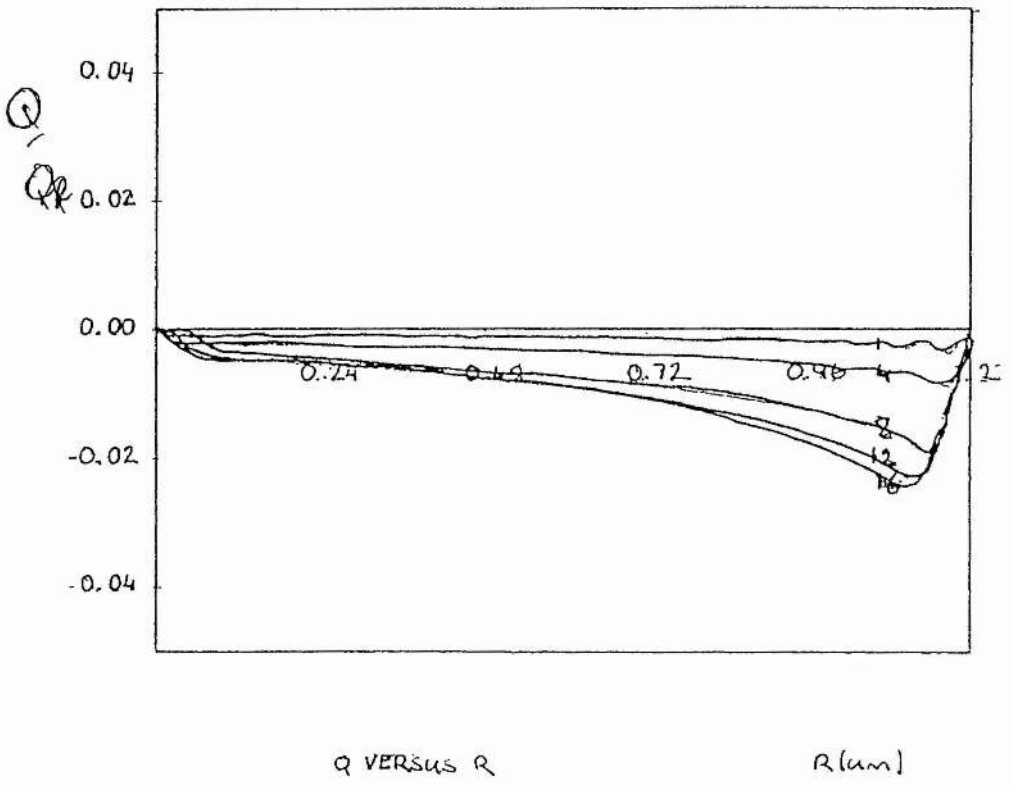

Figure 3.7 HEAT FLOW PROFILES FOR A NON-UNIFORM PLASMA WITH N_S/N_E = 2, T_H/T_C = 1 AND N_E = 10^{21} CM^{-3} AND T_E = 1.0KEV (t=1,4,8,12,16)

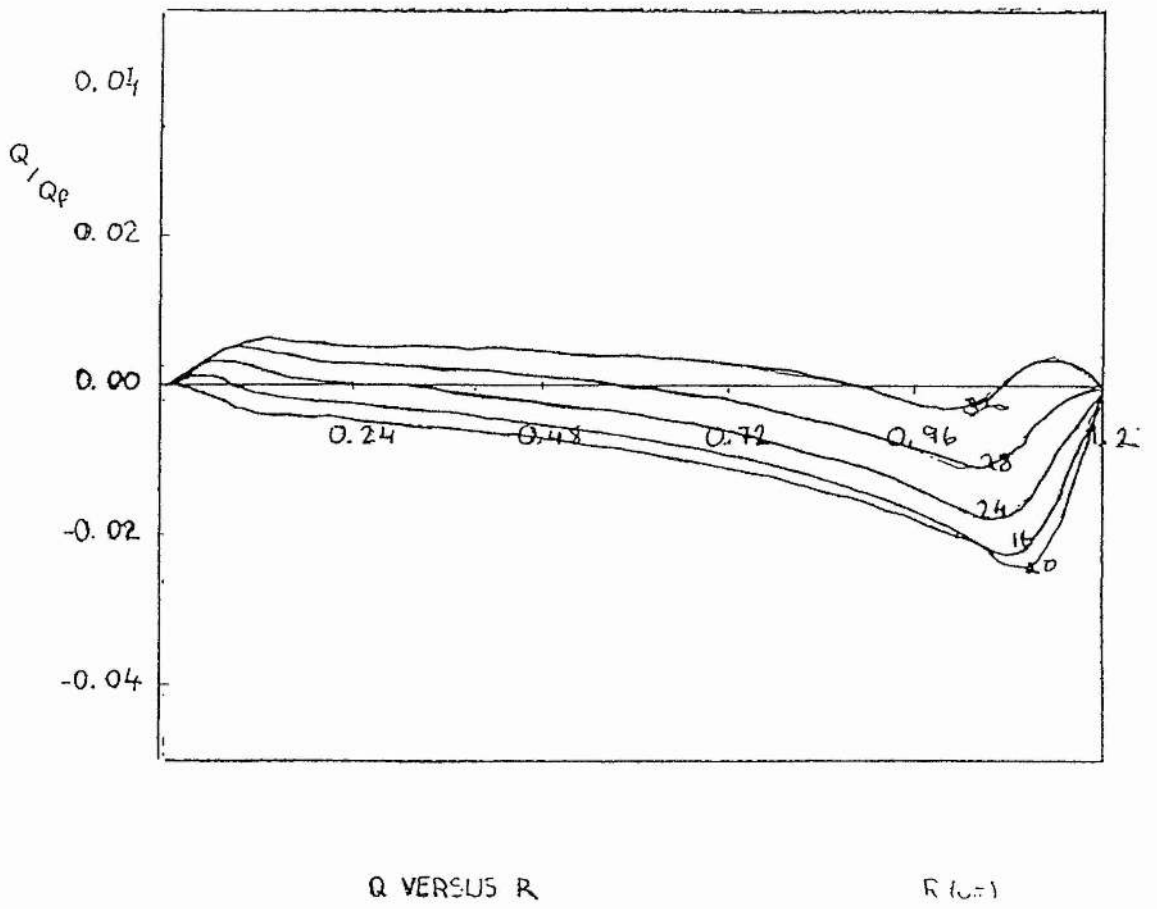

Figure 3.8 HEAT FLOW PROFILES FOR A NON-UNIFORM PLASMA WITH $N_S/N_E = 2$, $T_H/T_C = 1$ AND $N_E = 10^{21}$ CM^{-3} AND $T_E = 1.0KEV$ (t=16,20,24,28,32)

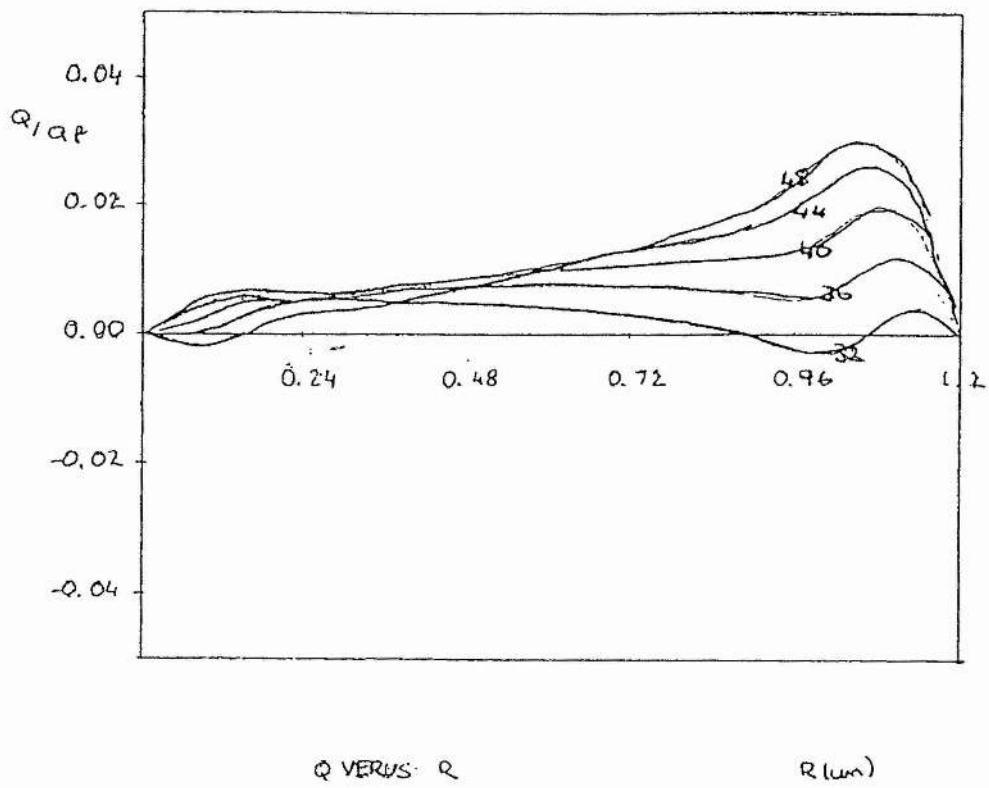

Figure 3.9 HEAT FLOW PROFILES FOR A NON-UNIFORM PLASMA WITH $N_S/N_E = 2$, $T_H/T_C = 1$ AND $N_E = 10^{21}$ CM^{-3} AND $T_E = 1.0KEV$ (t=32,36,40,44,48)

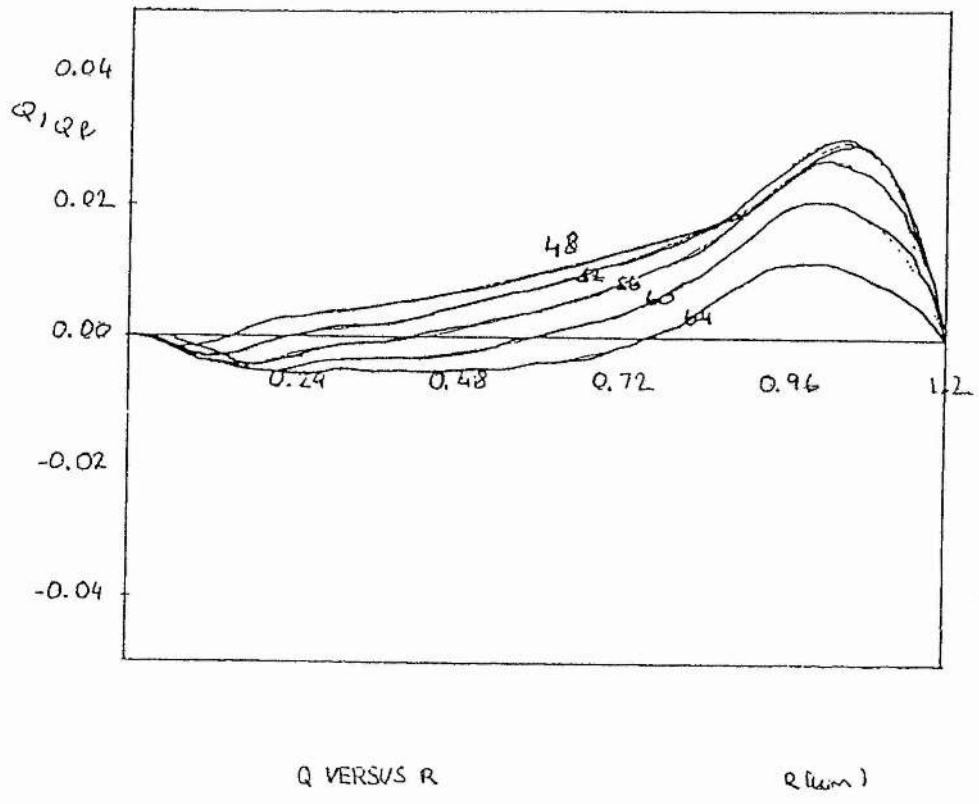

Figure 3.10 HEAT FLOW PROFILES FOR A NON-UNIFORM PLASMA WITH $N_S/N_E = 2$, $T_H/T_C = 1$ AND $N_E = 10^{21}$ CM^{-3} AND $T_E = 1.0KEV$ (t=48,52,56,60,64)

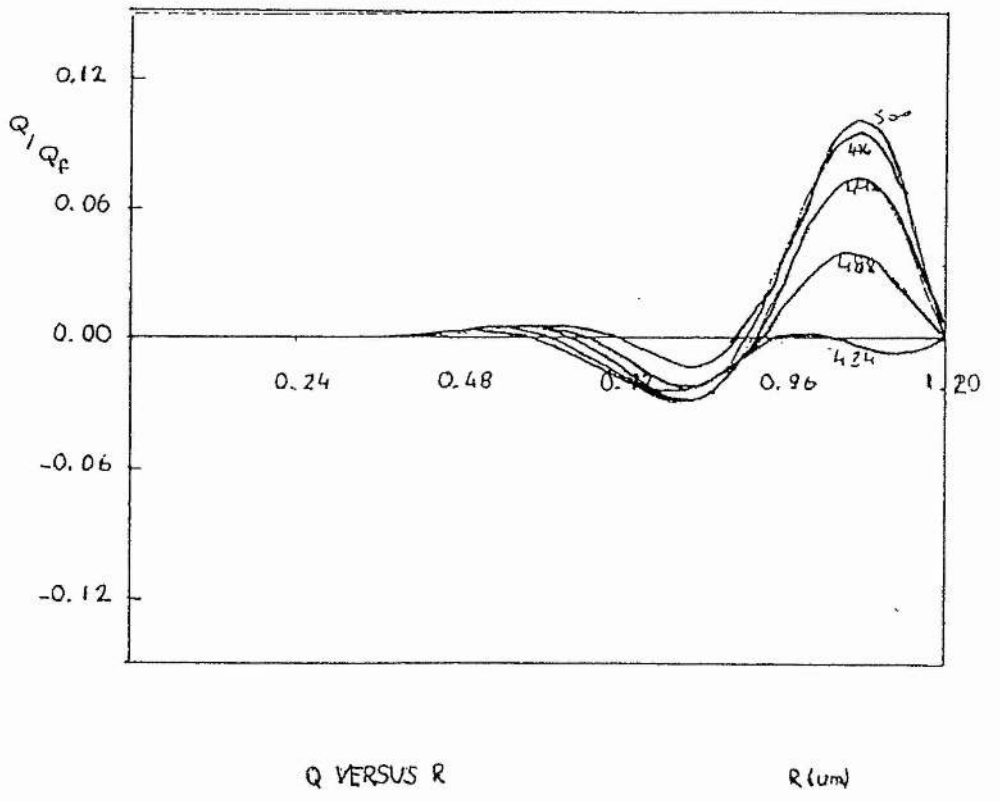

Figure 3.11 HEAT FLOW PROFILES FOR A NON-UNIFORM PLASMA WITH $N_S/N_E = 2$, $T_H/T_C = 1$ AND $N_E = 10^{21}$ CM^{-3} AND $T_E = 1.0KEV$ (t=484,488,492,496,500)

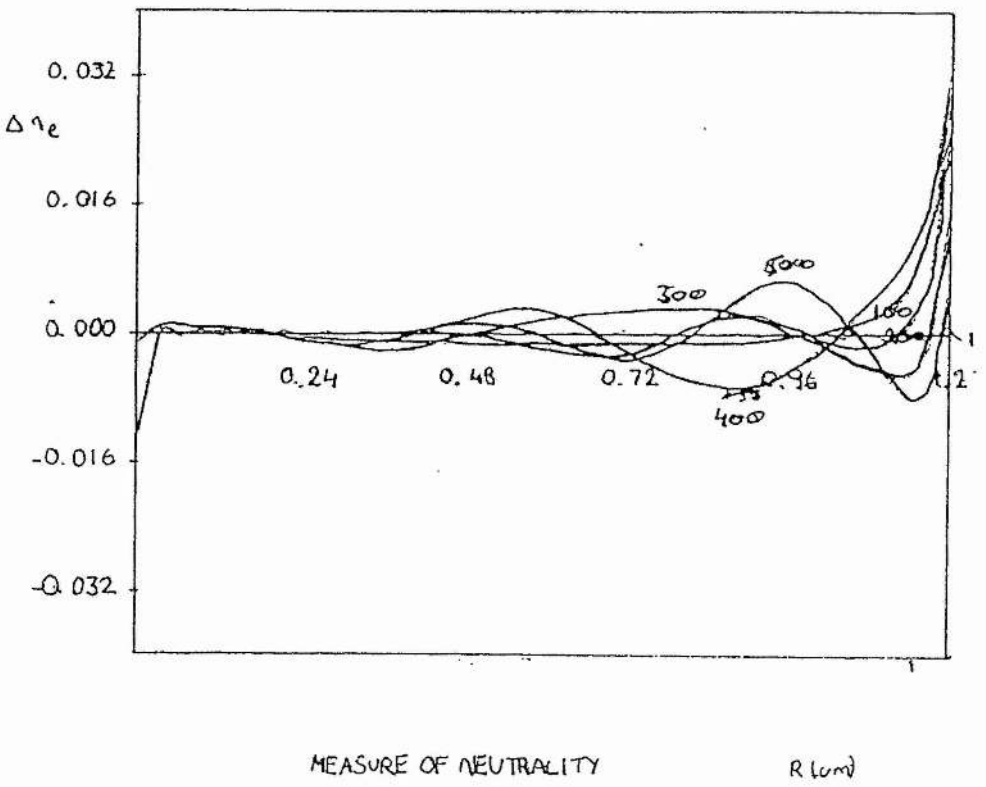

Figure 3.12 **DEPARTURE FROM NEUTRALITY FOR A NON-UNIFORM PLASMA WITH $N_S/N_E = 2$, $T_B/T_C = 1$ AND $N_E = 10^{21}$ CM^{-3} AND $T_E = 1.0KEV$ (t=100,200,300,400,500)**

3.3 Discussion of Density Gradient Simulations

In the previous section, it was shown that there were several problems with modelling thermal conduction with density gradients. When the plasma was heated with particle conservation switched on, it was shown that although the temperature profiles evolved satisfactorily, the heat flow developed an instability near the foot of the heat front. If the particle conservation was switched off when the plasma was being heated, it was shown that the temperature profiles cooled down near the inner boundary. Lastly, it was shown that when the particle conservation is switched on and no heat is added to the plasma, the plasma does not appear to relax to an equilibrium position.

It is thought that all of these problems are the result of two aspects of the original code.

Firstly, it is thought that the way in which the original code was artificially forced to conserve particles was unsatisfactory. To understand this explanation, consider the evolution of a Maxwellian distribution in an isotropic plasma without particle conservation switched on. Figure 3.13 shows how the distribution evolves. The distribution becomes underpopulated in the mid-velocity range and over-populated for low and high velocities. The distribution distorts more quickly when there are fewer velocity mesh points and when the collision frequency increases. The overall result of this distortion is that the distribution loses particles.

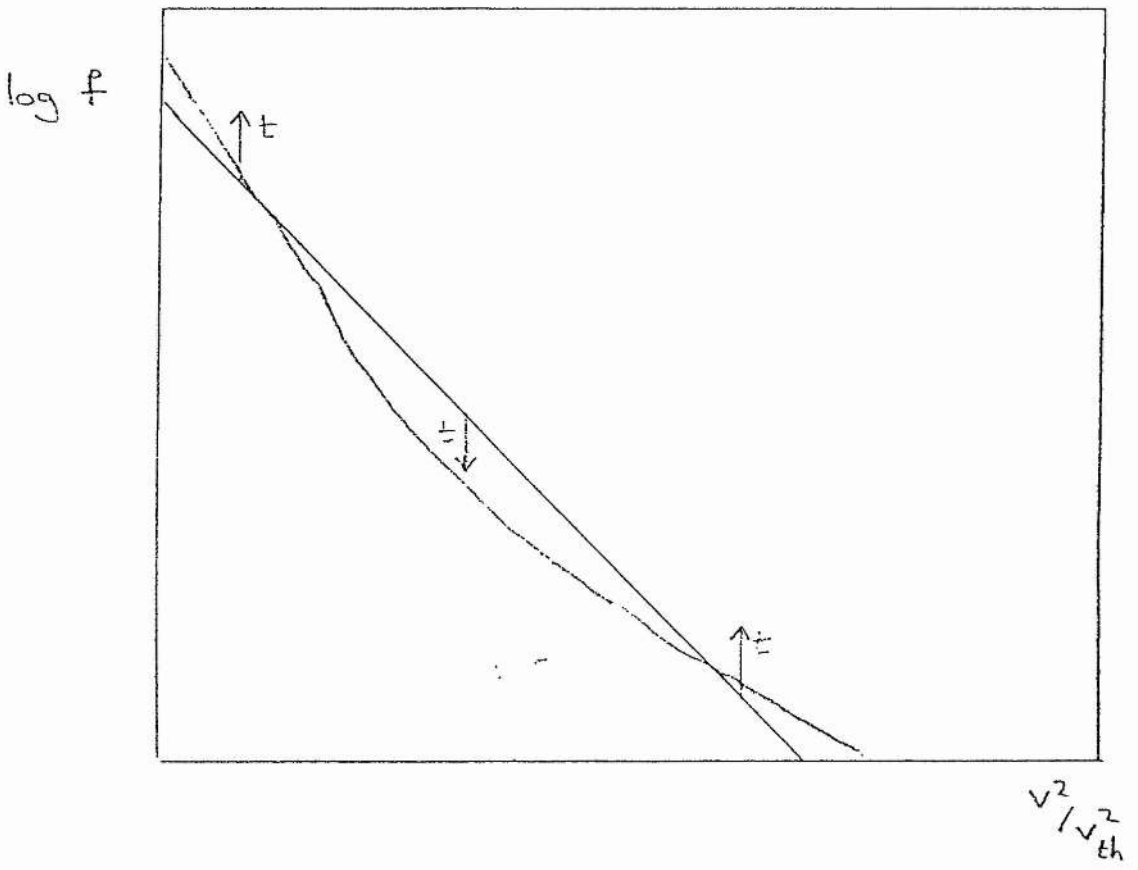

Figure 3.13 SCHEMATIC DIAGRAM OF DISTORTION OF DISTRIBUTION DUE TO VELOCITY DIFFERENCE EQUATION.

Now, as mentioned before, the original code was forced to conserve particles by calculating the particle loss at each radial mesh point and adding a Maxwellian at the current density and prevailing temperature if more than 0.1% is lost. This assumes that the particles lost form a Maxwellian distribution but from figure 3.13 we can see that it is not the case. The result of the correction to the particle loss is to add too few particles in the mid-velocity range and too many at high and low velocities. The particle loss may be reduced but the distortion of the distribution function remains.

The distortion of this method of conservation on Jorna and Wood's results will be discussed later in Chapter 5. In a non-uniform plasma, the result of this method of conservation is significant. As the particle loss is dependent on the collision frequency, the degree of distortion to the distribution will vary across the plasma. This will create artificial gradients across the plasma. It is possible, therefore, that the instability seen for the simulations in which heat is injected and particle conservation is on is due to these artificial gradients.

Secondly, it is thought that the method used to calculate the electric field was not accurate enough to stop large departures from neutrality. As mentioned previously, the electric field is reduced by 10^3 to decrease the effective plasma frequency to less than the collision frequency. In a uniform plasma, this is satisfactory but in a non-uniform plasma, the electric field has to act against the electron pressure down the density gradient. As the electric field is artificially reduced, then the electron pressure is never properly countered and departures from neutrality occur.

It is thought that it was the interaction of these two aspects of the original code that caused the problem with the density gradient simulations. In all of the simulations, deviations from neutrality would occur due to the time dilation method and the way in which the collision term was differenced. When particles were not artificially added, then this would result in the cooling seen in figure 3.13. When particles were artificially added, this would cause an artificial heat flow that disrupts the true heat flow.

To remove these two problems it was therfore necessary to improve the method used to conserve particles and the method used to calculate the electric field.

To deal with the problem of particle loss, it is necessary either to choose a different method of correcting the loss of particles or to alter the method used to difference the Fokker-Planck code so as to eliminate or significantly reduce the loss of particles.

Any method of correcting the loss of particles is fraught with difficulties. In these simulations, it is possible that if a different type of distribution is added to the plasma then the plasma may be distorted less while maintaining particle conservation. For example, if the distribution calculated at the previous timestep is added, instead of a Maxwellian, then the plasma will maintain its profile. Alternatively, the loss of particles may be corrected by only adding particles within a particular velocity range. A scheme could be devised where a Maxwellian distribution is added to the plasma up to about 2 thermal velocities. This would correct the particle loss and not distort the plasma at high velocities. However, the problem with all of these

schemes is to know which method to use before performing the simulation and what effect it will have on the simulation. Indeed, it seems unwise to artificially add particles throughout a plasma when the object of the simulation is to model the transportation of particles.

Rather than attempt to correct the loss of particles, it is better to choose a different scheme for the Fokker-Planck equation which does not lose particles.

The calculation of the electric field may be improved by replacing the time dilation method with the implicit moment method.

In the time dilation method, the plasma frequency was artificially decreased so that it was possible to have simulations on a timescale of the order of the self-collision time. In effect, the microscopic effect of the electric field was ignored by making the plasma period longer than the timescale of the simulation.

The implicit moment method of calculating the electric field was developed for particle codes when it became necessary to study problems on time-scales longer than the plasma period. It calculates the electric field not from the microscopic properties of the plasma but from the macroscopic properties of the plasma. The method involves taking the moments of the distribution and then using the fluid equations to calculate the electric field implicitly for the next timestep. This method can add significant algebraic complexity to the electric field calculation, but it does appear to offer a method that does not involve having to reduce the timestep or to decrease the elctric field.

3.5 Conclusion

In this chapter, we set out to examine the importance of including the anisotropic Rosenbluth potentials when a density gradient is introduced to Jorna and Wood's model. It has been discovered that it is not possible to model thermal conduction with density gradients with the current version of the code. It has been shown with the isotropic code that although the code could model the evolution of the temperature profile, it could not model the evolution of the heat fluxes.

It has been suggested that the original code cannot cope with density gradients because of the difference scheme employed in the solution of the velocity equation. The plasma loses particles which are artificially replaced in such a way that large artificial gradients are induced in the velocity range in which heat is carried. In addition, the time dilation method used to calculate the electric field is not sufficient to balance the electron pressure and therefore the plasma deviates from neutrality. Different methods to solve these two problems have been discussed.

It was decided to re-develop the original code in such a way that both the isotropic and anisotropic codes would conserve particles. In addition, it was decided to alter the method used to calculate the anisotropic portion of the Rosenbluth potentials to improve the performance of the anisotropic code and so that the numerical methods used to calculate the coefficients were consistent. By altering the code in this way it was hoped that it would be possible to determine what effect the original method of particle conservation has on the uniform plasma. For

example, as the methods used to calculate the Rosenbluth potentials were different for the original two codes, could the large differences discovered between the isotropic and ansisotropic codes be due to a different number of particles being added in the two simulations ?

It was our intention also to update the time dilation method but this was not possible in the time allowed. Consequently, the plan to investigate heat conduction in the presence of density gradients had to be abandoned in favour of (i) a re-investigation of Jorna and Wood's results using the new, particle-conserving, version of the code and (ii) a study of the collisional relaxation of non-thermal plasmas.

CHAPTER 4: THE NUMERICAL SOLUTION OF THE FOKKER-PLANCK EQUATION

4.1 Introduction

In this chapter, we describe the numerical methods used to solve the Fokker-Planck equation. The equation is cast in spherical geometry, with azimuthal symmetry, and is solved with and without the full anisotropic collision terms included. When the anisotropic collision terms are included, hereafter called the Anisotropic code, the collision term is solved using methods developed by Killeen et al (1980). If we are not interested in the anisotropic collision term, we use techniques that make use of the fact that the collision term is isotropic (Chang 1970, Langdon 1981); we shall call this the Isotropic code. The collisionless part of the code is differenced in the same way for both the Isotropic code and the Anisotropic code.

This code was developed from a code written by Jorna and Wood (1987a,1987b). Where applicable, we shall describe where the code was developed and how we have improved it.

In Section 4.2, the original equations are described. The methods used to solve the collisionless part of the equation are described in Section 4.3. Sections 4.4 and 4.5 describe how the collisional part of the isotropic and anisotropic code is discretized. Finally, in Section 4.6 we describe the calibration tests for the isotropic and the anisotropic codes.

4.2 Original Equations

The Fokker-Planck equation in spherical geometry, with azimuthal symmetry, is of the form

$$\frac{\partial f}{\partial t}+\frac{v\mu}{r^2}\frac{\partial}{\partial r}(r^2 f)+\frac{v}{r}\frac{\partial}{\partial \mu}[(1-\mu^2)f] + \frac{eE}{m}\left[\frac{(1-\mu^2)}{v}\frac{\partial f}{\partial \mu}+\mu\frac{\partial f}{\partial v}\right]=\left[\frac{\partial f}{\partial t}\right]_c$$

- eqn (4.2.1)

where the electron distribution function f depends on v, the total velocity, μ , the cosine of the angle between $\underline{v}$ and the radial vector $\underline{r}$, the radial distance r, and E is the radial component of the electric field.

The collision term for like particle interactions is, as defined by Rosenbluth, MacDonald and Judd (1957a),

$$\frac{1}{\Gamma}\left(\frac{\partial f}{\partial t}\right)_c = -\frac{1}{v^2}\frac{\partial}{\partial v}\left(fv^2\frac{\partial h}{\partial v}\right) - \frac{1}{v^2}\frac{\partial}{\partial \mu}\left[f(1-\mu^2)\frac{\partial h}{\partial \mu}\right] + \frac{1}{2v^2}\frac{\partial^2}{\partial v^2}\left(fv^2\frac{\partial^2 g}{\partial v^2}\right) + \frac{1}{2v^2}\frac{\partial}{\partial \mu}\left(f\left[\frac{\mu(1-\mu^2)}{v^2}\frac{\partial^2 g}{\partial \mu^2}+\frac{2\mu}{v}\frac{\partial g}{\partial v}\right]\right) + \frac{1}{2v^2}\frac{\partial}{\partial \mu}\left(f\left[\frac{(1-\mu^2)}{2v}\frac{\partial^2 g}{\partial \mu \partial v}-\frac{2}{v^2}\frac{\partial g}{\partial \mu}\right]\right)$$

$$+\frac{1}{2v^2}\frac{\partial^2}{\partial\mu^2}\left(f\left[\frac{(1-\mu^2)}{v^2}\frac{\partial^2 g}{\partial\mu^2}+\frac{(1-\mu^2)}{v}\frac{\partial g}{\partial v}-\frac{\mu(1-\mu^2)}{v^2}\frac{\partial g}{\partial\mu}\right]\right)$$

$$+\frac{1}{2v^2}\frac{\partial}{\partial v}\left(f\left[-\frac{(1-\mu^2)}{v}\frac{\partial^2 g}{\partial\mu^2}-2\frac{\partial g}{\partial v}+\frac{2\mu}{v}\frac{\partial g}{\partial\mu}\right]\right)$$

$$+\frac{1}{v^2}\frac{\partial^2}{\partial\mu\partial v}\left(f(1-\mu^2)\left[\frac{\partial^2 g}{\partial\mu\partial v}-\frac{1}{v}\frac{\partial g}{\partial\mu}\right]\right)$$

- eqn (4.2.2)

where the Rosenbluth potentials h and g are given by

$$h(\underline{v})=2\int f(\underline{v'})\,|\underline{v}-\underline{v'}|^{-1}\underline{dv'}$$

- eqn (4.2.3)

$$g(\underline{v})=\int f(\underline{v'})\,|\underline{v}-\underline{v'}|\underline{dv'}$$

- eqn (4.2.4)

and

$$\ln\Lambda=24-\frac{\ln\sqrt{n_e}}{T_e}$$

$$\Gamma=4\pi\frac{e^4}{m_e}\ln\Lambda$$

Chapter 4

It will be seen later that it is useful to re-write the right hand side of the Fokker-Planck equation as

$$\left(\frac{\partial f}{\partial t}\right)_c = \frac{1}{2v^2}\frac{\partial}{\partial v}\left(Af + B\frac{\partial f}{\partial v} + C\frac{\partial f}{\partial \mu}\right) + \frac{1}{2v^2}\frac{\partial}{\partial \mu}\left(Df + E\frac{\partial f}{\partial \mu} + F\frac{\partial f}{\partial v}\right)$$

- eqn (4.2.5)

where

$$A = -2v^2\frac{\partial h}{\partial v} + 2v\frac{\partial^2 g}{\partial v^2} + v^2\frac{\partial^3 g}{\partial v^3} - 2\frac{\partial g}{\partial v} + 2\frac{\mu}{v}\frac{\partial g}{\partial \mu} - \frac{(1-\mu^2)}{v}\frac{\partial^2 g}{\partial \mu^2}$$

- eqn (4.2.6)

$$B = v^2\frac{\partial^2 g}{\partial v^2}$$

- eqn (4.2.7)

$$C = (1-\mu^2)\frac{\partial^2 g}{\partial \mu \partial v} - \frac{(1-\mu^2)}{v}\frac{\partial g}{\partial \mu}$$

- eqn (4.2.8)

$$D = -2(1-\mu^2)\frac{\partial h}{\partial \mu} + 2\frac{(1-\mu^2)}{v}\frac{\partial^2 g}{\partial \mu \partial v} + \frac{(1-\mu^2)^2}{v^2}\frac{\partial^3 g}{\partial \mu^3} + (1-\mu^2)\frac{\partial^3 g}{\partial \mu \partial v^2} - 2\frac{(1-\mu^2)}{v^2}\frac{\partial g}{\partial \mu} - 4\frac{\mu(1-\mu^2)}{v^2}\frac{\partial^2 g}{\partial \mu^2}$$

- eqn (4.2.9)

$$E=\frac{(1-\mu^2)^2}{v^2}\frac{\partial^2 g}{\partial \mu^2}+\frac{(1-\mu^2)}{v}\frac{\partial g}{\partial v}-\frac{\mu(1-\mu^2)}{v^2}\frac{\partial g}{\partial \mu}$$

- eqn (4.2.10)

$$F=(1-\mu^2)\frac{\partial^2 g}{\partial \mu \partial v}-\frac{(1-\mu^2)}{v}\frac{\partial g}{\partial \mu}$$

- eqn (4.2.11)

The Fokker-Planck equation, (4.2.1) and (4.2.5), is solved by the method of fractional steps. The method of fractional steps is chosen because of the mixed derivative terms in equation (4.2.5). The mixed derivative terms are treated explicitly and it is therefore an advantage to treat the rest of the terms implicitly. Otherwise it is possible that the code may become unstable. In addition, the method of fractional steps is chosen because of its simplicity to program and the ease with which it allows additional physics to be added. We allow a degree of flexibility by permitting a mixture of implicit and explicit terms in the velocity, equation (4.2.13), and angular, equation (4.2.14), steps.

Therefore, the equations to be solved are:

$$\frac{\partial f^{n+\frac{1}{3}}}{\partial t} = -v\mu \frac{\partial f^{n+\frac{1}{3}}}{\partial r}$$

- eqn (4.2.12)

$$\frac{\partial f^{n+\frac{2}{3}}}{\partial t} = \left[a_r \mu \frac{\partial f}{\partial v} + \frac{1}{2v^2}\frac{\partial}{\partial v}\left(Af + B\frac{\partial f}{\partial v}\right)\right]^{\alpha(n+\frac{2}{3});(1-\alpha)(n+\frac{1}{3})} + \frac{1}{2v^2}\frac{\partial}{\partial v}\left(C\frac{\partial f}{\partial \mu}\right)^{n+\frac{1}{3}}$$

- eqn (4.2.13)

$$\frac{\partial f^{n+1}}{\partial t} = \left[\left((1-\mu^2)\left(\frac{a_r}{v}+\frac{v}{r}\right)\right)\frac{\partial f}{\partial \mu} + \frac{1}{2v^2}\frac{\partial}{\partial \mu}\left(Df + E\frac{\partial f}{\partial \mu}\right)\right]^{\alpha(n+1);(1-\alpha)(n+\frac{2}{3})} + \frac{1}{2v^2}\frac{\partial}{\partial \mu}\left(F\frac{\partial f}{\partial v}\right)^{n+\frac{2}{3}}$$

- eqn (4.2.14)

where α represents the fraction of the difference equation that is treated implicitly. If $\alpha = 0.5$ then the difference equations are second order accurate while if $\alpha = 1.0$ then the difference equations are only first order

accurate. It is worth noting that on the problems considered in this thesis, the results were insensitive to α when α is in the 0.5 to 1.0 range.

4.3 Discretization of the Collisionless Portion

The advection equation, (4.2.12), is solved by the implicit Wendroff method. This method has no numerical diffusion but it does have significant dispersion when $v\Delta t/\Delta r << 1$ or $v\Delta t/\Delta r >> 1$ and it does not preserve monotonicity. The algorithm can be written as:

$$f^{n+1}_{i+1,j,k} = f^{n}_{i,j,k} + \frac{1-pv_j\mu_k}{1+pv_j\mu_k}\left(f^{n}_{i+1,j,k} - f^{n+1}_{i,j,k}\right)$$

- eqn (4.3.1)

where $p = \Delta t/\Delta r$. The i,j,k subscripts are associated with the r,v and μ respectively while the n superscript denotes the number of time steps that have elapsed.

Despite the drawbacks of the method, the implicit Wendroff method is accurate enough for our purposes.

The remaining collisionless terms, in equations (4.2.13) and (4.2.14), are all centre differenced.

4.4 Discretization of Velocity and Angular Equations for the Anisotropic Code

The velocity and angular equations, (4.2.13) and (4.2.14) respectively, are discretized as follows.

$$\frac{\partial}{\partial v}(Af)\Big|_{j,k}=\frac{(A_{j+1,k}f_{j+1,k}-A_{j-1,k}f_{j-1,k})}{2\Delta v_j}$$

- eqn (4.4.1)

$$\frac{\partial}{\partial v}\left(B\frac{\partial f}{\partial v}\right)\Big|_{j,k}=$$
$$\left(B_{j+1/2,k}\left(\frac{f_{j+1,k}-f_{j,k}}{\Delta v_{j+1/2}}\right)-B_{j-1/2,k}\left(\frac{f_{j,k}-f_{j-1,k}}{\Delta v_{j-1/2}}\right)\right)/\Delta v_j$$

- eqn (4.4.2)

$$\frac{\partial}{\partial v}\left(C\frac{\partial f}{\partial \mu}\right)\Big|_{j,k}=$$
$$\frac{(C_{j+1,k}(f_{j+1,k+1}-f_{j+1,k-1})-C_{j-1,k}(f_{j-1,k+1}-f_{j-1,k-1})}{4\Delta v_j\Delta\mu_k}$$

- eqn (4.4.3)

The remaining terms in equation (4.2.5) are differenced similarly. It is essential to difference the angular and velocity derivatives in this way to conserve particle density. The earlier version of the code did not difference the derivatives in this way and thus the particle density was poorly conserved. To correct the particle loss, particles were periodically added to the plasma.

Jorna and Wood calculated the Rosenbluth potentials exactly. However, this process requires a large amount of memory and consumed 95% of the total processing time. Instead of calculating h and g exactly, the Rosenbluth potentials are calculated from a Legendre decomposition in μ. This process only consumes 10 % of the total processing time and leads to a much faster code. Therefore g and h become

$$h(v,\mu,t) = 2\sum_{j=0}^{\infty} \ln\Lambda_{ee} h_j(v,t)\, P_j(\mu)$$

- eqn (4.4.4)

$$g(v,\mu,t) = \sum_{j=0}^{\infty} \ln\Lambda_{ee} g_j(v,t)\, P_j(\mu)$$

- eqn (4.4.5)

where

$$h_j(v,t) = \frac{4\pi}{(2j+1)} \left(v^{-j-1}N_j + v^j M_j\right)$$

- eqn (4.4.6)

$$g_j(v,t) = \frac{4\pi}{(2j+1)} \left(\frac{1}{(2j+3)} \left[v^{-j-1}E_j + v^{j+2}M_j\right] - \frac{1}{(2j-1)} \left[v^{-j+1}N_j + v^j R_j\right] \right)$$

- eqn (4.4.7)

and

$$M_j = \int_v^\infty f_j(u)\, u^{1-j} du$$

- eqn (4.4.8)

$$R_j = \int_v^\infty f_j(u)\, u^{3-j} du$$

- eqn (4.4.9)

$$N_j = \int_0^v f_j(u)\, u^{2+j} du$$

- eqn (4.4.10)

$$E_j = \int_0^v f_j(u)\, u^{4+j} du$$

- eqn (4.4.11)

$$f_j(v,t) = \frac{(2j+1)}{2} \int_{-1}^{+1} f(v,\mu,t)\, P_j(\mu)\, d\mu$$

- eqn (4.4.12)

The integrals over v are done using the trapezoidal rule while the μ-integration is completed using Simpson's rule.

The derivatives with respect to v can now be done analytically. The results are:

$$\frac{\partial h_j}{\partial v} = \frac{4\pi}{(2j+1)} \left[j v^{j-1} M_j - (j+1)\, v^{-j-2} N_j \right]$$

- eqn (4.4.13)

$$\frac{\partial g_j}{\partial v} = \frac{4\pi}{(2j+1)} \left(\frac{1}{(2j+3)} \left[(j+2)\, v^{j+1} M_j - (j+1)\, v^{-j-2} E_j \right] - \frac{1}{(2j-1)} \left[j v^{j-1} R_j - (j-1)\, v^{-j} N_j \right] \right)$$

- eqn (4.4.14)

$$\frac{\partial^2 g_j}{\partial v^2} = \frac{4\pi}{(2j+1)} \left(\frac{(j+1)(j+2)}{(2j+3)} \left[v^{-j-3} E_j + v^j M_j \right] - \frac{j(j-1)}{(2j-1)} \left[v^{-j-1} N_j + v^{j-2} R_j \right] \right)$$

- eqn (4.4.15)

$$\frac{\partial^3 g_j}{\partial v^3} = \frac{4\pi}{(2j+1)} \left(\frac{1}{(2j+1)} \left[j(j+1)(j+2) v^{j-1} M_j - (j+1)(j+2)(j+3) v^{-j-4} E_j \right] - \frac{1}{(2j-1)} \left[j(j-1)(j-2) v^{j-3} R_j - (j+1) j (j-1) v^{-j-2} N_j \right] \right)$$

- eqn (4.4.16)

The μ-derivatives are also done analytically.

4.5 Discretization of Velocity and Angular Equations for the Isotropic Code

The isotropic code can be used for problems where the anisotropic portion is not needed by only including the first term in the Legendre decomposition in the Rosenbluth potentials. Indeed, the angular equation in the isotropic code is discretized in exactly the same way as in the anisotropic code. However, it is possible to discretize the velocity equation in the isotropic code in such a way that both particles and energy are conserved, with much fewer mesh points than in the anisotropic code (Langdon, 1981). The number density is conserved by differencing the collisional term as in Section 4.4.

$$\frac{\partial f}{\partial t} = \frac{1}{2v^2{}_j} \frac{F_{j+1/2} - F_{j-1/2}}{\Delta v_j}$$

and

$$F_{j+1/2} = (Af)_{j+1/2} + (B\frac{\partial f}{\partial v})_{j+1/2}$$

- eqn (4.5.1)

If this expression is multiplied by v_j^2 and summed over

all possible velocities then it is zero. The conservation of energy depends on how the coefficients A_j and B_j are determined. The coefficients are determined by considering the energy equation. If we multiply equation (4.2.5) by v^4, while ignoring the angular components, and then integrate over velocity, we find that (4.2.5) becomes:

$$\int_0^\infty \frac{v^2}{2} \frac{\partial}{\partial v} \left(Af + B\frac{\partial f}{\partial v}\right) dv = \int_0^\infty \left(-Av + \frac{\partial}{\partial v}(vB)\right) f dv$$

- eqn (4.5.2)

For these two terms to cancel and for energy to be conserved, it is necessary that:

$$\frac{\partial}{\partial v}(vB) = vA$$

- eqn (4.5.3)

Now for an isotropic plasma

$$A=N_0=\int_0^v v^2 f dv$$

- eqn (4.5.4)

and so we require that B be calculated by differencing

$$\frac{\partial}{\partial v}(vB)=\int_0^v v^3 f dv$$

- eqn (4.5.5)

By differencing the equation in this fashion, the velocity equation conserves energy and particles.

When the collisional part of the distribution is not too far away from Maxwellian, it is possible to use the Chang-Cooper method (Chang 1970) to difference equation (4.5.1). The Chang- Cooper method anticipates how f varies when the distribution is close to Maxwellian. The method does not use linear interpolation to calculate $f_{j+1/2}$ but expresses as

$$f_{j+1/2} = (1-\delta_j) f_{j+1} + \delta_j f_j$$

- eqn (4.5.6)

where δ_j is calculated in such a way that when $F_{j+1/2}$ is expressed as a centre difference, $f_{j+1/2}$ equals the quasi-equilibrium solution.

The advantage of this scheme is that it prohibits negative distributions which can occur at large velocities unless the mesh is very fine. The disadvantage of this scheme is that it assumes that the plasma is close to equilibrium.

4.6 Calibration Tests

4.6.1 Landau Damping

To test the collisionless part of the code, the code is used to simulate Landau damping. The collisions are switched off and a small perturbation is applied to the electron distribution function, ie

$$f(r, v, \mu, t=0) = f_{maxw}(v, 0)\,(1.0 + A\cos(kr)) \qquad \text{- eqn (4.6.1)}$$

$A = 0.05$, $k = 1/2\lambda_d$, $4\pi\lambda_d = r_2 - r_1$, where r_1 and r_2 are the minimum and maximum values of r respectively and λ_d is the Debye length. The system is forced back to equilibrium by the electric field at a frequency equal to the plasma frequency. Figure 4.1 shows the amplitude of the electric field as time progresses. The theoretical value of the Landau decrement is 0.15 and the value of the decrement predicted from the code is 0.18. The plasma frequency is within 1 % of the theoretical value.

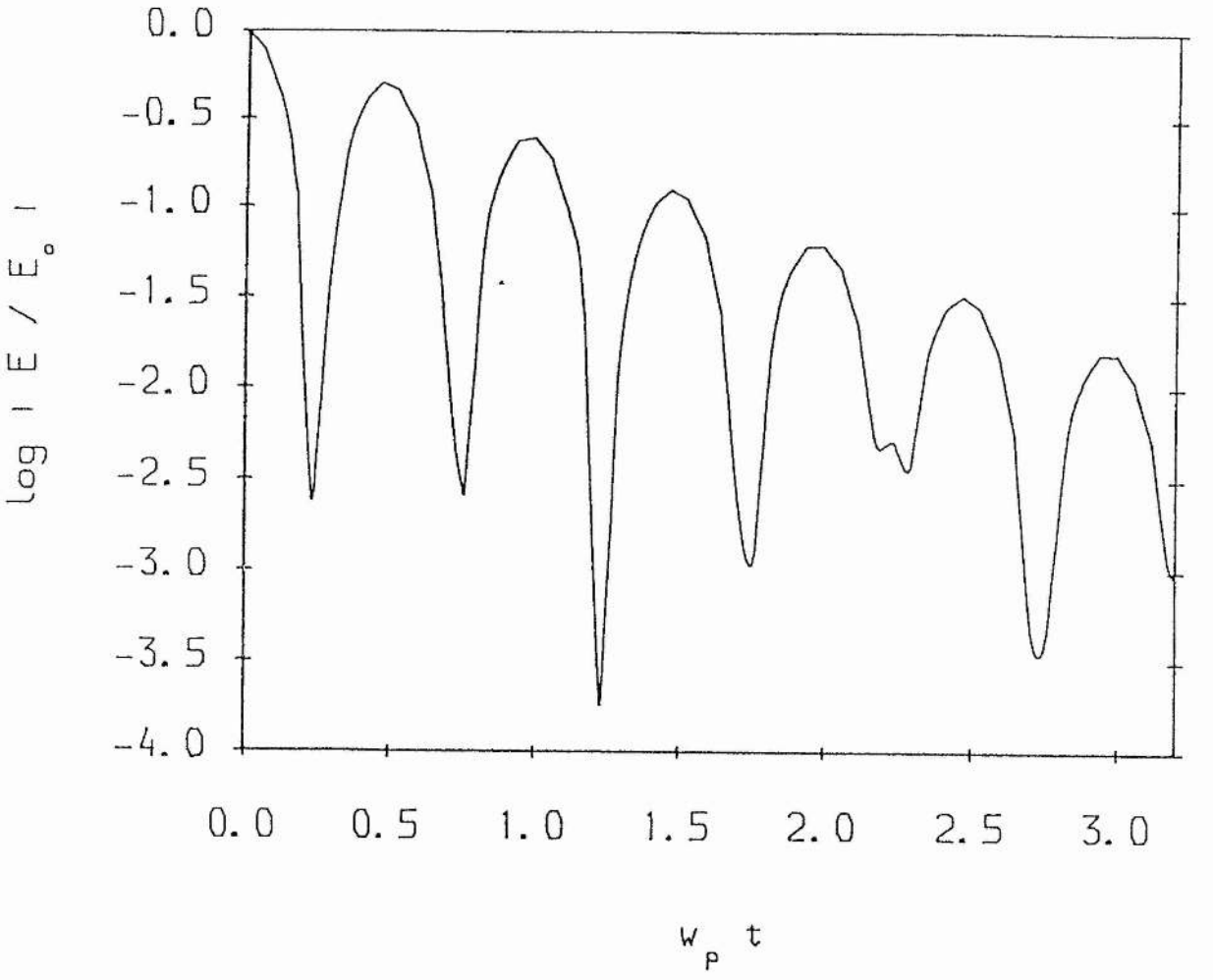

Figure 4.1: **LANDAU DAMPING OF ELECTRIC FIELD DUE TO PLASMA OSCILLATIONS**

4.6.2 Relaxation of a Gaussian Hump on a Maxwellian Distribution

To test the velocity component of the anisotropic Fokker-Planck collision term, the code is used to simulate the relaxation of a high-energy Gaussian hump on a Maxwellian distribution. The initial distribution is given by

$$f(r,v,t=0) = 1.7453\left(\frac{3}{2\pi}\right)^{\frac{3}{2}}\exp\left(-\frac{3v^2}{1.28v^2_{th}}\right) + 0.001192\exp\left(-100\left(\frac{v}{v_{th}}-2\right)^2\right)$$

- eqn (4.6.2)

It can be seen that this distribution has a sharp Gaussian hump at 2 v_{th}. The magnitude of the pertubation is chosen to match that of Dolinsky (1965). Figure 4.2 shows the time evolution of f where log f is plotted against v/v_{th}. The points are the results from work completed by Dolinsky (1965) and the agreement is good.

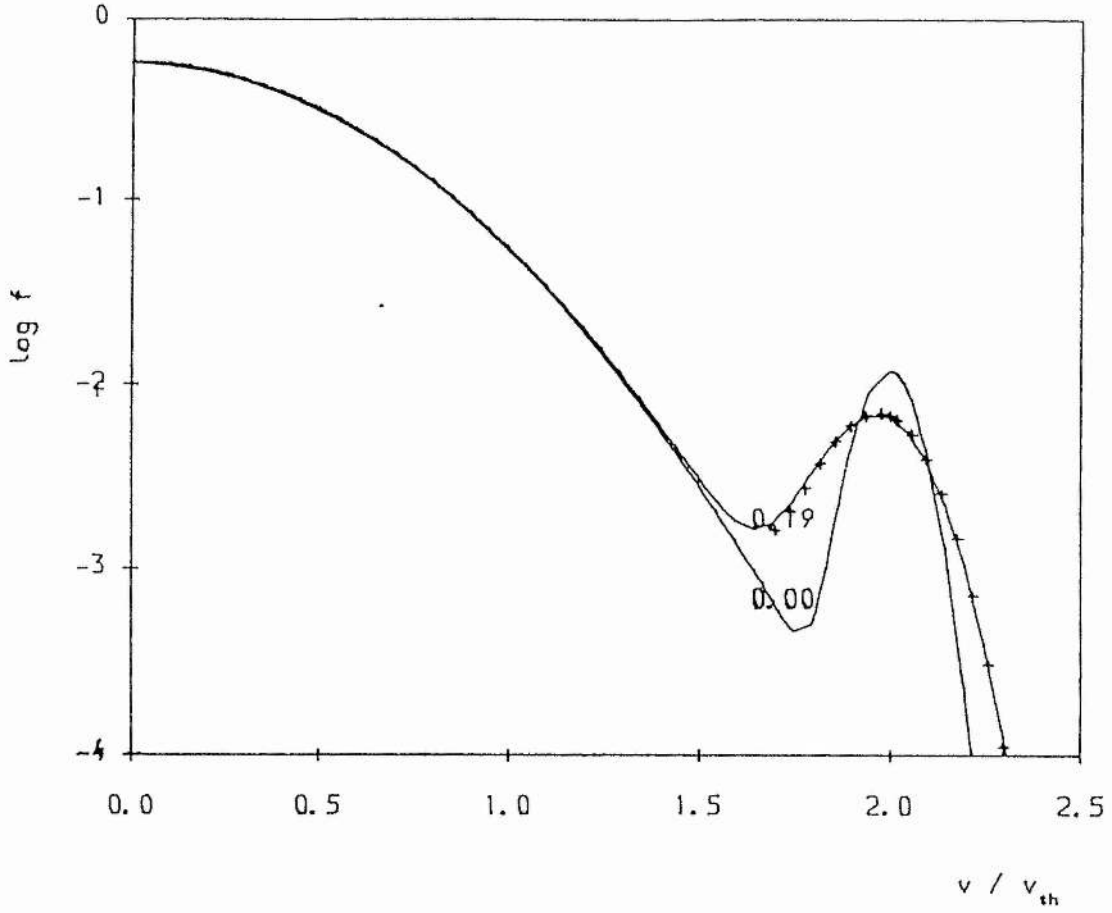

Figure 4.2: RELAXATION OF A GAUSSIAN HUMP ON A MAXWELLIAN DISTRIBUTION AT T=0 AND T=0.19 WHERE TIME IS SCALED TO SELF COLLISION TIME

4.6.3 Relaxation of an Anisotropic Velocity Distribution

The angular component of the Fokker-Planck equation collision term is tested by simulating the relaxation of a bi-Maxwellian distribution, ie

$$f(v,\mu,t) = \frac{n_e}{(\pi v_{th})^{3/2}} \exp\left(-\mu^2 v^2/T_{perp} - (1-\mu^2)\, v^2/T_{par}\right)$$

- eqn (4.6.3)

Initially T_{perp} / T_{par} = 2. Figure 4.3 shows the time development of T_{perp} / T_{par} versus t where t is normalised to the Spitzer self-collision time and the Spitzer self-collision time given by:

$$t_0 = \frac{3\sqrt{m_e}(KT_e)^{3/2}}{4\sqrt{2\pi}n_e e^4 \ln\Lambda}$$

- eqn (4.6.4)

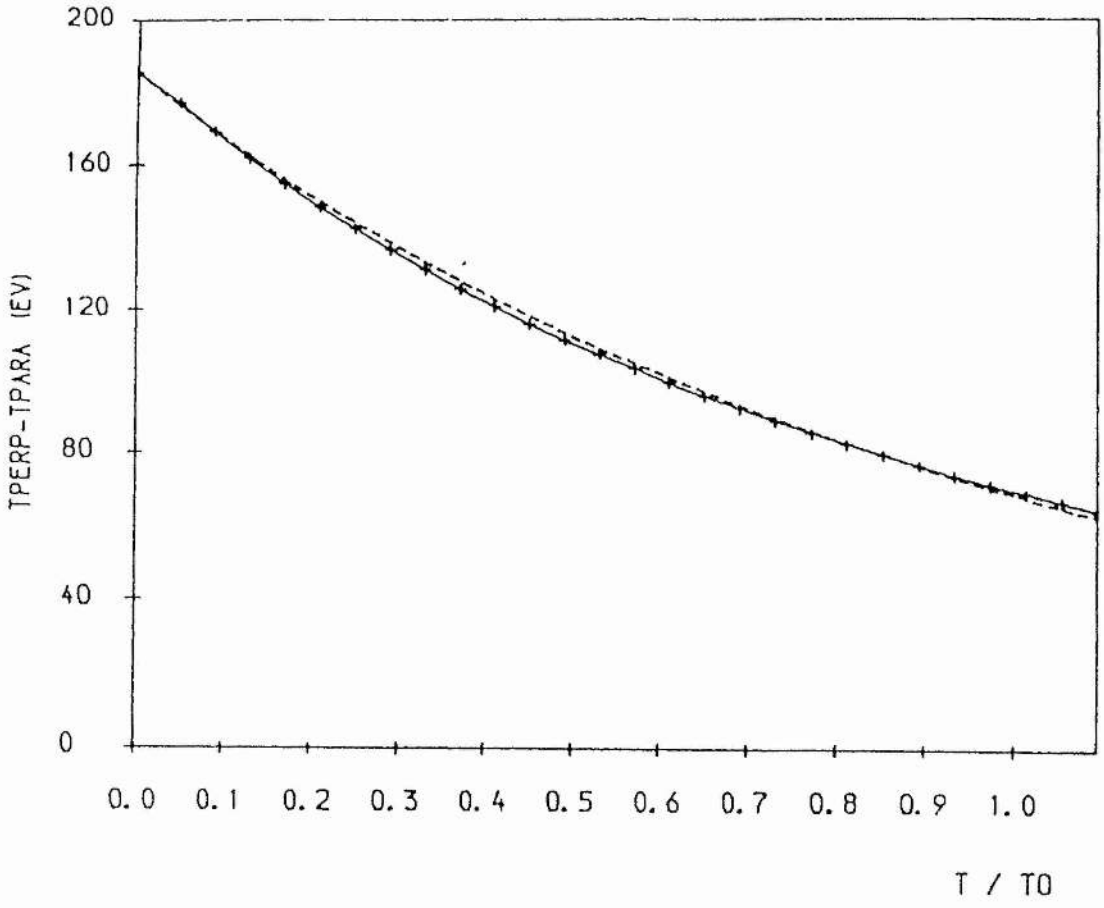

Figure 4.3: RELAXATION OF A BI-MAXWELLIAN. Initially epsilon=2. Time is scaled to self-collision time. Dashed line is analytical result.

The dashed line is the relaxation rate predicted by Shkarofsky (1966) from analytical work which is given by:

$$\frac{d}{dt}(T_{perp}-T_{par}) = \frac{-3\ 2^{1/2}}{5}(T_{perp}-T_{par})$$

- eqn (4.6.5)

4.6.4 Relaxation of an Isotropic Gaussian Distribution

To test the improved particle and energy conservation of the isotropic Fokker-Planck Code, the collisional part of the isotropic Fokker-Planck equation is used to simulate the relaxation of an isotropic Gaussian distribution. The initial distribution is:

$$f(v, t=0) = 0.01 \exp\left(-10\left[\frac{v-0.3}{0.3}\right]^2\right)$$

- eqn (4.6.4)

The evolution of the distribution is shown in Figure 4.4. It is seen that the distribution relaxes back to the correct Maxwellian in about 500 time steps. It was pointed out by Kho (1985) that unless the Isotropic Fokker-Planck equation is differenced in this way, then the distribution will relax back to a cooler Maxwellian due to the poor energy conservation. This is a common drawback of methods using other differencing schemes.

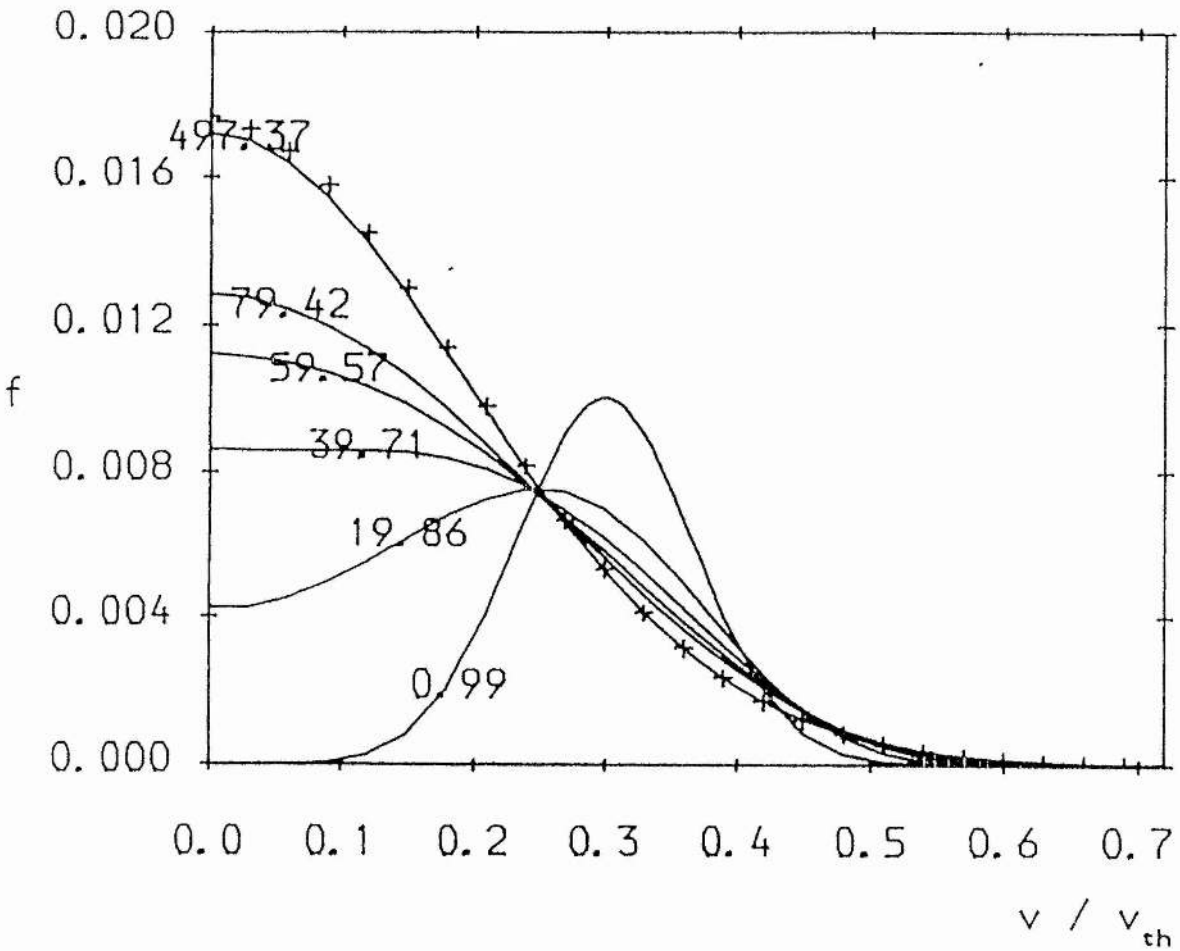

Figure 4.4: RELAXATION OF A GAUSSION HUMP TO A MAXWELLIAN DISTRIBUTION. Crosses are the Maxwellian distribution.

CHAPTER 5: THERMAL ELECTRON TRANSPORT IN DIRECT DRIVE LASER FUSION REVISITED

5.1 Introduction

In Chapter 4, the new version of the Fokker-Planck code was described. In this chapter, the new Fokker-Planck code is used to re-investigate the original model adopted by Jorna and Wood. The new calculations were carried out to seek to verify Jorna and Wood's results and to attempt to understand what causes them.

In Section 5.2, we describe the model that we used to study thermal electron transport and show typical temperature and heat flow profiles.

In Section 5.3, we examine the effect of curvature on the temperature and heat flow profiles.

Section 5.4 analyses the differences between describing the angular component of the distribution function discretely and describing the angular component of the distribution function by a Legendre decomposition in μ.

In Section 5.5 we analyse the importance of including the anisotropic portion of the Rosenbluth potentials.

Finally, in Section 5.6, we discuss the different results discovered with the two different codes.

5.2 The Numerical Experiment

To study thermal electron transport, we considered the cathode model used by Matte (1982). In spherical geometry, the cathode model is described by the transport of energy between two concentric shells of radii r_1, the cold cathode, and r_2, the hot cathode. Between the two shells there is a homogeneous plasma of uniform density n_e which is at a temperature T_o. The ions are of charge Z and since the ion mass is very much greater than the electron mass, it is a very good assumption to assume that the ions are at rest in the plasma. In addition, it is reasonable to assume that the ions have zero heat capacity and that there is no energy exchange between the ions and the electrons.

The plasma is heated up by gradually increasing the temperature of the distribution injected at the hot cathode. The exact form of the hot distribution injected at r_2, the hot cathode, is dependent on the problem under consideration. However, if the plasma is to remain quasi-neutral, it is necessary to inject the boundary distributions in such a way that the total current in the plasma is zero. This is achieved by setting the updated electron distribution function to

$$f(r_2, v, \mu, t+\delta t) = \begin{bmatrix} f(r_2, v, \mu, t+\delta t) \; if \mu > 0 \\ c_2 f_h(v, \mu, t+\delta t) \; if \mu < 0 \end{bmatrix}$$

-eqn (5.2.1)

where C_2 is given by

$$C_2 = \frac{\int_0^1 \mu d\mu \int_0^{v_{max}} f(r_2, v, \mu, t+\delta t)\, v^3 dv}{\int_0^1 \mu d\mu \int_0^{v_{max}} f_h(v, \mu, t)\, v^3 dv}$$

-eqn (5.2.2)

and $f_h(v,\mu,t)$, the hot distribution, depends on the problem being considered. The exact form of the hot distribution is linked to the value of C_2. In theory, it is desirable to increase the temperature at the hot cathode as quickly as possible. However, there is a limit to how quickly the temperature of the hot cathode can be increased. Although the boundary condition at the hot cathode ensures that there is no net current added, it does not enforce conservation of the total number of particles. It is necessary to ensure that the value of C_2 does not vary by more than 10% from unity. If the value of C_2 does drop below 0.9, then the hot cathode temperature is not increased until C_2 becomes larger than 0.9. In practice this doesn't take longer than 2 time steps. A similar expression to equation (5.2.1) is used at r_1 where f_h is replaced by f_c which is generally a Maxwellian at the temperature of the cold cathode . The boundary conditions for f(v) are that f is an even function around v=0 and that f decreases to zero at v = vmax. For f(μ) it is assumed that f is linear in μ at μ = +1 and μ = -1.

Let us now consider a typical simulation for which the initial conditions are that the initial density is 10^{21} cm^{-3}, the ambient temperature is 1 kev and Z = 5. These conditions correspond to a mean free path of 29.4 μm where the mean free path is defined as (Book, 1987)

$$\lambda(T_e) = 1.987 \times 10^{13} \frac{T_e^{\,2}}{n \ln\Lambda}$$

- eqn (5.2.3)

The inner radius, r_1, was set to 120 μm and the shell thickness was 12 μm. The form of the distribution injected at r_2 is a half-Maxwellian and the temperature of the hot cathode was increased from 1 kev to 2 kev over 0.5 t_o, where t_o is the electron self collision time, which is defined as (Book, 1987)

$$t_0 = 3.44 \times 10^{5} \frac{T_e^{\,3/2}}{n \ln\Lambda}$$

-eqn (5.2.4)

We used the isotropic Fokker-Planck equation with the velocity equation solved using the Chang-Cooper method. We used 30 radial and angular mesh points, 60 velocity mesh points and a time step of $t_o/200$.

Figures 5.1 and 5.2 show the heat flow and temperature profiles at a number of different time steps. It is seen in figure 5.1 that the heat flow is much less than the free-streaming limit. In fact, the inferred value of the flux limiter is about 0.3 for this simulation which is still an order of magnitude greater than most experiments predict. The small ripples in the temperature profiles are due to the dispersion in the advection equation. If we increase the number of radial mesh points, these ripples disappear but the form of the temperature profiles does not change. In addition, the form of the profiles does not change when we consider more collisional systems. When the density is increased to $5.0 * 10^{21}$ cm^{-3}, there is little change in the profiles.

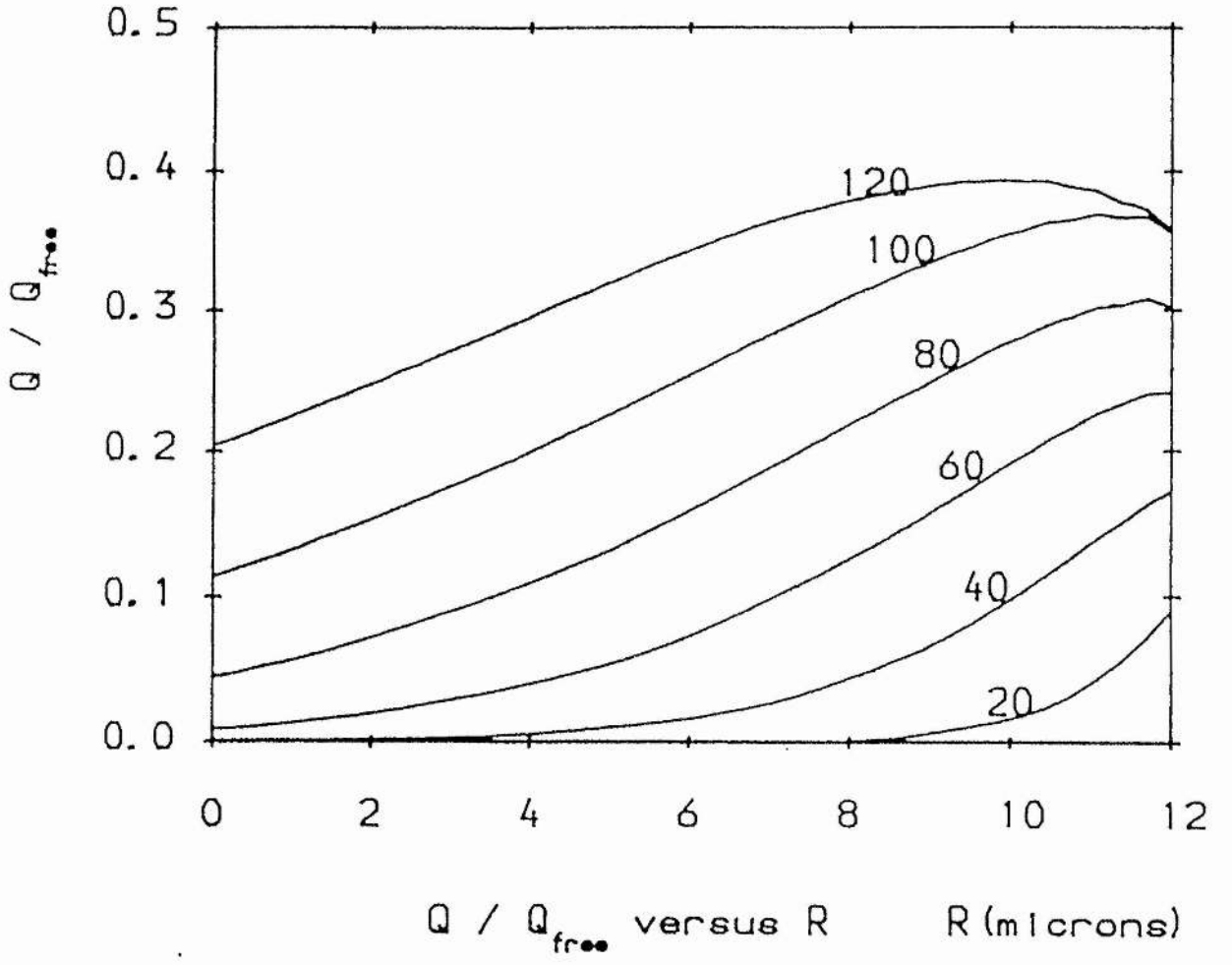

Figure 5.1: **HEAT FLOW PROFILES FOR UNIFORM PLASMA WITH Th/Tc=2, ne=10^{21}cm^3, Te=1keV**

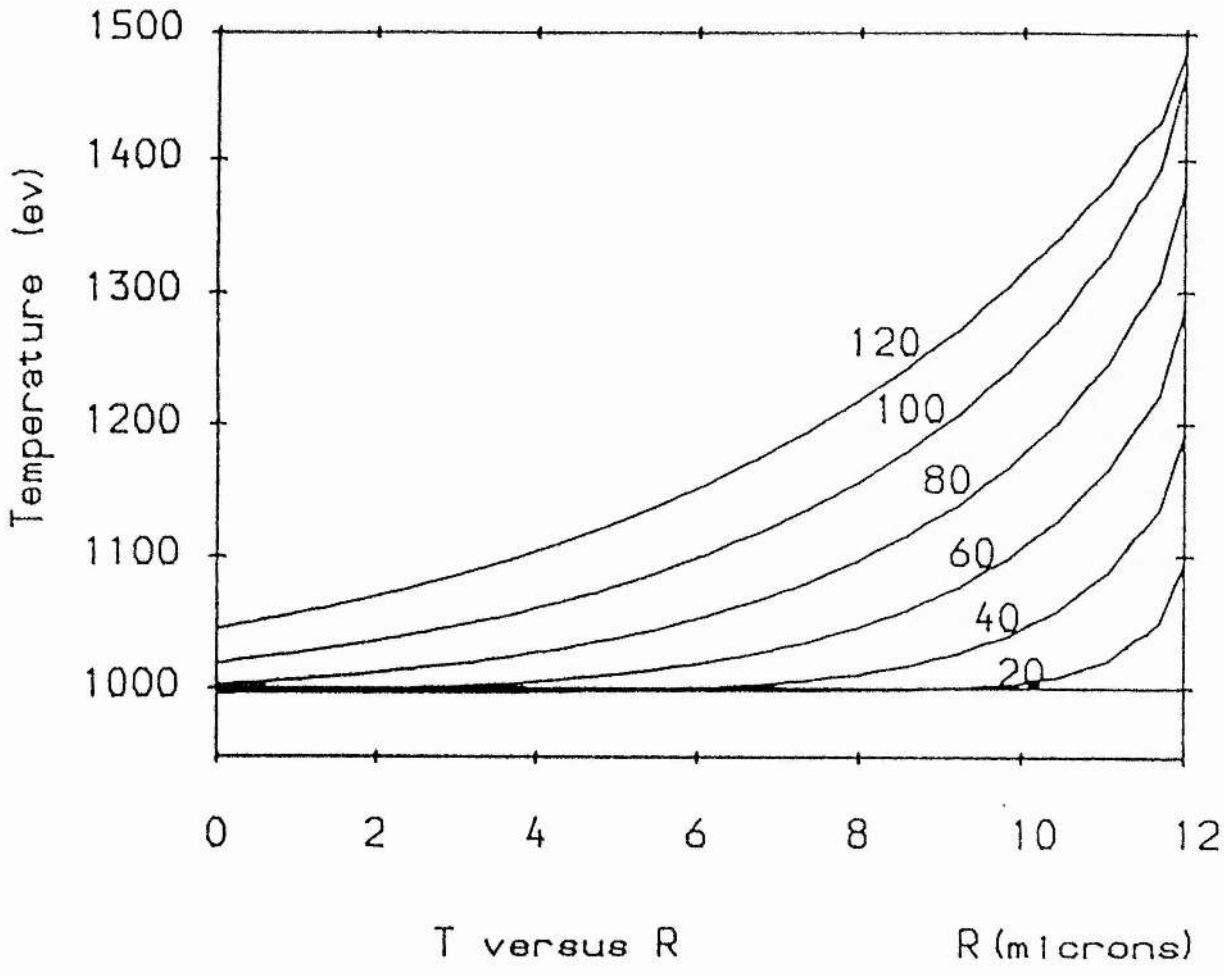

Figure 5.2: **TEMPERATURE PROFILES FOR UNIFORM PLASMA WITH Th/Tc=2, ne=10^{21}cm^3, Te=1keV**

5.3 Effects of Curvature on Heat Flow

The importance of curvature on the heat flow was examined by varying the radius of the inner shell, r_1, while keeping the shell separation constant at 12 μm. The initial state of the plasma was the same as that described in Section 5.2. The heat flux was measured near the inner boundary once steady state had been reached. The heat flux for each value of r_1 was compared to the heat flux at steady state for an r_1 of 300 μm. A plot of the heat flux versus aspect ratio is shown in figure 5.3 where the aspect ratio is defined as:

$$a=\frac{r_2}{(r_2-r_1)}$$

-eqn (5.3.1)

As the aspect ratio approaches infinity, we return to planar geometry. It can be seen from figure 5.3 that the effect of curvature is to reduce the heat flow at r_1 compared to the planar case. Most experiments that use spherical targets have an aspect ratio of about 10 and at this value the heat flux is reduced by approximately 10%. Very similar results were obtained when the density was increased to $5*10^{21}$ cm^{-3} and 10^{22} cm^{-3}.

It is possible to estimate the effect of curvature on the heat flow from purely geometric arguments. From figure 5.4, it can be seen that when electrons are ejected from point A, only a fraction of those electrons will enter the sphere defined by r_1.

The solid angle is given by

$$\Omega = 2\pi(1-\cos\theta) = 2\pi(1-\Delta r/r_2)$$

-eqn (5.3.2)

and so the fraction to enter the surface at r_1 is

$$F = \Omega_0/2\pi = 1-\Delta r/r_2 = 1-1/a$$

-eqn (5.3.4)

The dashed line in figure 5.3 is the predicted reduction, by the factor (1 - 1/a), in the heat flow at r_1 from geometrical arguments. The agreement between the geometric result and the Fokker-Planck code is very good. The reason for the good agreement is that the heat carrying electrons are effectively collisionless for the three systems considered here. Therefore, in the absence of magnetic fields, the electrons will move in straight lines as assumed in the geometric calculation.

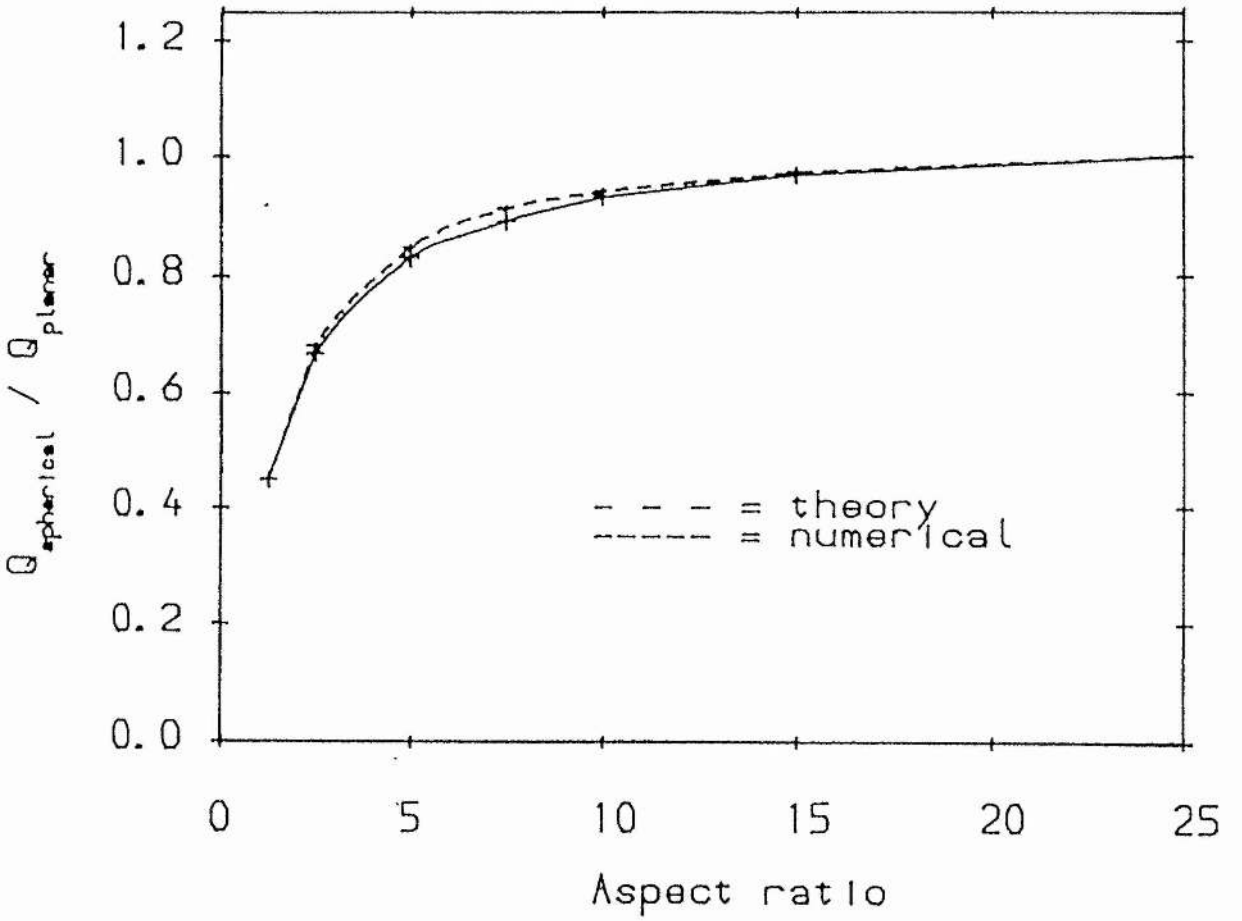

Figure 5.3: REDUCTION IN HEAT FLOW AT INNER BOUNDARY AS A FUNCTION OF ASPECT RATIO.

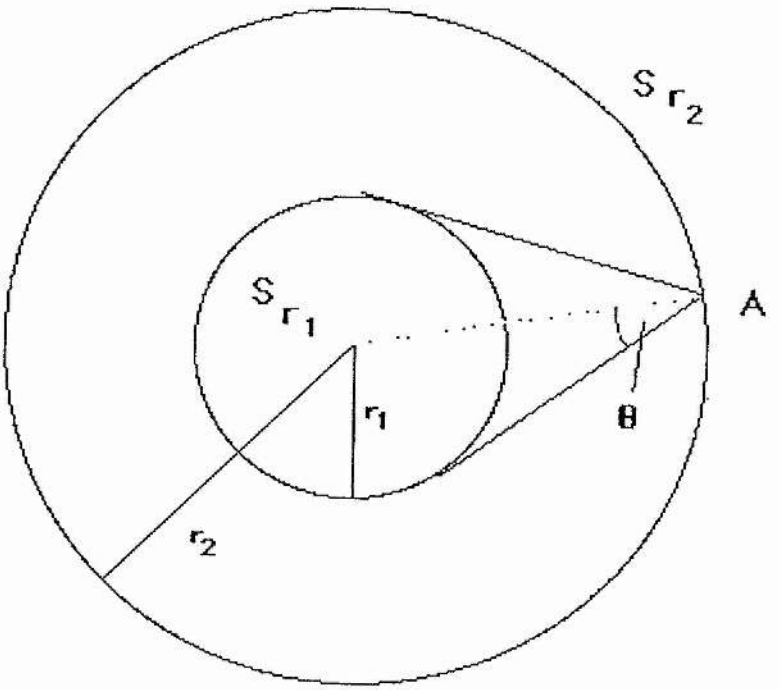

Figure 5.4:

5.4 Differences between the discrete ordinate method and the Legendre polynomial method

In this section, we examine the differences between representing the angular component of the electron distribution discretely and representing the angular component of the electron distribution function by a Legendre decomposition of f in μ, ie:

$$f(v,\mu) = \sum_{l=0}^{l_{max}} P_l(\mu)\, f_l(v)$$

-eqn (5.4.1)

The only previous comparison was made by Kho (1983) at the 1983 CECAM workshop. Kho solved the Fokker-Planck equation in a time-independent form without including electron-electron collisions and with an approximate electron-ion collision term. Kho showed that the heat flow calculated using the Legendre decomposition method may deviate by approximately 30% when compared with the heat flow calculated using discrete coordinates.

We can examine the importance of the higher order terms in equation (5.4.1) by including a routine between the velocity and angular equations, equations (4.2.13) and (4.2.14) respectively, that acts as a filter to the higher order terms in (5.4.1). The filtering routine calculates $f_l(v)$ using equation (4.4.12) for the first l_{max} terms. The distribution is then reassembled using equation (5.4.1). In this way we can examine how important the higher order terms are in thermal electron transport. Figure 5.5 compares the heat flow profile for the case of $l_{max} = 4$ to the case where the μ-filter

was not used. We see that the agreement between the two is reasonably good. Figure 5.6 is the same as figure 5.5 except that only the first two terms in equation (5.4.1) are included. In this case, the agreement appears to be poor. However, this figure is misleading. Although the Legendre polynomial method underestimates the heat flow near the cold boundary, it can be seen from figure 5.1 that the absolute value of the heat flow is small in this region. As the bulk of the heat flow reaches the cold boundary, the Legendre polynomial method becomes more accurate.

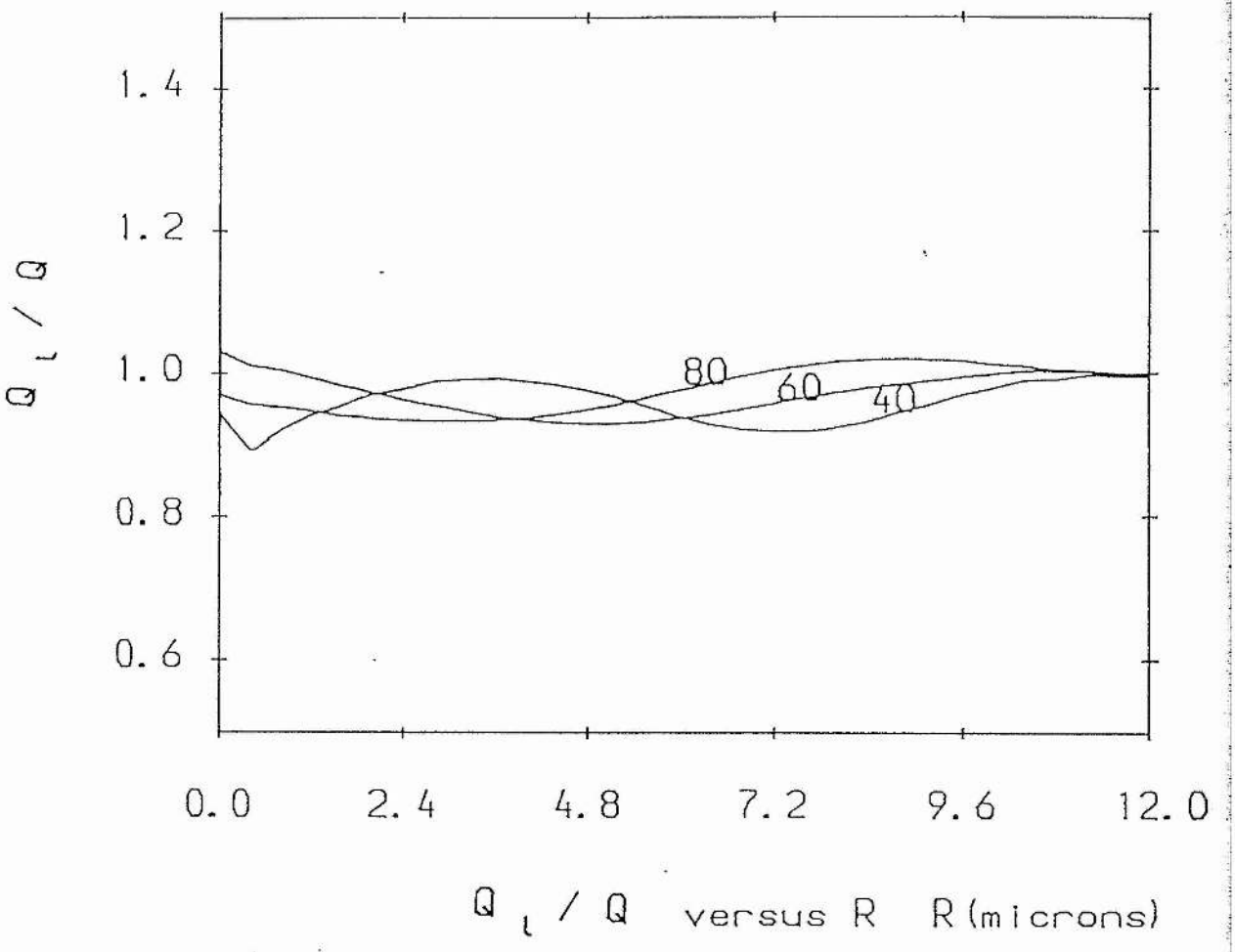

Figure 5.5: **RATIO OF HEAT FLOWS CALCULATED FROM DISCRETE METHOD AND LEGENDRE POLYNOMIAL METHOD WITH $L_{MAX}=4$**

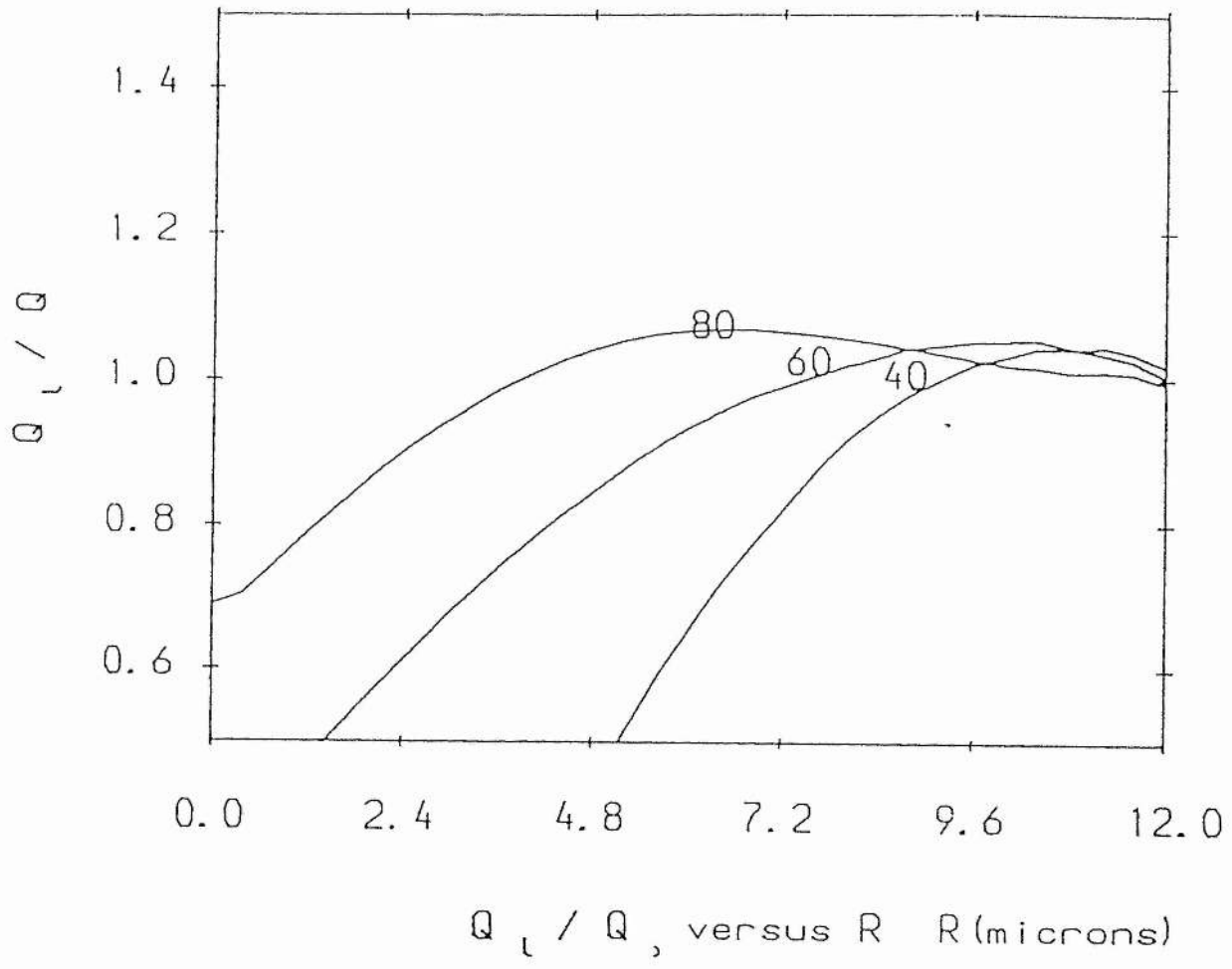

Figure 5.6: RATIO OF HEAT FLOWS CALCULATED FROM DISCRETE METHOD AND LEGENDRE POLYNOMIAL METHOD WITH $L_{MAX}=2$

5.5 Effect of Anisotropic Rosenbluth Potentials on Heat Flow

As has been stated previously, most treatments of thermal electron transport in direct-drive laser fusion have neglected the anisotropic portion of the Rosenbluth potentials. Jorna and Wood included the anisotropic portion of the Rosenbluth potentials by calculating h and g exactly and then numerically differentiating appropriately. However, as described in Chapter 4, we have represented the anisotropic portion of the Rosenbluth potentials by a Legendre decomposition of h and g in μ ie:

$$h(v,\mu) = \sum_{l=0}^{l_{max}} P_l(\mu)\, h_l(v)$$

and

$$g(v,\mu) = \sum_{l=0}^{l_{max}} P_l(\mu)\, g_l(v)$$

-eqn (5.5.1)

It is possible to obtain an order of magnitude estimate of the first angular moment of the Rosenbluth potentials, h_1 and g_1, from a local extension to the Spitzer-Harm theory.

Let us assume that the angular dependence of f can be described by

$$f(x, v, \mu, t) = f_0(x, v, t) + \mu f_1(x, v, t)$$

-eqn (5.5.2)

Then in a time-independent Lorentzian plasma, that is one with no electron-electron collisions, the Fokker-Planck equation becomes (Schvartz, 1981)

$$f_1(x, v) = -\lambda(v) \left(\frac{\delta}{\delta x} - \frac{eE}{m_e v} \frac{\delta}{\delta v} \right) f_0(x, v)$$

-eqn (5.5.3)

where $\lambda(v)$ is a velocity dependent mean free path defined by

$$\lambda(v) = \lambda_0(T_e) \frac{v^4}{v_{th}^4}$$

-eqn (5.5.4)

where λ_0 (T_e) is the normal mean free path defined in equation (5.2.3). If f_o is assumed to be a Maxwellian and the current is zero then it follows that

$$\frac{f_1}{f_0} = \frac{\lambda_0}{L} \left(\frac{v}{v_{th}}\right)^4 \left(\left(\frac{v}{v_{th}}\right)^2 - 4.0\right)$$

-eqn (5.5.5)

For large values of λ_0 / L, f_1 becomes larger than f_o which is physically unreasonable if equation (5.5.2) is to be valid since then when $\mu < 0$ the distribution will become negative. Therefore, Shvartz et al put an upper limit on f_1 and assumed that f_1 / f_o must be less than unity. If f_1 does become larger than unity then f_1 is set equal to f_o. From f_1 it is possible to numerically calculate h_1 and g_1. Figures 5.7, 5.8 and 5.9 show f_1, h_1 and g_1 versus v respectively for $\lambda/L = 0.1$. It is seen from these figures that the anisotropic portion of h and g can be as large as 10% of the isotropic part. The anisotropic portion of h and g is due to the current that flows from the cold boundary to the hot boundary that is necessary to counter the flow of hot electrons.

However, these results only tell us how large the anisotropic portion of h and g may be. It does not tell us how the heat flow is affected by the inclusion of the anisotropic portion of h and g. To discover this and to include the important non-local effects, we must solve the Fokker-Planck equation.

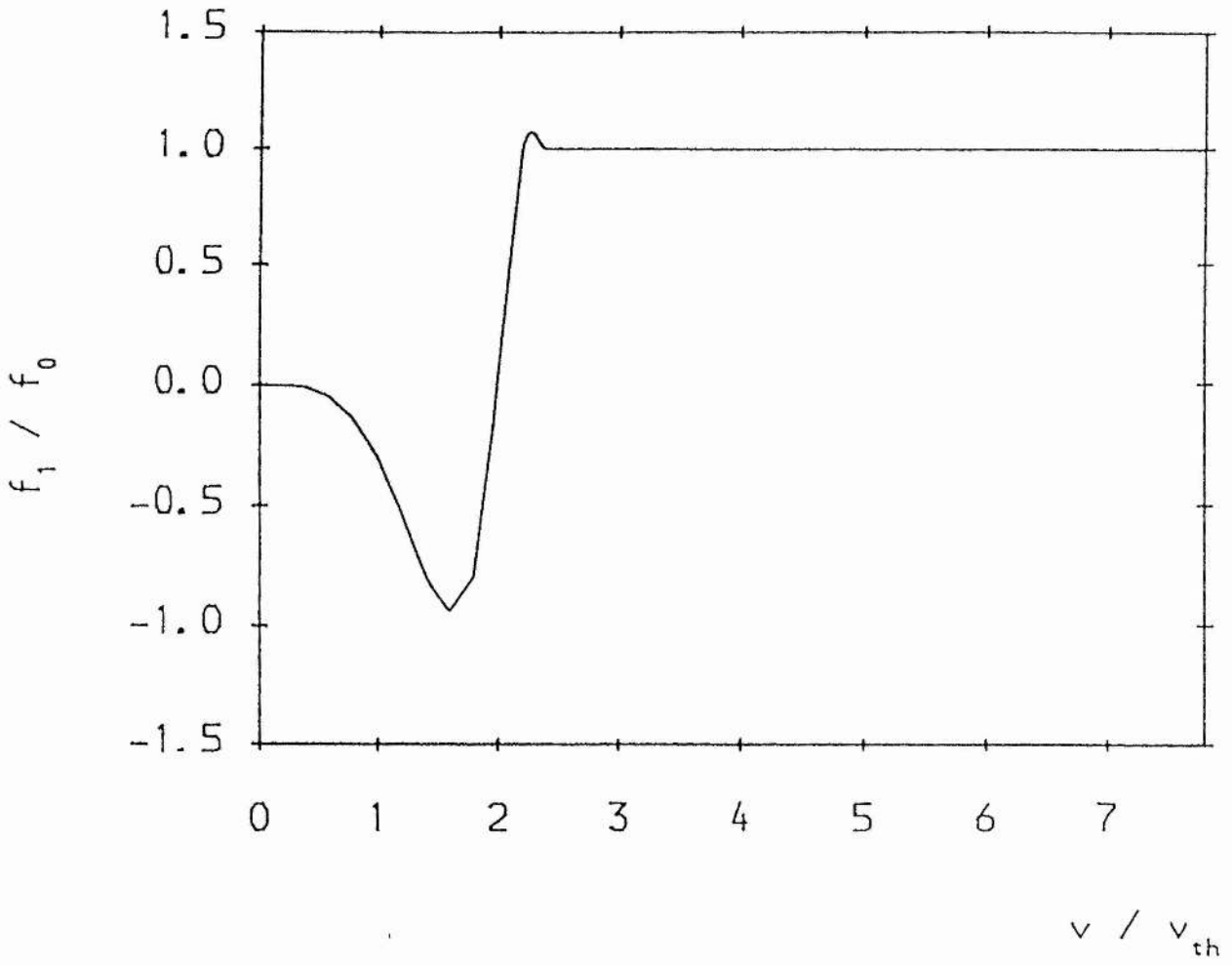

Figure 5.7: PLOT OF f_1/f_0 VERSUS v/v_{th} FROM USING SCHVARTZ'S MODEL WITH $\lambda/L = 0.1$

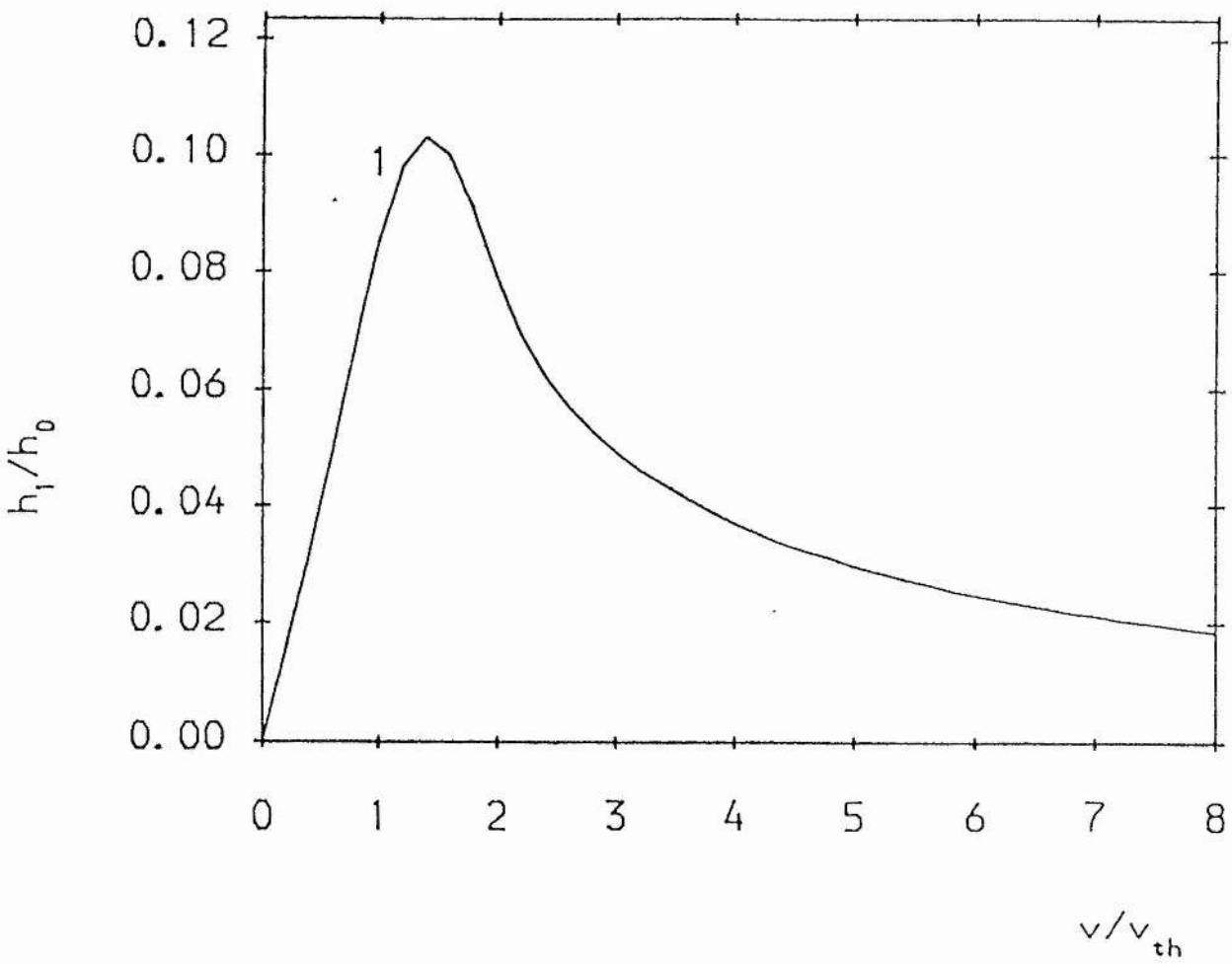

Figure 5.8: PLOT OF h_1/h_0 VERSUS v/v_{th} FROM USING SCHVARTZ'S MODEL WITH $\lambda/L = 0.1$

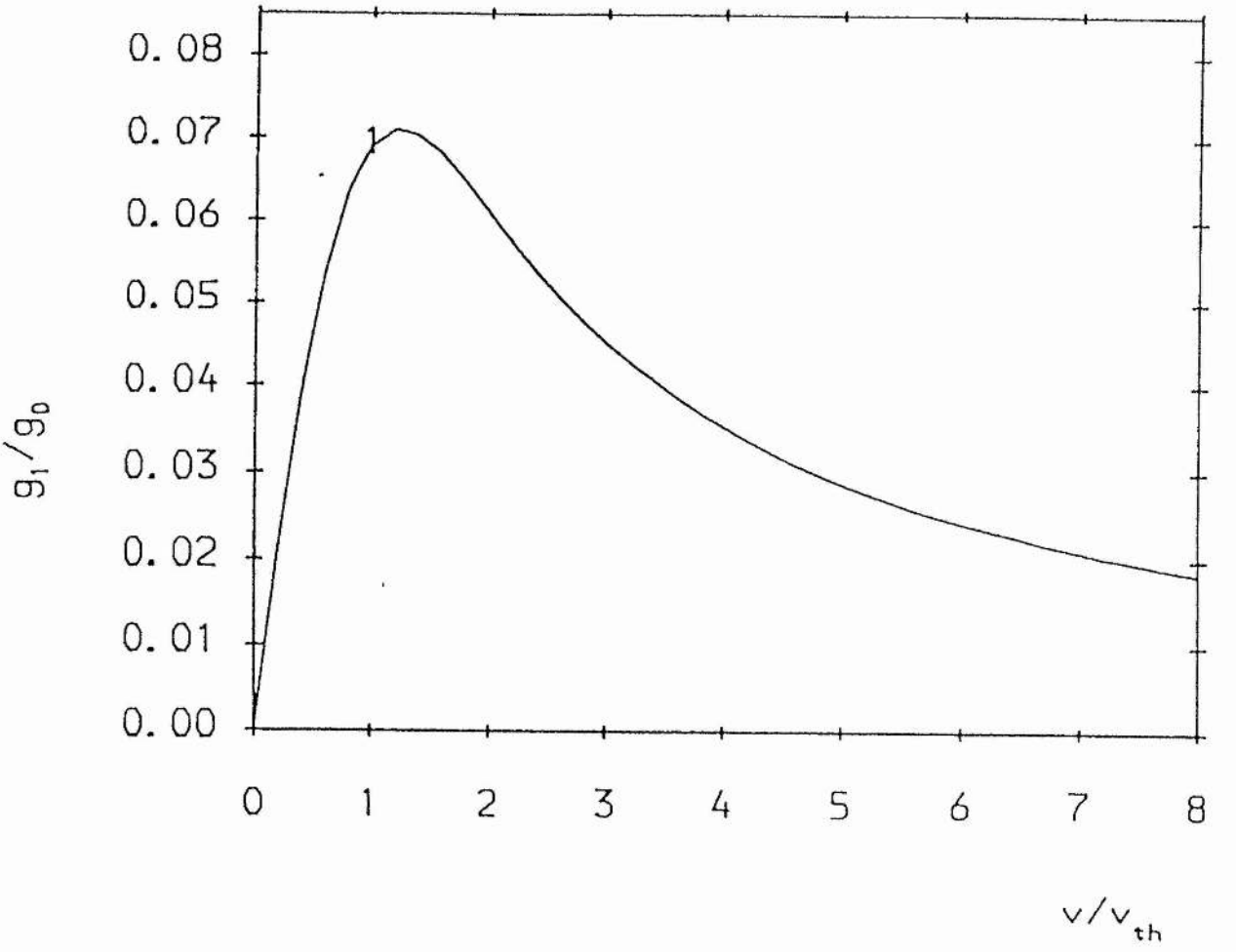

Figure 5.9: PLOT OF g_1/g_0 VERSUS v/v_{th} FROM USING SCHVARTZ'S MODEL WITH $\lambda/L = 0.1$

We used the anisotropic code with the anisotropic portion of the Rosenbluth potentials represented by the first three terms in the Legendre polynomial expansion. The initial state of the plasma was the same as that described in Section 5.2 except that the density was increased to $5 * 10^{21}$ cm $^{-3}$ and we have doubled the number of velocity mesh points.

One run was done with the anisotropic portion of h and g included and one without. Figure 5.10 shows the ratio of the two heat flow profiles after 48 and 60 time steps. We see that if the anisotropic portion of the Rosenbluth potentials is included, the heat flow can be up to 10% greater.

Figures 5.11 and 5.12 show g_1/g_0 and h_1/h_0 versus v near the hot boundary where the temperature gradient is steepest. Both g_1/g_0 and h_1/h_0 reach a maximum at around v_{th}. Again, we see that the anisotropic portion of h and g is due to the thermoelectric current. The value of g_1/g_0 and h_1/h_0 is much reduced at high velocities compared to figures 5.8 and 5.9 . This is because f_0 is far from being a Maxwellian. It can be seen from figure 5.13 that the isotropic part of the electron distribution function evolves to a two-temperature Maxwellian. Therefore g_1/g_0 and h_1/h_0 are reduced at high velocities because the plasma is hotter and therefore more collisionless.

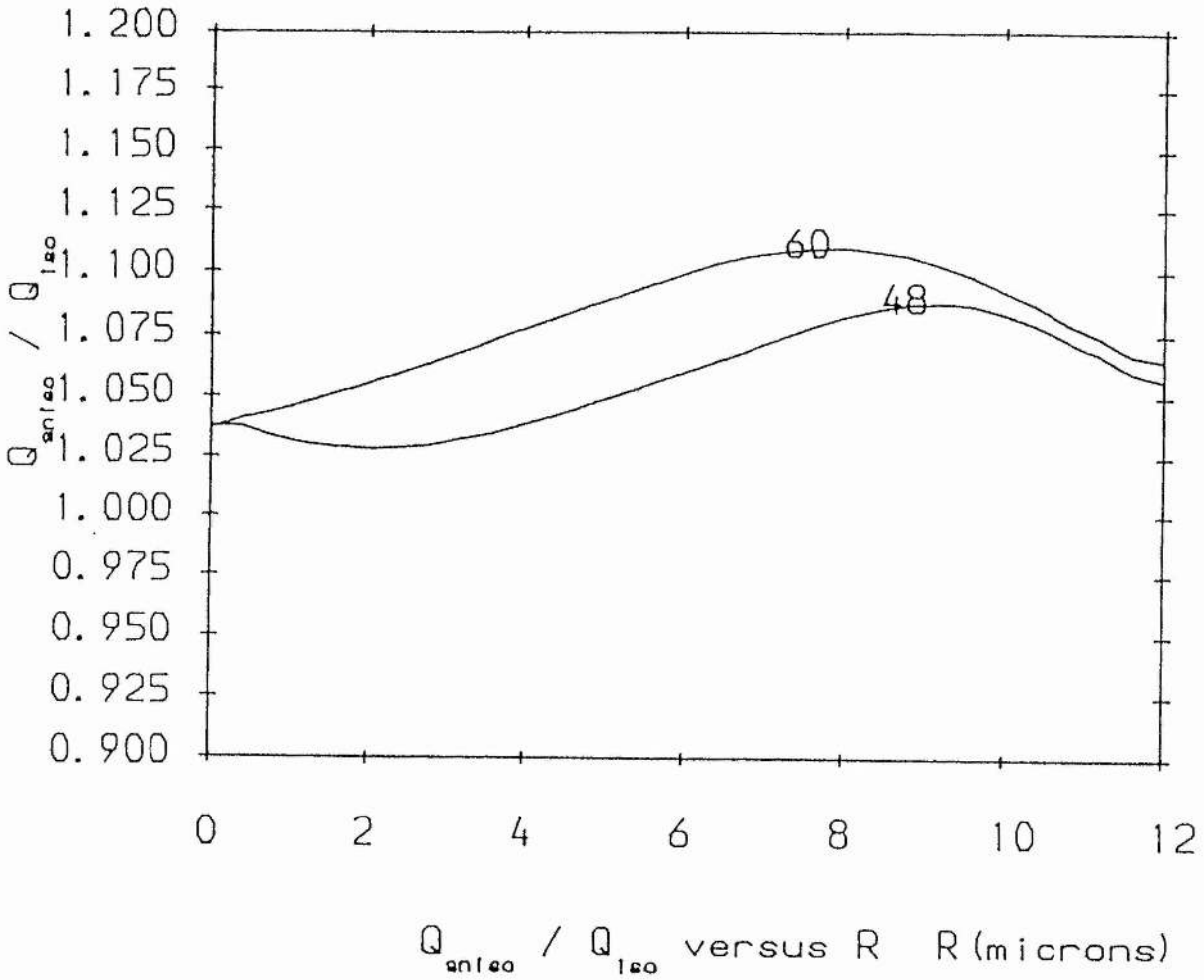

Figure 5.10: RATIO OF HEAT FLUXES CALCULATED FROM THE ANISOTROPIC AND ISOTROPIC CODES

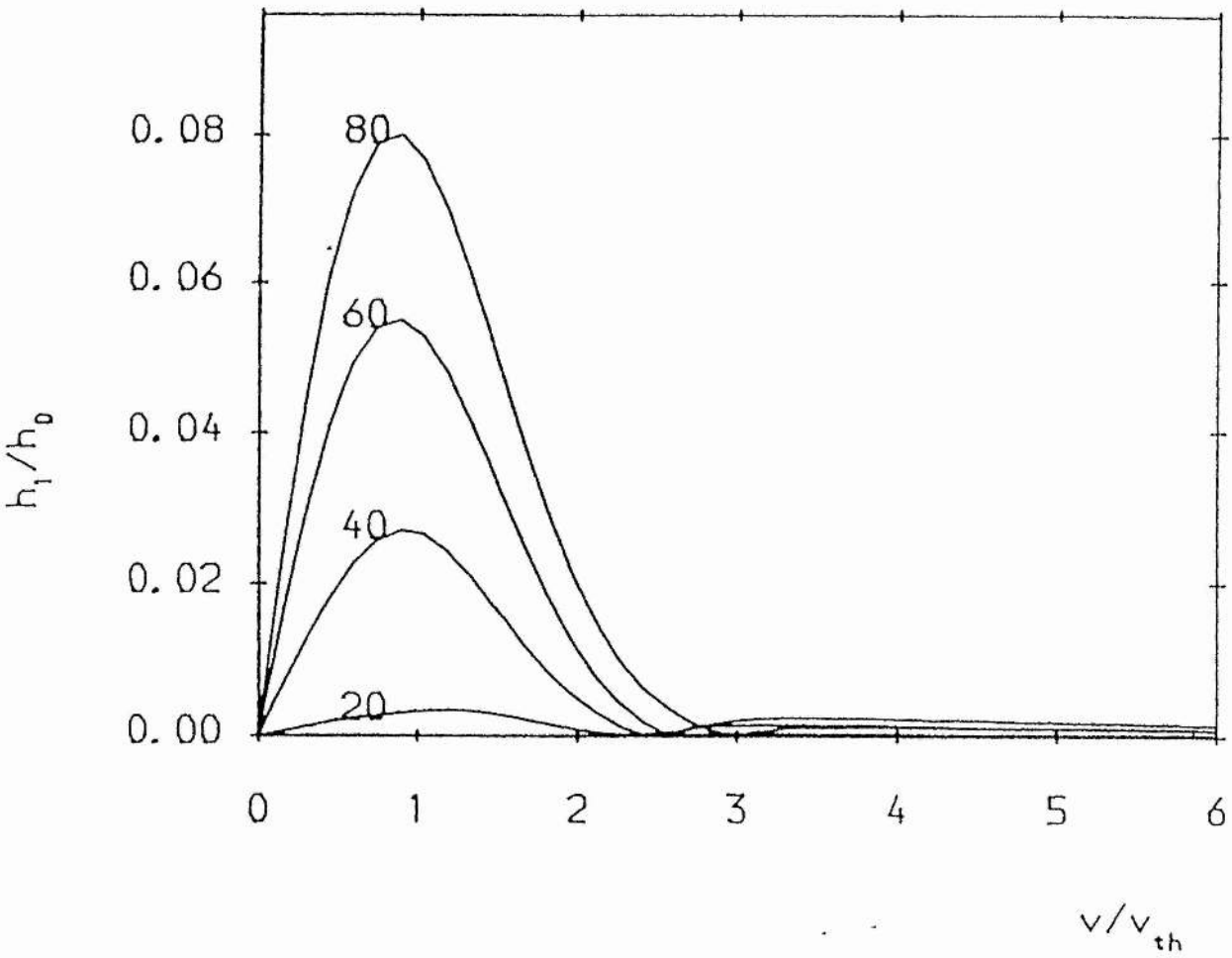

Figure 5.11: RATIO OF h_1/h_0 CALCULATED FROM THE ANISTROPIC CODE NEAR HOT BOUNDARY

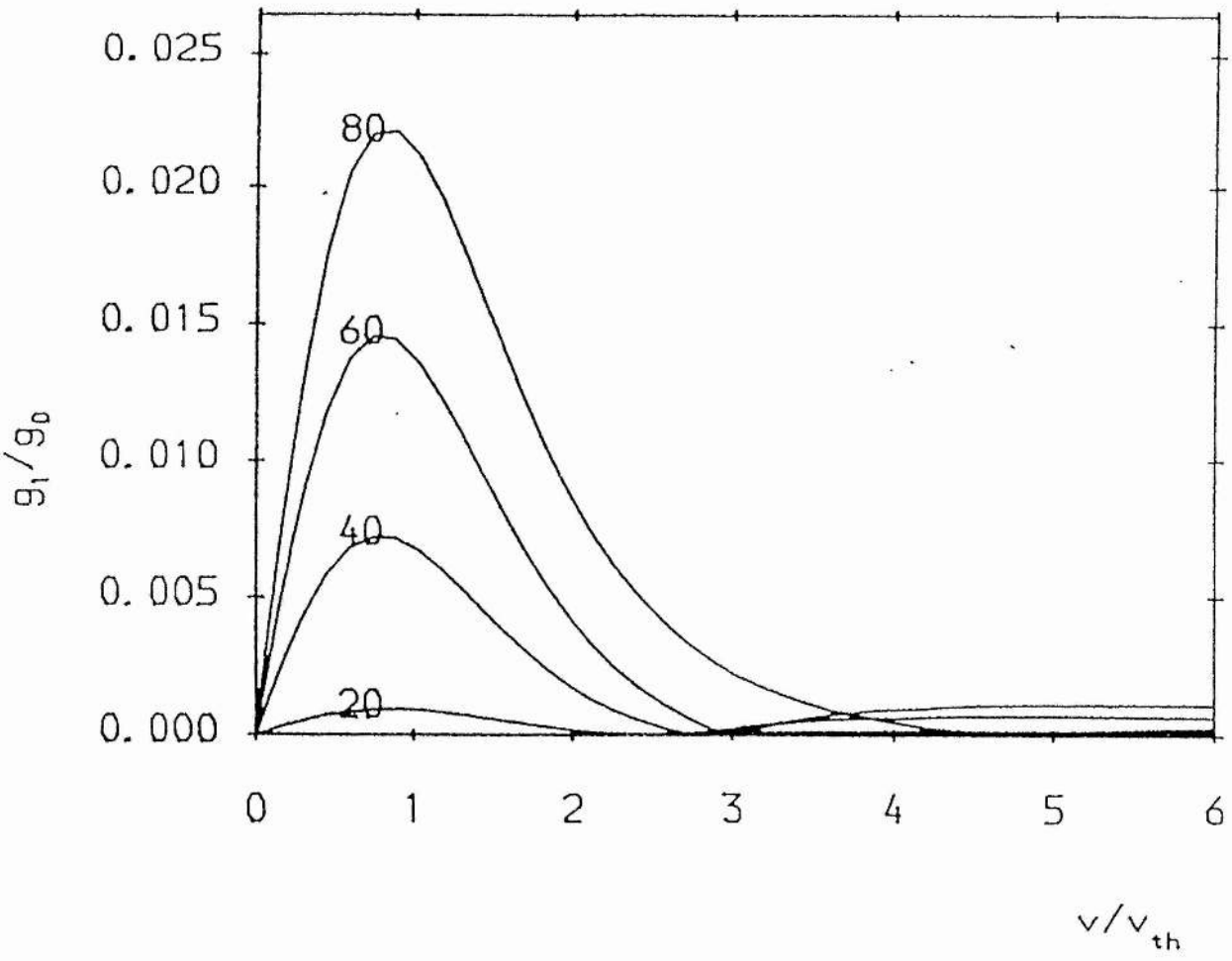

Figure 5.12: RATIO OF g_1/g_0 CALCULATED FROM THE ANISOTROPIC CODE NEAR HOT BOUNDARY

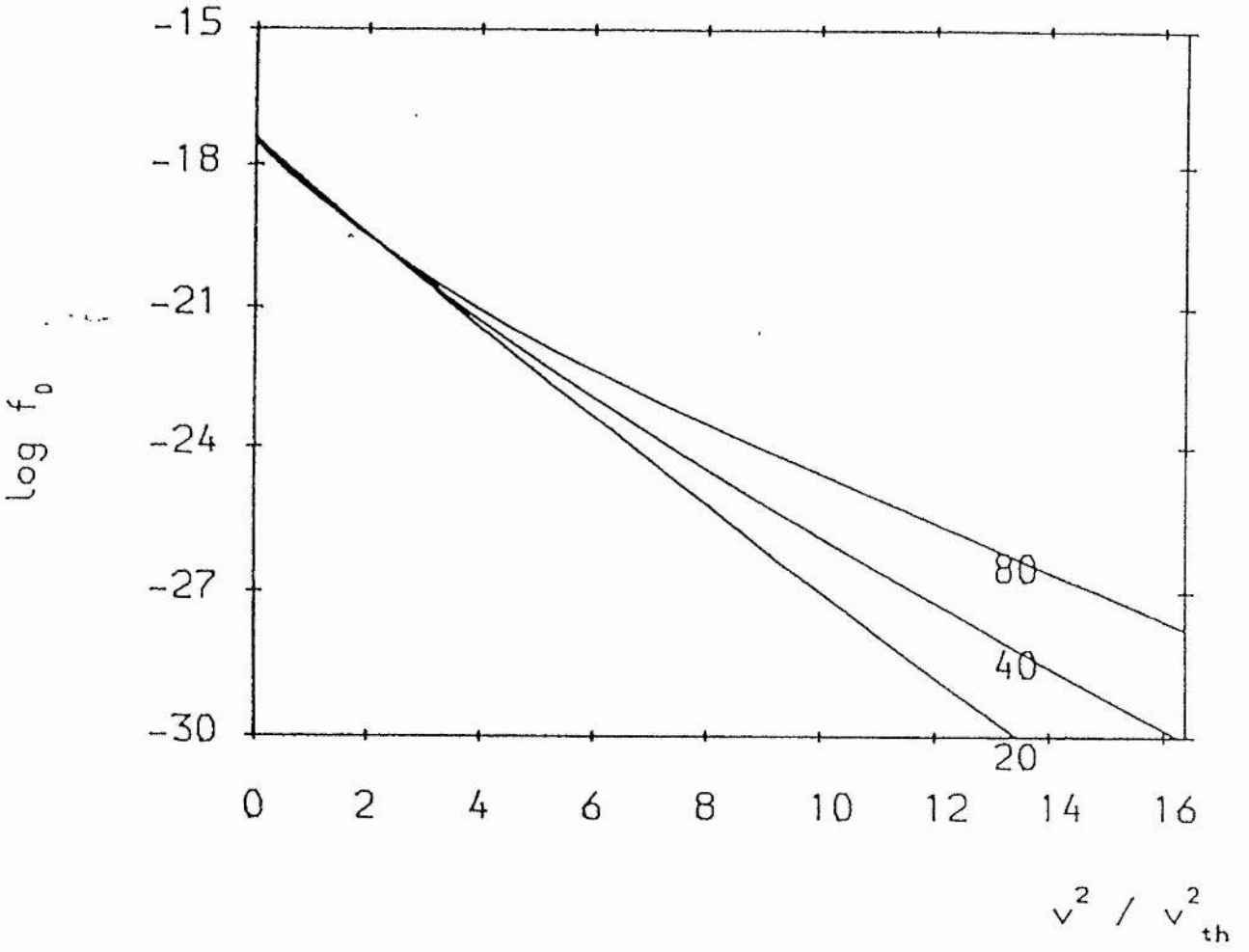

Figure 5.13: LOGARITHM OF f_0 VERSUS v^2/v_{th}^2

Chapter 5

So far we have only injected an isotropic hot distribution at the hot cathode. However, in experiments the form of the distribution function created in the corona will be far from being isotropic. The exact form of the distribution function will depend on a variety of related processes.

However, it seems likely that the distribution function will probably be hotter in the direction parallel to the radial vector rather perpendicular to it ie there will be more hot particles travelling along $\mu = -1$ than $\mu = 0$.

We can model this by injecting a bi-Maxwellian distribution at the hot cathode where the bi-Maxwellian distribution is given by

$$f(v,\mu,t) = \frac{n_e}{\pi^{3/2} v_{th}^{3/2}} \exp\left(-\mu^2 v^2 / T_{perp} - (1-\mu^2)\, v^2 / T_{par}\right)$$

-eqn (5.5.7)

In these simulations, ϵ is increased from 1 to 4.0 where $\epsilon = T_{par} / T_{perp}$ while increasing the temperature of the hot distribution from 1 keV to 2keV. The resulting heat flow and temperature profiles are show in figures (5.14) and (5.15). When these profiles are compared to the profiles for the isotropic hot distribution, figures (5.1) and (5.2), we see that the temperature profile is little changed but that the heat flow is significantly larger. When we include the anisotropic portion of the Rosenbluth potentials, we see from figure (5.16) that the heat flow is increased by about 12 %. This value is larger than the value for the isotropic heating

distribution. This is because the bi-Maxwellian distribution produces a larger flux which in turn requires a larger thermoelectric current. This larger current distorts h and g more and causes the slightly larger heat flow.

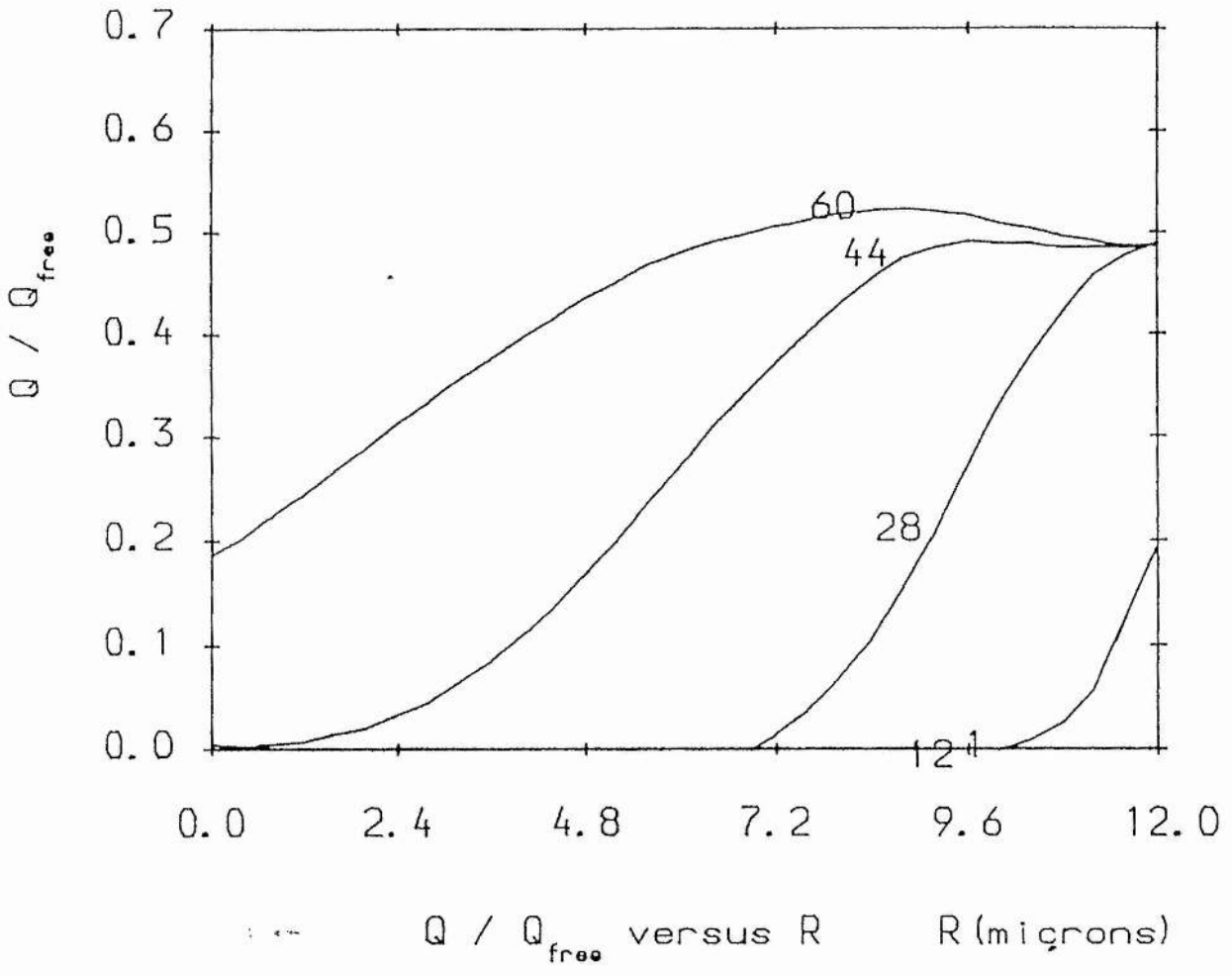

Figure 5.14: HEAT FLOW VERSUS DISTANCE FOR A HEATED BI-MAXWELLIAN DISTRIBUTION OF INITIAL TEMPERATURE RATIO $T_{para}/T_{perp} = 2$

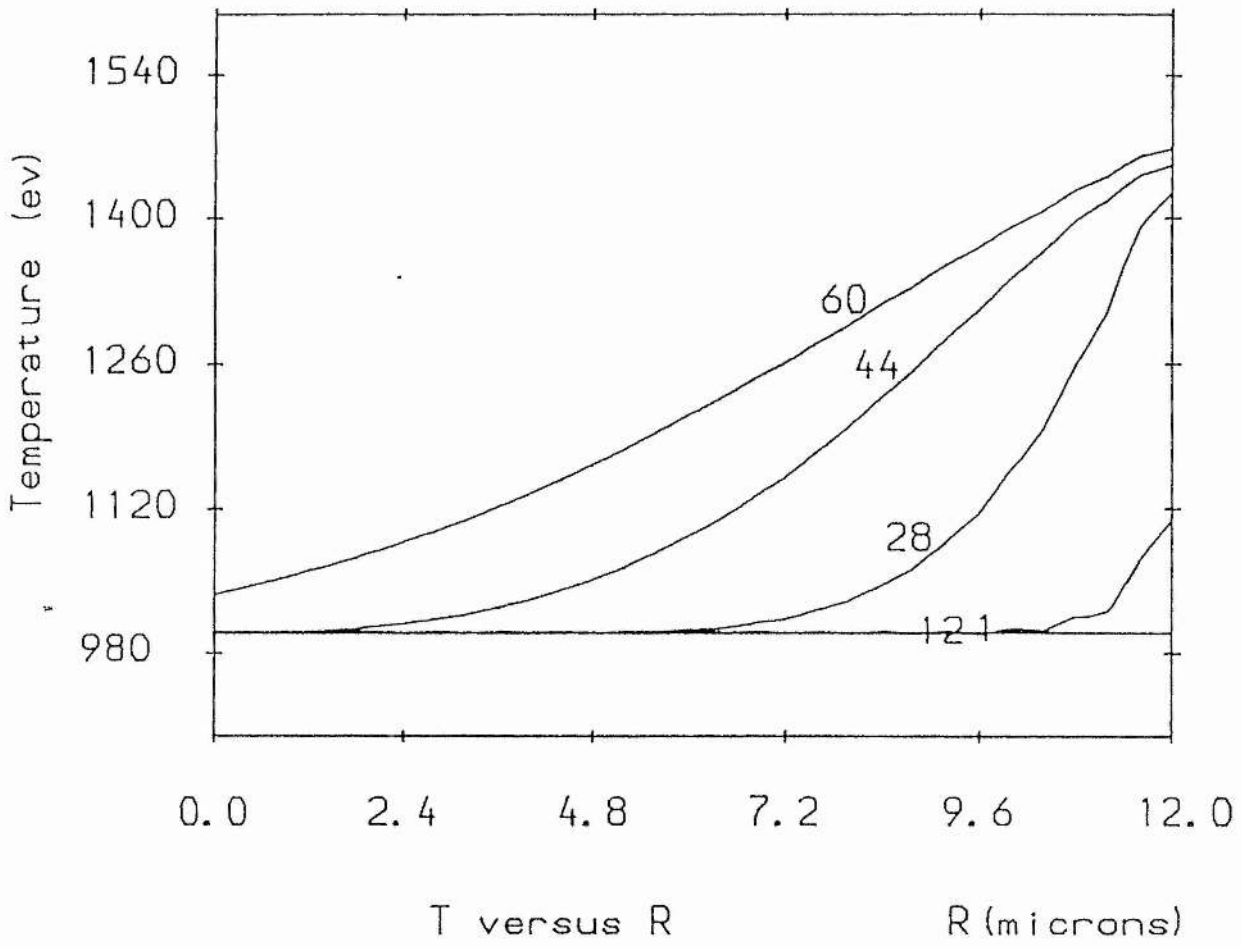

Figure 5.15: **TEMPERATURE PROFILES VERSUS DISTANCE FOR A HEATED BI-MAXWELLIAN DISTRIBUTION OF INITIAL TEMPERATURE RATIO $T_{para}/T_{perp} = 2$**

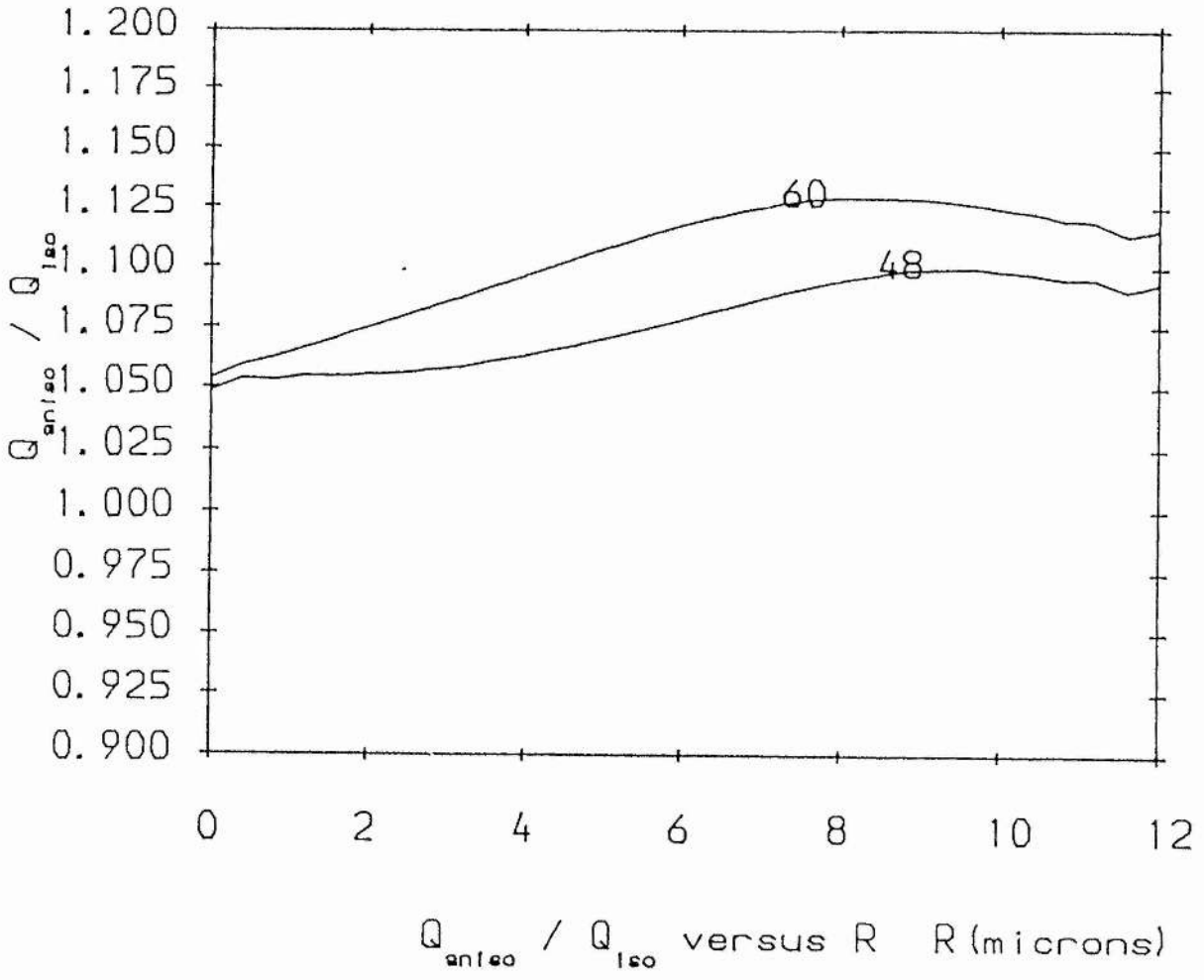

Figure 5.16: **RATIO OF HEAT FLUXES CALCULATED FROM THE ANISOTROPIC AND ISOTROPIC CODES**

5.5 Differences between original code and new code

The simulations presented in the previous sections were similar to those performed by Jorna and Wood with the original Fokker-Planck code. The new code gave similar results to Jorna and Wood when the isotropic code was used. However, with the isotropic code it was shown that the effect of sphericity on heat flow was a purely geometric effect. The heat flow at the inner boundary decreased as the curvature increased not because of the stronger electric field, as suggested by Jorna and Wood, but because more particles missed the inner sphere.

The most significant differences between the old and the new Fokker-Planck codes were when measuring the importance of the anisotropic Rosenbluth potentials on the heat flow. The new code predicted that the heat flow could be affected by between 10 and 15% if the anisotropic potentials are included. However, this was far less than the 20% to 180% predicted by the old code. Jorna and Wood argued that the anisotropic code produced a larger value for the heat flow because the anisotropic, less collisional electrons are not averaged over angles and therefore more reach the inner boundary. This arguement seems unlikely as the heat carrying electrons have an average velocity of about 3 v_{th} and are therefore almost entirely collisionless.

It seems more likely that the increase in the heat flow is due to the thermoelectric current. Those electrons in the thermoelectric current, which have an average velocity of less than v_{th} , will not be averaged and they will produce a larger heat flux at the outer boundary. This will increase the value of c_2 in equation (5.2.2) and therefore more hot particles will be added to the plasma.

What caused the large ratios discovered by Jorna and Wood ? It is believed that these results were due to the method used to calculate the collision coefficients in the original isotropic and anisotropic codes. As described in section 2.3, the original code was differenced in such a way that the distribution was artificially distorted with the result of lost particles. How the distribution is distorted is a function of the collision coefficients. As the collision coefficients were different in the two codes, then the distortion would be different. Therefore, a different number of particles was added to the plasma at each timestep. It is likely that it was this numerical effect that caused the large ratios found with the original code.

5.6 Conclusion

In this chapter, we have considered several aspects of thermal conduction in laser - produced plasmas. The effect of curvature on heat flow has been studied and it has been shown that it is possible to explain the effect of curvature on heat flow from purely geometrical arguments. We have compared the discrete ordinate method of solving the angular equation with the Legendre polynomial method and shown that the Legendre polynomial method is a satisfactory method provided that enough terms in the expansion are retained. In the weakly collisional example that we considered here, it was found that 4 terms in the expansion were adequate to describe the heat flow. Finally, we examined how the anisotropic components of the Rosenbluth potentials affected thermal conduction. Our analysis showed, in contradiction with the earlier version of the code, that including the anisotropic components of the Rosenbluth potentials had a minimal effect on the heat flow.

Jorna and Wood had also applied the original code to the relaxation of a bi-Maxwellian distribution. As the new code has contradicted Jorna and Wood's results for thermal conduction, it was decided to re-investigate the relaxation problem. This is presented in the following chapter.

CHAPTER 6: ENERGY RELAXATION OF MODEL DISTRIBUTION FUNCTIONS

6.1 Introduction

In Chapter 5, it was shown that in the presence of steep temperature gradients, the electron distribution function deviates significantly from thermal equilibrium. The production of non-thermal distributions is a common occurrence in plasma physics. In tokamak research, for example, highly distorted distribution functions are generated by heating processes such as neutral beam injection and r.f heating and significantly non-Maxwellian behaviour appears in slideaway and runaway discharges where the distortions are driven by the longitudinal electric field.

Laser produced plasmas produce highly distorted distribution functions in the coronal region where the plasma is distorted by the production of parametric instabilities. The primary absorption mechanism in laser produced plasmas, inverse bremmstrahlung, drives the distribution function away from thermal equilibrium. If space plasmas are considered, then it becomes apparent that very few space plasmas are in thermodynamic equilibrium. For example, the plasma in the solar wind is far from equilibrium because of the interplanetary magnetic field.

It is important to understand how non-thermal distribution functions relax to thermal equilibrium because the transport processes are directly related to the rate of relaxation. The Fokker-Planck equation can be used to determine how a non-Maxwellian distribution relaxes back to thermal equilibrium. Most of the

analysis on the energy relaxation of non-Maxwellian distributions has been restricted to either a test particle treatment or a linearised perturbative treatment of the Fokker-Planck equation. These treatments have given relaxation times that are normally dependent on the thermodynamic properties of the plasma and not on the detailed structure of the distribution function. However, to follow the temporal evolution of non-Maxwellian distributions that deviate significantly from Maxwellian, it is normally necessary to solve the Fokker-Planck equation numerically.

In this chapter, the temporal evolution of several model distribution functions is analysed. Each of the model distributions has the Maxwellian distribution as a special case. We sought to determine whether or not the model distribution function relaxed within its own class since some of these model distributions have been investigated analytically under this assumption. In addition, if the model distribution was anisotropic, we sought to determine how sensitive the relaxation was to truncations of the collision operator.

6.2 The Bi-Maxwellian Distribution Function

As has been stated in the introduction, the analysis of the energy relaxation of anisotropic distributions is normally restricted to small deviations from thermal equilibrium. However, Kogan (1961), and then Schamel et al (1989), have investigated analytically the relaxation of a bi-Maxwellian distribution without linearising the Fokker-Planck collision operator. The only restriction that is placed on the Fokker-Planck equation is that the relaxation process takes place within the class of bi-Maxwellian distributions. With this restriction, they found that the equation describing the relaxation process reduces to a single ordinary differential equation given by

$$\frac{d\epsilon}{d\tau} = \frac{(1+2\epsilon)^{5/2}}{4(1-\epsilon)} \left[(2+\epsilon)\, g(\epsilon) - 3 \right]$$

- eqn(6.2.1)

where

$$g(\epsilon) = \begin{pmatrix} \tanh^{-1}\sqrt{1-\epsilon}/\sqrt{1-\epsilon}, & \epsilon \le 1 \\ \tan^{-1}\sqrt{\epsilon-1}/\sqrt{\epsilon-1}, & \epsilon \ge 1 \end{pmatrix}$$

- eqn(6.2.2)

$$\tau = \nu_E t$$

- eqn(6.2.3)

$$\nu_E^{-1} = \sqrt{m_e (3T_e)^3/\pi}[1/8\,(Ze)^4 n \ln\Lambda]$$

- eqn(6.2.4)

$$\epsilon = T_{perp}/T_{par}$$

- eqn(6.2.5)

Schamel's definition of the slowing down time ν_E^{-1} differs from Spitzer's by $2/\sqrt{3}$. To test the validity of the analytic model, equation (6.2.1) was solved numerically, to find the time evolution of the temperature ratio $\epsilon(t)$ and the result was compared with the graph obtained for $\epsilon(t)$ by a full numerical solution of the Fokker-Planck equation using the code. Good agreement would indicate that the assumption that the distribution function remains bi-Maxwellian during the relaxation process is satisfactory for an investigation of anisotropic temperature relaxation though not necessarily strictly true as we discuss below.

The anisotropic Fokker-Planck code was solved using 200 velocity mesh points and 50 angular mesh points with the collision coefficients represented by the first 6 Legendre polynomials. As the function is an even function, it was possible to reduce the range of the angular mesh from [-1,+1] to [0,1]. The boundary conditions were that the function had to be even in μ at $\mu = 0$ and linear in μ at $\mu = 1$. These conditions were less strict than those chosen by Jorna and Wood, and Schamel. The velocity boundary conditions used were the same as those in Chapter 5. The time step was varied to obtain results that are essentially independent of it.

Typical results are shown in figures 6.1 and 6.2 in which the solutions of the analytic model are represented by the crosses.

The isotropisation of an oblate, $\epsilon > 1$, and a prolate, $\epsilon < 1$, distribution function is shown by the solid lines in figures 6.1 and 6.2 where ϵ is plotted against time for an initial ϵ of 5.0 and 0.2 respectively. The agreement between the analytic and the numerical result is very good in the oblate case while in the prolate case the distribution relaxes slightly slower than predicted by the analytic result.

Jorna and Wood (1987b) studied this problem with the earlier version of the Fokker-Planck code. Their results were slightly different. In both cases, the agreement with Schamel's analytic results was not as good. It was found that the numerical result relaxed faster than the analytic model in the oblate case and in the prolate case, the numerical result relaxed much faster than the analytic result. Schamel's numerical results are much closer to our results. There is no difference in the oblate case, but in the prolate case, their code showed a slightly quicker relaxation than our code.

Despite the fact that the agreement between the analytic and numerical results is good, it does not prove that the distribution remains bi-Maxwellian throughout the isotropisation process. It only proves that the approximate combination of second moments is similar in both cases.

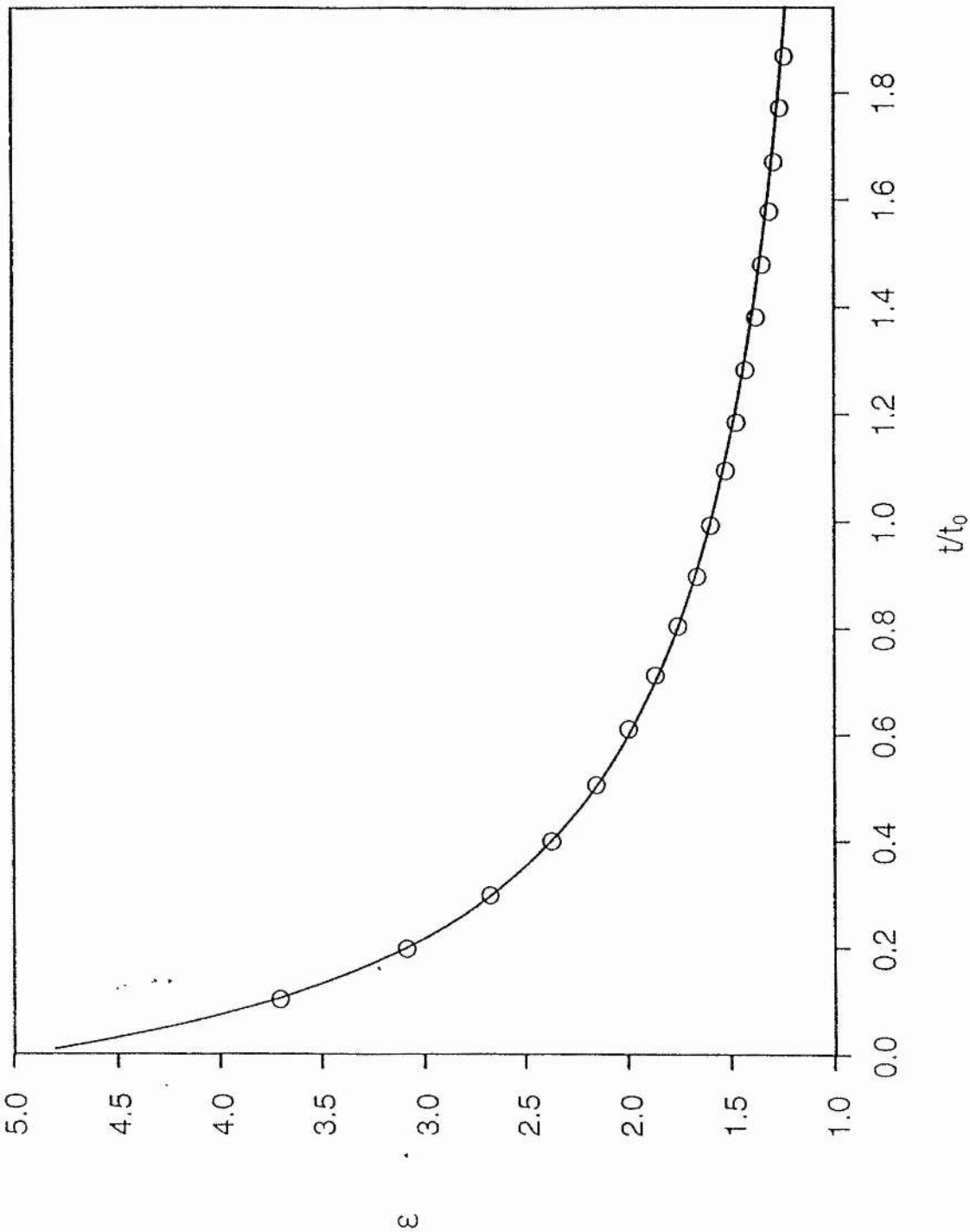

Figure 6.1: **RELAXATION OF AN OBLATE DISTRIBUTION WITH $\epsilon = 5$**

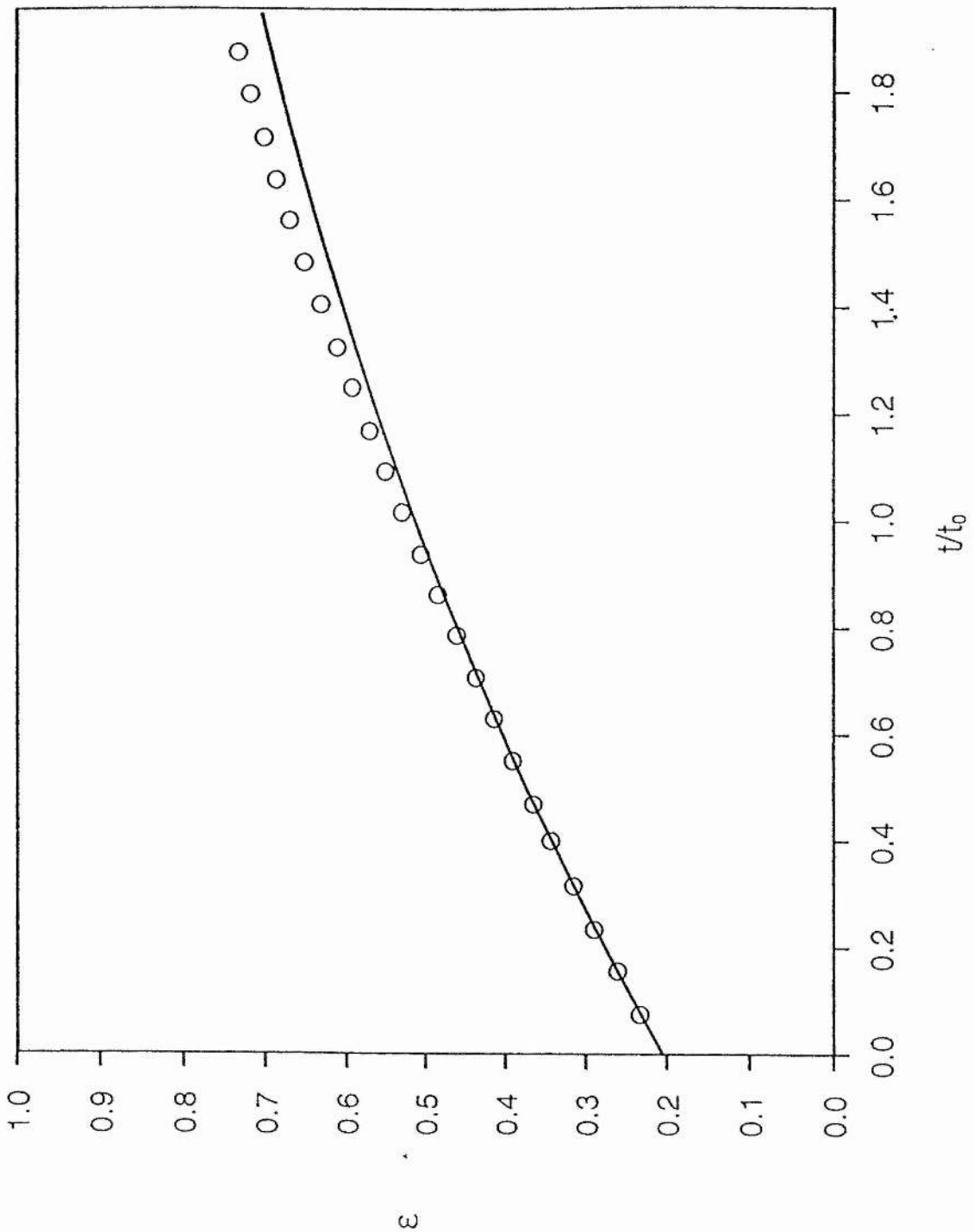

Figure 6.2: **RELAXATION OF AN PROLATE DISTRIBUTION WITH ϵ = 0.2**

In figures 6.3 and 6.4 we show the ratio of the calculated distribution function to the bi-Maxwellian (with T_{perp} and T_{par} calculated from the distribution function) as a function of μ for the oblate and prolate cases respectively. The ratios are given at the thermal velocity (the full line) and twice the thermal velocity (the broken line) at 0.05 t_0, 0.5 t_0, 1.0 t_0, 1.5 t_0 where t_0 is the self-collision time as defined in chapter 5. It can be seen that in the oblate case, figure 6.3, the distribution significantly deviates from bi-Maxwellian only at μ = 1 where the distribution, relative to a bi-Maxwellian, is over-populated at the thermal velocity and under-populated at twice the thermal velocity. However, the oblate case is strongly peaked around μ = 0 and so the bulk of the distribution does remain bi-Maxwellian throughout the isotropisation process. In the prolate case, the distribution deviates from Maxwellian for all values of μ. In the prolate case the bulk of the distribution is around μ' = 1 and it can be seen that the distribution deviates by as much as 10 % at this point. It can be seen in both cases that the distribution is relaxing back to thermal equilibrium.

It should be noted that the departure of the distribution from bi-Maxwellian in both cases is notably less than that found by Jorna and Wood (1987a). Figures 2 and 3 in that paper show deviations which are qualitatively similar but an order of magnitude larger in the prolate case and spread over a greater range of μ in the oblate case. Another significant difference between the earlier results and our results is that figures 6.3 and 6.4 clearly show the return of f to the bi-Maxwellian form as t increases beyond 0.5 t_0. This is not shown in the Jorna and Wood figures where deviation of the distribution from bi-Maxwellian is still increasing at t = 0.6 t_0, the

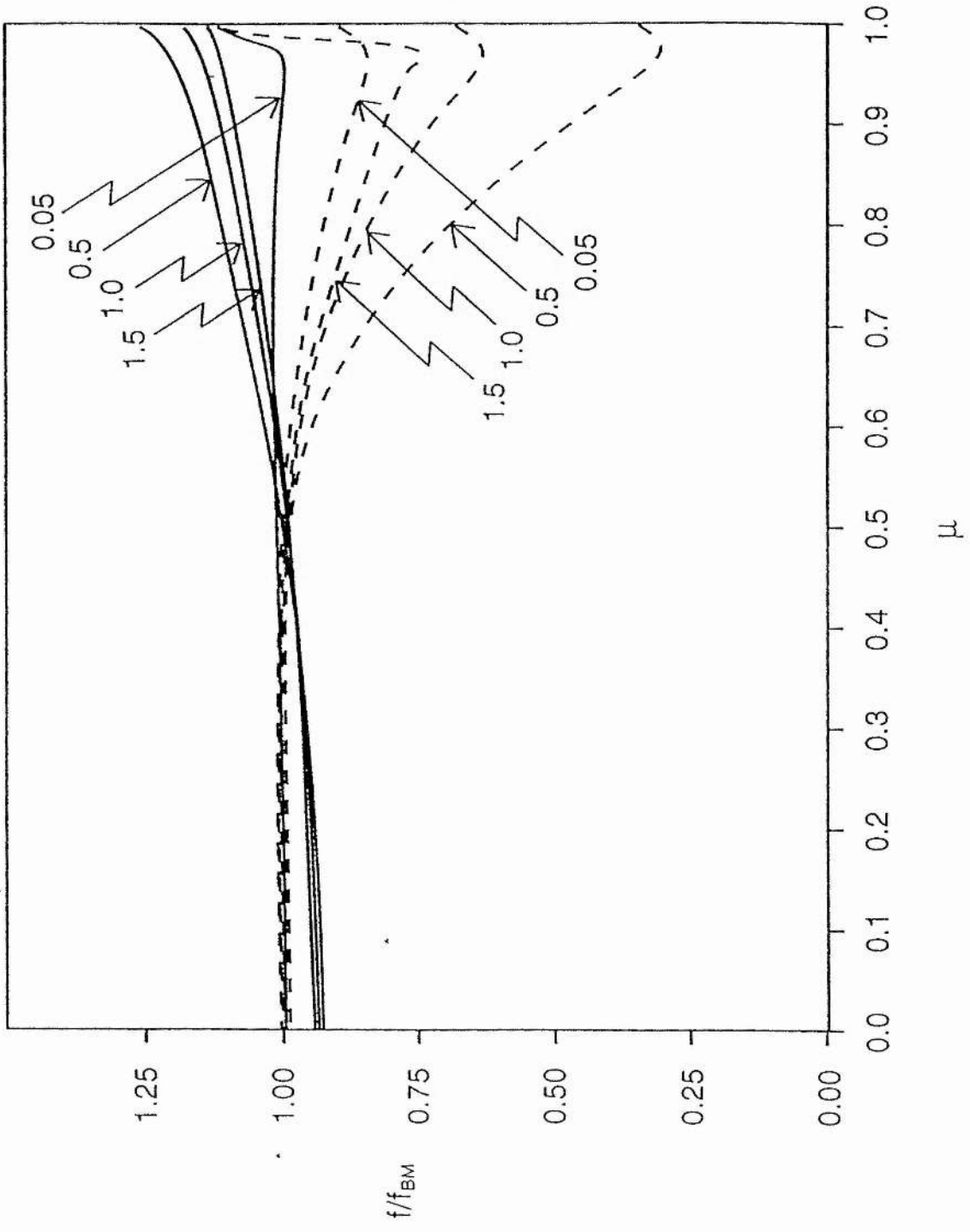

Figure 6.3 DEVIATION OF THE DISTRIBUTION FUNCTION FROM BI-MAXWELLIAN FOR AN OBLATE DISTRIBUTION AT t = 0.05 t_o, 0.5 t_o, 1.0 t_o and 1.5 t_o.

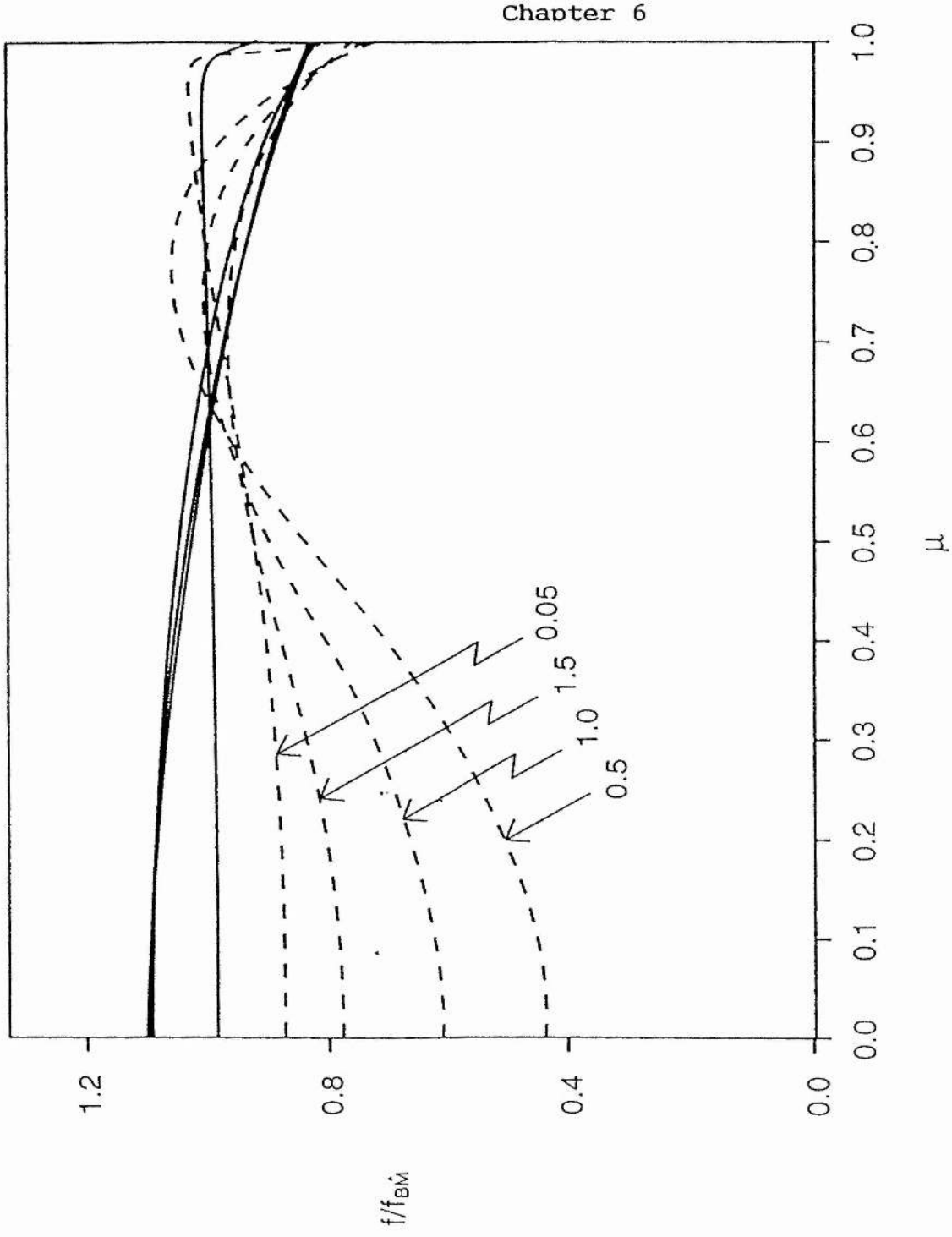

Figure 6.4 DEVIATION OF THE DISTRIBUTION FUNCTION FROM BI-MAXWELLIAN FOR A PROLATE DISTRIBUTION AT $t = 0.05\ t_o$, $0.5\ t_o$, $1.0\ t_o$ and $1.5\ t_o$.

latest time for which the comparison was made. Particle conservation was less accurate in this earlier version of the code and it is possible that the method of adding particles exaggerated the departure from bi-Maxwellian.

Another way of analysing the difference between the calculated distribution and the bi-Maxwellian is by calculating the following integrals

$$\Delta n_{par} = \frac{\int_0^\infty \int_0^1 v^2 \mu^2 \, | f(v,\mu) - f_{BM} | \, d\mu \, dv}{\int_0^\infty \int_0^1 f(v,\mu) \, v^2 \mu^2 \, d\mu \, dv}$$

- eqn(6.2.6)

$$\Delta T_{par} = \frac{\int_0^\infty \int_0^1 v^4 \mu^2 \, | f(v,\mu) - f_{BM} | \, d\mu \, dv}{\int_0^\infty \int_0^1 f(v,\mu) \, v^4 \mu^2 \, d\mu \, dv}$$

- eqn(6.2.7)

$$\Delta n_{perp} = \frac{\int_0^\infty \int_0^1 v^2 (1-\mu^2) \, | f(v,\mu) - f_{BM} | \, d\mu \, dv}{\int_0^\infty \int_0^1 f(v,\mu) \, v^2 (1-\mu^2) \, d\mu \, dv}$$

- eqn(6.2.8)

$$\Delta T_{perp} = \frac{\int_0^{\infty}\int_0^{1} v^4 (1-\mu^2) \, | f(v,\mu) - f_{BM} | \, d\mu \, dv}{\int_0^{\infty}\int_0^{1} f(v,\mu) \, v^4 (1-\mu^2) \, d\mu \, dv}$$

- eqn(6.2.9)

These integrals give a measure of the total departure of the distribution function from the bi-Maxwellian distribution. They are weighted to determine the departure from Maxwellian in different regions of velocity space. The integrals which involve the second velocity moments, Δn_{par} and Δn_{perp}, measure the departure from Maxwellian at low velocities while the fourth velocity moments, ΔT_{par} and ΔT_{perp}, measure the departure at higher velocities. The difference between Δn_{par} and Δn_{perp} is that Δn_{par} is weighted to measure the difference in the parallel direction while Δn_{perp} is weighted to measure the difference in the perpendicular direction and likewise for ΔT_{par} and ΔT_{perp}.

We see in figures 6.5 and 6.6 that the departure from bi-Maxwellian grows quickly for the low and high velocity parts of the distribution after which the moments decay as the distribution relaxes to equilibrium. In the oblate case, figure 6.5, the departure is strongest for the suprathermal moments. The perpendicular suprathermal moment (ΔT_{perp}) dominates which might be expected as the distribution is strongly stretched in that direction. For the prolate distribution, figure 6.6, both of the parallel moments (Δn_{par} and ΔT_{par}) dominate the perpendicular moments. Also, the maximum value of the suprathermal moment is twice the maximum found in the oblate case.

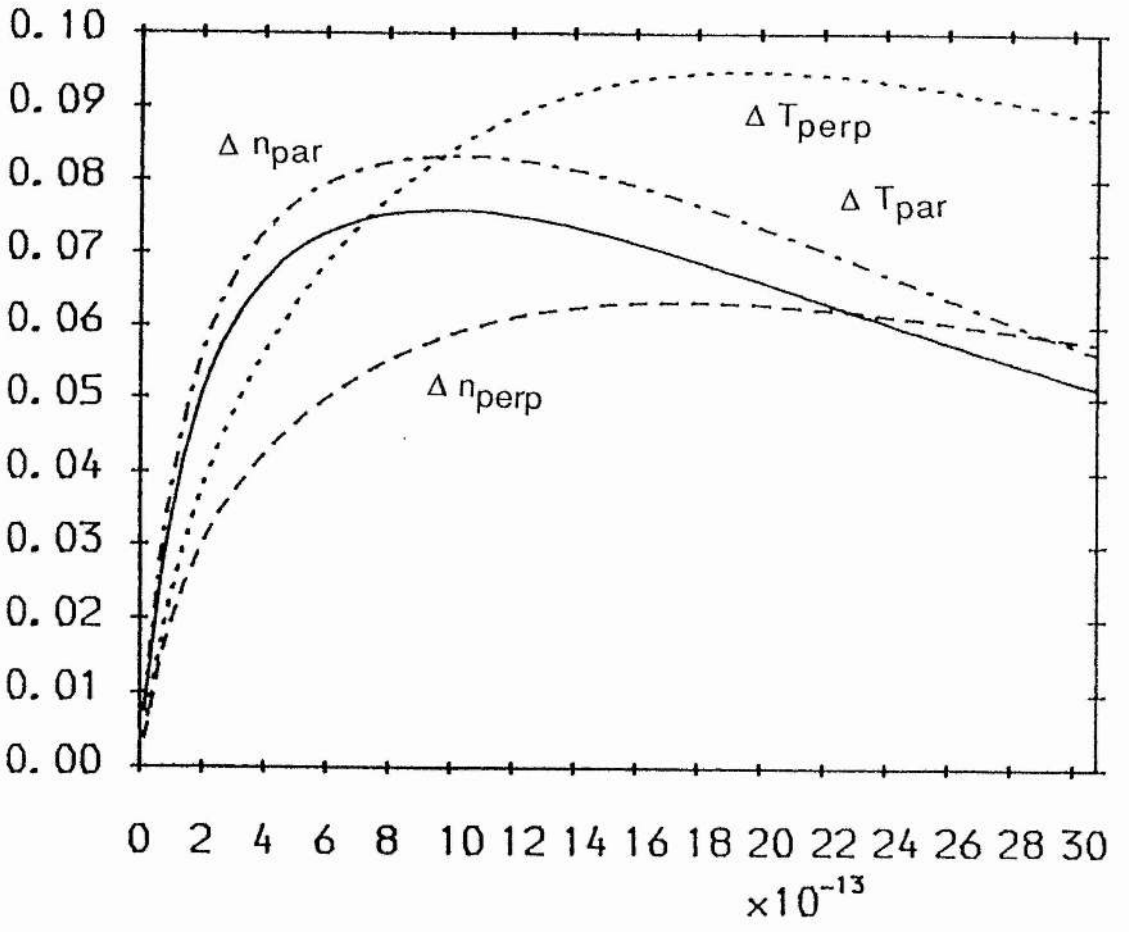

Figure 6.5: MOMENTS OF DEPARTURE FROM BI-MAXWELLIAN FOR AN OBLATE DISTRIBUTION

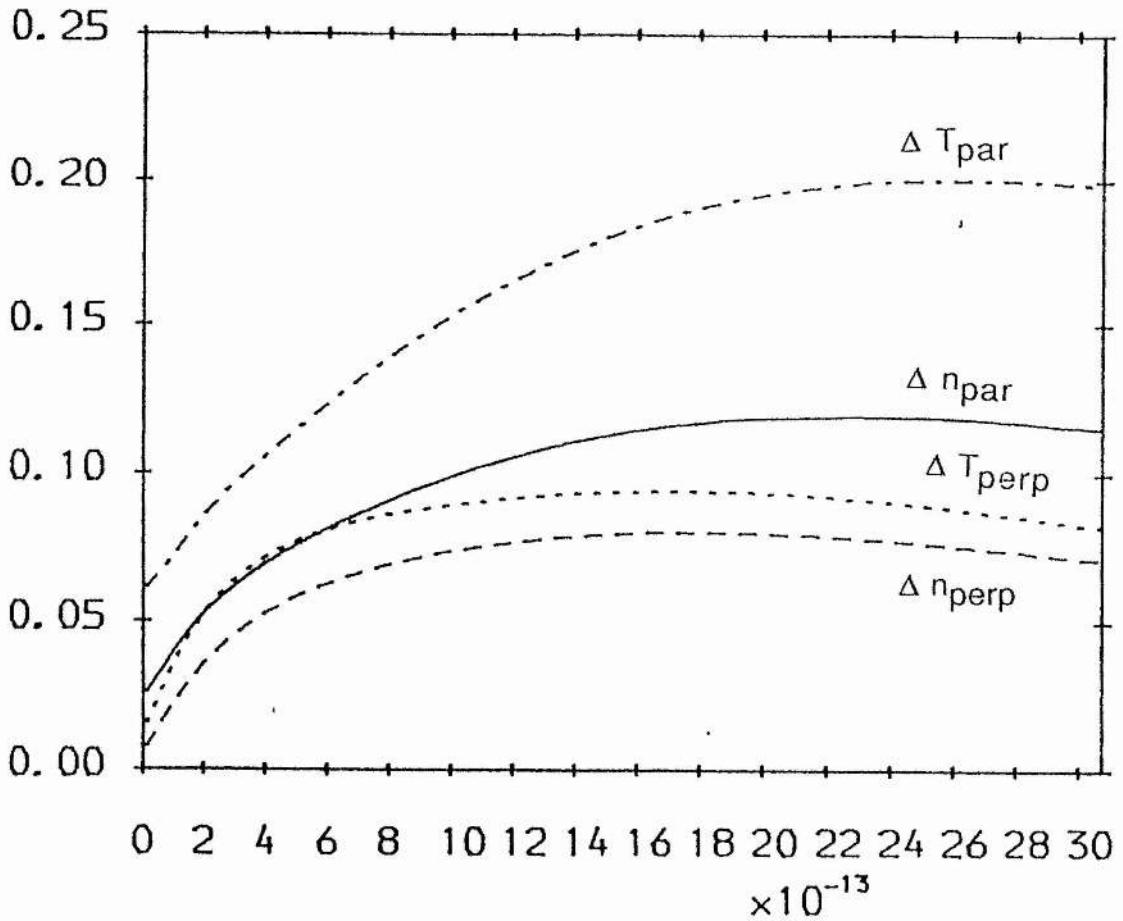

Figure 6.6: MOMENTS OF DEPARTURE FROM BI-MAXWELLIAN FOR A PROLATE DISTRIBUTION

Therefore, as in figure 6.3 and 6.4, the greatest deviation from the bi-Maxwellian distribution occurs when the distribution is stretched in the parallel direction.

It is not clear why the oblate distribution agrees with the bi-Maxwellian model better that the prolate distribution. Wood and Jorna argued that the oblate distribution agreed with the bi-Maxwellian model better than the prolate distribution because of the boundary conditions used by the code. In the oblate case, the boundary conditions that they applied were also satisfied by a Maxwellian distribution. However, in the prolate case this was not the case. Jorna and Wood then claimed that the prolate bi-Maxwellian distribution was invalid. This does not appear to be self-consistent. Schamel does not explain why the prolate distribution deviates further from bi-Maxwellian than the oblate distribution.

Finally, we examine the sensitivity of the results to the truncation of the collision operator by reducing the number of Legendre polynomials in f when calculating the collision integrals. Figures 6.7 and 6.8 show the results for the oblate and prolate cases respectively when l_{max} = 0,2 and 4. In both cases the relaxation is faster for isotropic Rosenbluth potentials (l_{max} = 0) in qualitative agreement with the results of Jorna and Wood; it should be noted, however that the Jorna and Wood code did not expand f in Legendre polynomials so although the effect is the same the method of obtaining it is different. The faster relaxation is to be expected since an isotropic distribution is cooler than the corresponding anisotropic distribution so collisions are more effective.

The more interesting point about these results is the insensitivity to truncation beyond $l_{max} = 2$. The isotropisation curves for both oblate and prolate cases for $l_{max} = 2$ and $l_{max} = 4$ agree to within 2%.

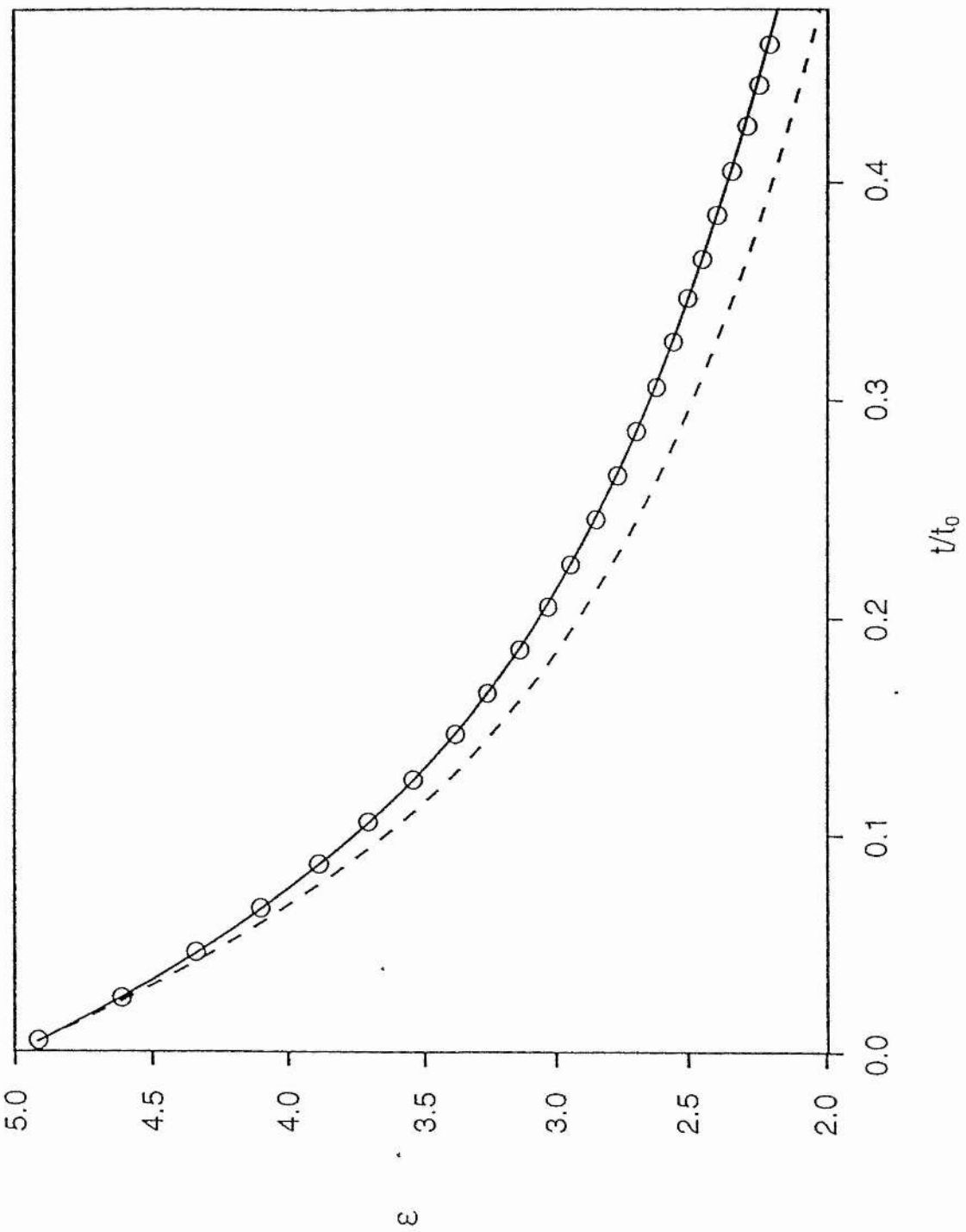

Figure 6.7: RELAXATION OF AN OBLATE DISTRIBUTION WITH l_{max} = 0 (broken line), 2 (circles) and 4 (full line).

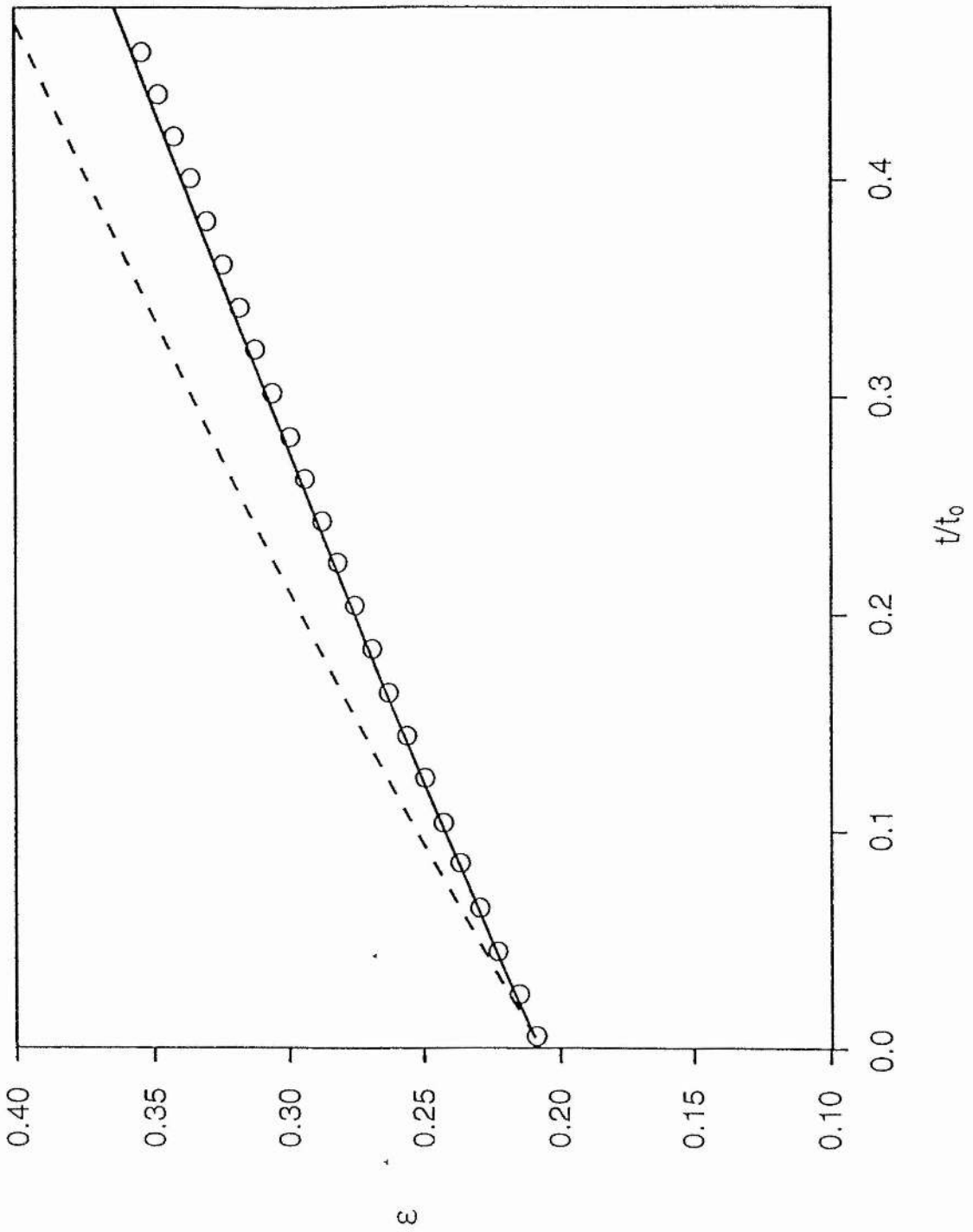

Figure 6.8: RELAXATION OF A PROLATE DISTRIBUTION WITH l_{max} = 0 (broken line), 2 (circles) and 4 (full line).

6.3 The Self-Similar Distribution Function

The self similar distribution is defined as (Marsch et al,1985)

$$f_e(v) = \frac{c_s n_e}{\pi^{3/2} {v_0}^3} \exp\left(-\frac{v^s}{{v_0}^s}\right)$$

- eqn(6.3.1)

where the normalisation constants, c_s and v_0, are defined as

$$c_s = \frac{3\ \pi^{1/2}}{4\Gamma(1+3/s)}$$

- eqn(6.3.2)

and

$${v_{th}}^2 = {v_0}^2 \frac{2\Gamma(5/s)}{s\Gamma(1+3/s)}$$

- eqn(6.3.3)

n_e is the electron density, v_{th} is the thermal velocity and Γ is the Gamma function. From equation (6.3.3) and the properties of the Gamma function, it can be seen that for s > 2, the reference velocity, v_0, is always greater than the thermal velocity. Therefore, around v_{th} the self-similar distribution is over-populated relative to the Maxwellian. Once we go above v_0, the distribution falls off much more quickly than the Maxwellian and is therefore depleted at high velocities.

Several authors have pointed out the importance of self-similar distributions in a variety of plasmas. Interest first arose in the field of weak turbulence theory where anomalous transport coefficients were derived from self-similar distributions (see eg. Dum (1978)). Jones (1980), Langdon (1980) and Balescu (1982) have shown that laser irradiated, high z plasmas reach a self-similar state with s = 5 for the electrons and s = 2 (Maxwellian) for the ions. Compared with the Maxwellian distribution, self-similar distributions with s > 2 are flat-topped and for this reason they have been of interest to space plasma physicists to explain the frequently observed electron distributions at the earth's bow shock (Feldman et al. (1983)).

Marsch and Livi have considered the coulomb collision rates for the self-similar distribution and the kappa distribution (see section 6.4). They showed that the Fokker-Planck equation could be written in a relaxation time form i.e.

$$\frac{\partial f}{\partial t} = \nu_s(f, \underline{v})\, f$$

-eqn (6.3.4)

where υ_s is the effective collision frequency and is defined as

$$\nu_s(f, \underline{v}) = 2\pi f(\underline{v}) + \frac{1}{4}\nu^d(\underline{v}) : \Delta \ln f(\underline{v})$$

- eqn (6.3.5)

and

$$\nu^{d}(\underline{v}) = \frac{\partial^2}{\partial \underline{v} \partial \underline{v}} g(\underline{v})$$

- eqn (6.3.6)

$$\Delta \ln f(\underline{v}) = \left(\frac{\partial}{\partial \underline{v}} \ln f \frac{\partial}{\partial \underline{v}} \ln f + \frac{\partial^2}{\partial \underline{v} \partial \underline{v}} \ln f \right)$$

- eqn (6.3.7)

are the normalised diffusion rate and the logarithmic second derivative of the normalised distribution. Marsch and Livi showed that the effective collision frequency for a self-similar distribution is:

$$\nu_s(v) = \frac{2C_s}{\sqrt{\pi}} e^{-v^s} - \frac{s}{2} v^{s-3} \left(\Phi_s + \frac{(s-2-sv^s)}{v^2} \Pi_s \right)$$

- eqn (6.3.8)

where

$$\Phi_s = \int_0^v G_s(z)\, dz$$

- eqn (6.3.9)

$$\Pi_s = \int_0^v z^2 G_s(z)\, dz$$

- eqn(6.3.10)

$$G_s = \frac{2c_s}{\sqrt{\pi}} \frac{2}{s} \int_{z^2}^{\infty} e^{-t^2} t^{\frac{2}{s}-1} dt$$

-eqn (6.3.11)

Marsch and Livi solved equation (6.3.8) numerically. They showed that for self-similar distributions with s > 2.5, the effective collision frequency rises dramatically. In fact, it was shown that the effective collision frequency for a self-similar distribution increases according to a power law at high velocities. As the effective collision frequency increases with s, the effective collision time of the self-similar distribution becomes smaller. In fact for a distribution with s = 5, they showed that the collision time is about one order of magnitude less than the Spitzer collision time.

However, Marsch and Livi were unable to examine the temporal evolution of the plasma. Their analysis was only valid at t = 0, before the collision rates had time to modify the distribution. They were unable to say if the distribution remained self-similar during the relaxation process. It was decided to use the Isotropic code to investigate if the distribution did remain self-similar during the relaxation process.

For these results, the Isotropic code was used with 300 velocity mesh points and the maximum velocity mesh point at 6 v_{th}. The time step was kept at $t_o/200$. The index of the initial self-similar distribution was 5.

Figure 6.9 shows a log log plot of the temporal evolution of the initially self - similar distribution for t = 0.0 t_0, 2.0 t_0, 4.0 t_0 and 6.0 t_0. The dotted line in the figure represents the equilibrium value. If the distribution had relaxed back within the class of self-similar distributions, then all the lines in figure 6.9 would have been straight lines. However, as can be seen from the figure, the distribution does not relax back within the class of self-similar distributions. The distribution function returns to equilibrium within t_0 below v_{th} (= 0 on x-axis). Above v_{th}, the distribution takes much longer to relax.

Figure 6.10 shows the effective collision frequency of the distribution against velocity where the effective collision frequency was calculated from eqn (6.3.4) for the same time sequence as in figure 6.9. The dotted line in figure 6.10 is the equilibrium value. The collision frequency for small times remains similar to the self-similar distribution. At less than v_{th}, the collision frequency is small and positive where there is a hole in the distribution. Around v_0, about 1.5 v_{th} for s = 5, the collision frequency is small and negative as the distribution is over-populated. At high velocities, there is a dramatic increase in the collision frequency.

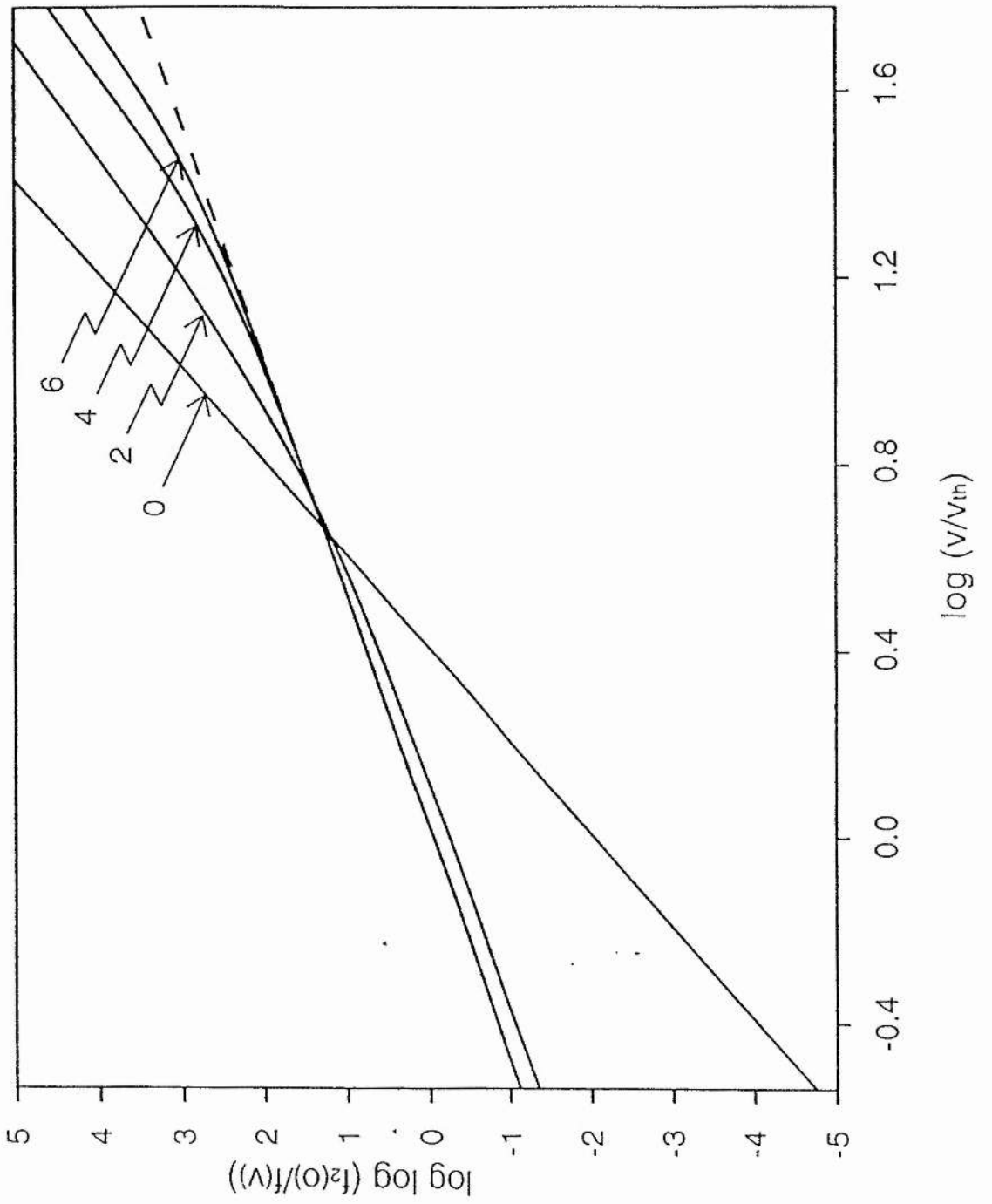

Figure 6.9: **TEMPORAL EVOLUTION OF A SELF-SIMILAR DISTRIBUTION (S = 5) AT t = 0, $2t_o$, $4t_o$ and $6t_o$**

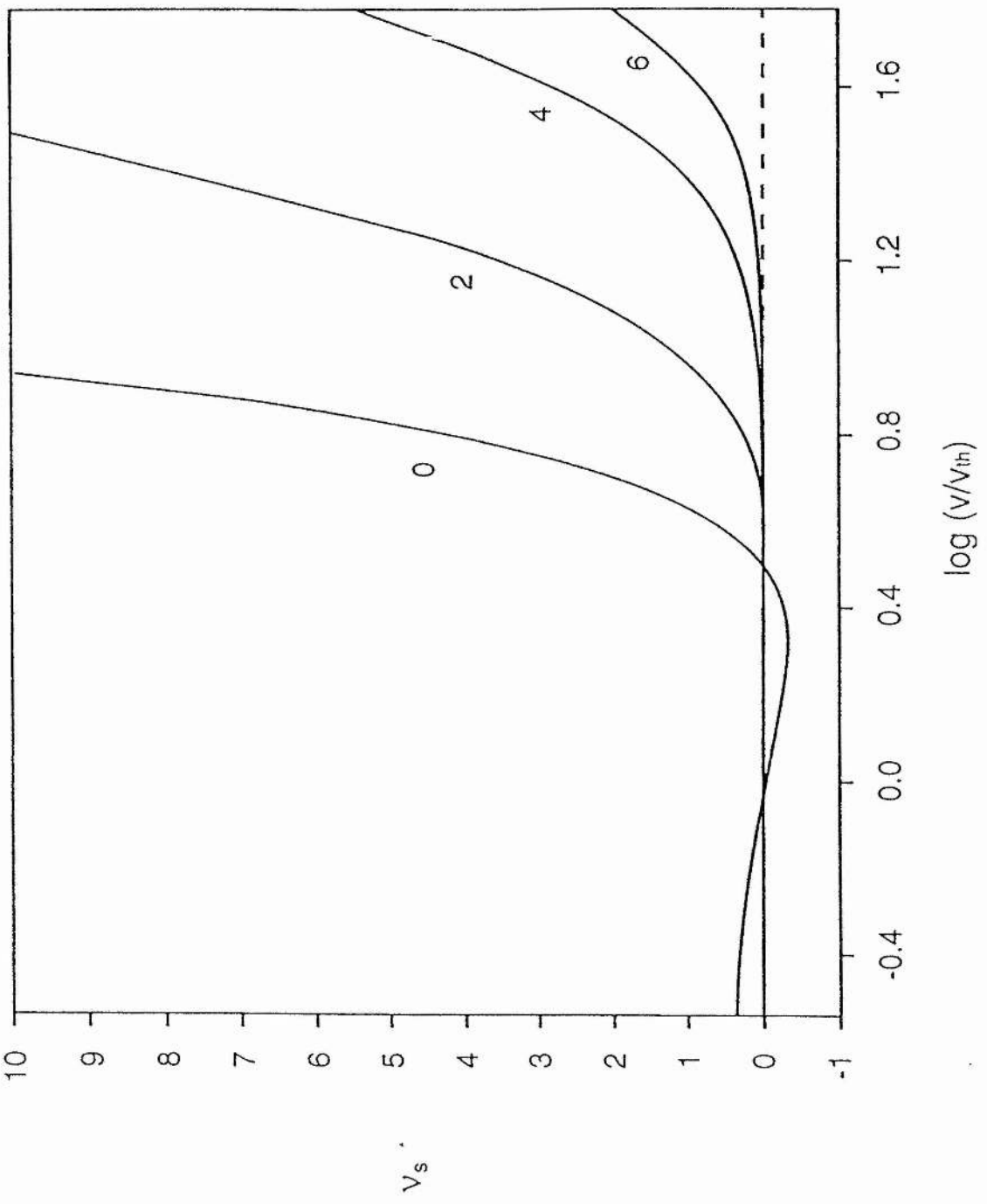

Figure 6.10: TEMPORAL EVOLUTION OF THE EFFECTIVE COLLISION FREQUENCY FOR A SELF-SIMILAR DISTRIBUTION (S = 5) AT t = 0, $2t_o$, $4t_o$ and $6t_o$

After t_0, the collision frequency has lost its self-similar shape. The relaxation process has filled in the hole at v = 0 and smoothed out the hump at v = $v_{th.}$ However, there is still a very large collision frequency at high velocities. This at first sight may seem a surprising result. One might have thought that a high collision frequency would have implied that the distribution will thermalise rapidly. This is not necessarily the case as the rate of change of the distribution depends on the collision frequency and the distribution. As the distribution is exponentially small at large velocities, the rate of change of the distribution is also small.

6.4 The Kappa Distribution

The kappa distribution is defined as:

$$f_e(v) = \frac{A_K n_e}{\pi^{3/2} v_0^3}\left[1+\frac{v^2}{v_0^2}/K\right]^{-K}$$

- eqn (6.4.1)

where the normalisation constants, A_K and v_0, are

$$A_K = \frac{\Gamma(K)}{\Gamma(K-3/2)K^{3/2}}$$

- eqn (6.4.2)

and

$$v_{th}^2 = v_0^2\left[\frac{K}{K-5/2}\right]$$

- eqn (6.4.3)

when K > 5/2. It can be shown that this distribution approaches the Maxwellian distribution asymptotically as K tends to infinity. If we expand the right hand side of equation (6.4.1) and let K tend to infinity then:

$$\left[1+\frac{v^2}{v_0^2}/K\right]^{-K} = 1 - K\frac{(v/v_0)^2}{K} + \frac{K(K+1)}{2}\frac{(v/v_0)^4}{K^2} + \ldots$$

$$= 1 - \left(\frac{v}{v_0}\right)^2 + \frac{1}{2}\left(1+\frac{1}{K}\right)\left(\frac{v}{v_0}\right)^4 + \ldots$$

$$= \exp -\left(\frac{v}{v_0}\right)^2$$

and we return to the Maxwellian distribution. For small values of K, the kappa distribution has a hotter thermal tail than the Maxwellian distribution. At low velocities, the kappa distribution is similar to the Maxwellian distribution except that the Maxwellian distribution tails off less quickly as the velocity increases.

The distribution was first suggested by Obert (1979) to explain the observed electron distributions in interplanetary space where the distribution has a hot tail. However, the Kappa distribution could also be used in wave-particle interactions where a tail is formed in the electron distribution.

As mentioned in Section 3, Marsch and Livi examined the coulomb collision rate for the kappa distribution and showed that the effective collision frequency is given by:

$$\nu_K(v) = \frac{2A}{\sqrt{\pi}}\frac{1}{(1+v^2/K)^K} - \frac{1}{(1+v^2/K)}\left(\frac{\Phi_K}{v} + \frac{K+1}{K}\frac{2}{1+v^2/K}\frac{\Pi_K}{v}\right)$$

- eqn (6.4.4)

where the velocity is normalised to the reference velocity and ϕ_κ and Π_κ are analogous to ϕ_s and Π_s defined in equations (6.3.9) and (6.3.10) and where G_κ is given by:

$$G_K = \frac{2A_K}{\sqrt{\pi}} \frac{K}{K-1} \frac{1}{(1+v^2/K)^{K-1}}$$

- eqn (6.4.5)

Marsch and Livi solved equation (6.4.4) numerically and showed that the effective collision frequency was much smaller than that for the self-similar distribution. They also deduced that the effective collision time was approximately 10 times larger than the Spitzer collision time in the tail of the distribution.

However, Marsch and Livi's analysis suffers from the same restrictions as those described in Section 3. To obtain an accurate picture of how the kappa distribution relaxes, it is necessary to solve the Fokker-Planck equation. The relaxation was simulated with the isotropic Fokker-Planck code with the same parameters as for the self-similar distribution except that the maximum velocity was set to 10 $v_{th.}$

Figures 6.11 and 6.12 show the evolution of a Kappa distribution with K = 10 at t = 0.0 t_0, 2.0 t_0 , 4.0 t_0 and 6.0 t_0. Figure 6.11 is a plot of the log of the distribution against the velocity normalised to the thermal velocity. The cold part of the distribution returns to thermal equilibrium within 2 t_0 while the high velocity part of the distribution relaxes on a timescale similar to the two - temperature distribution. Figure

6.12 is a plot of the effective collision frequency against the velocity. Compared to the self-similar distribution, the magnitude of the collision frequency is much smaller for the kappa distribution. The magnitude of the collision frequency is much smaller at higher velocities because the distribution is over - populated in this range and therefore requires the hot distribution to diffuse to lower velocities which is a much slower process than the diffusion of cold particles into the tail of the self - similar distribution. It can be seen from both figure 6.11 and 6.12 that the kappa distribution does not relax within its own class of distributions.

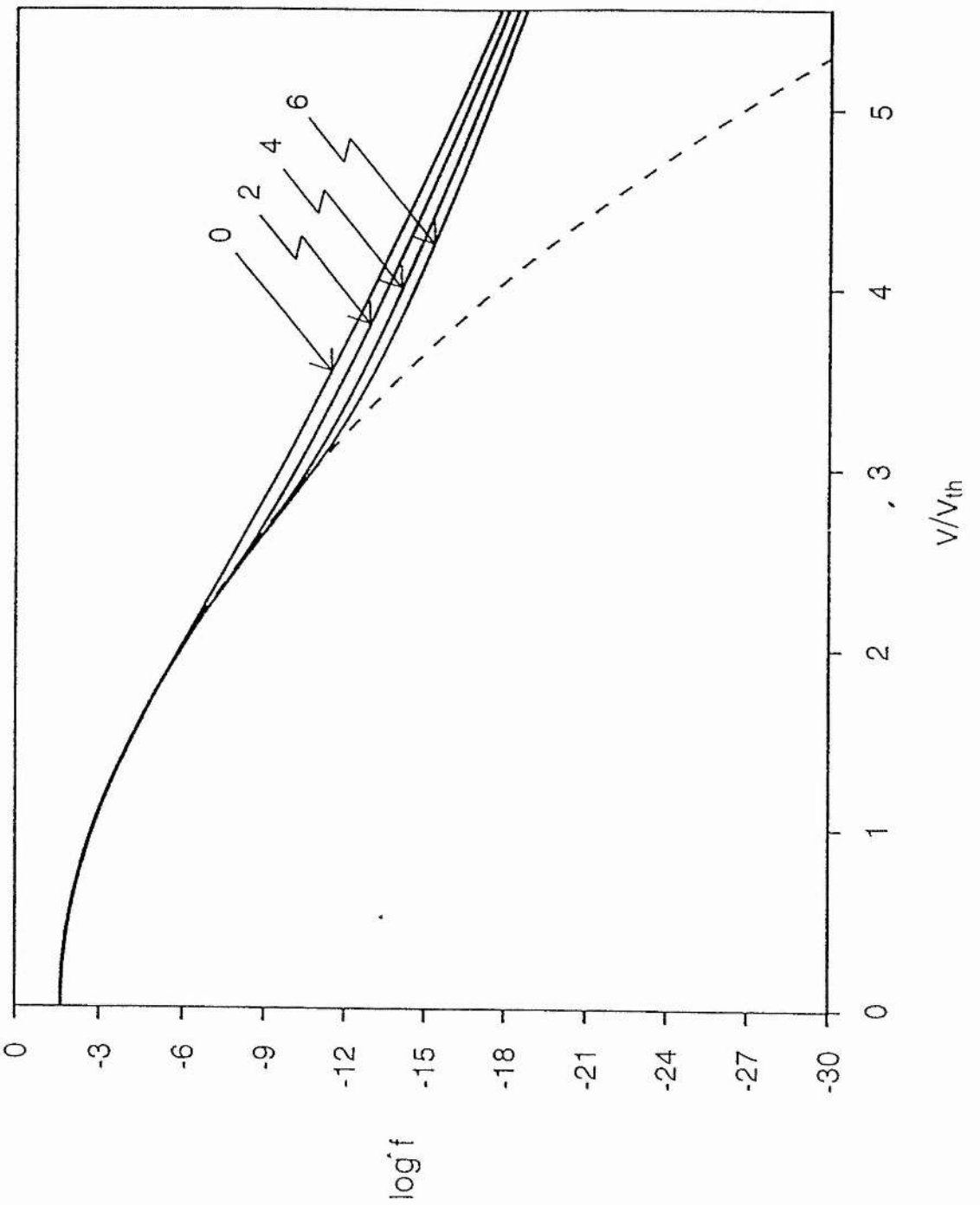

Figure 6.11: TEMPORAL EVOLUTION OF A KAPPA DISTRIBUTION (K = 10) at t = 0, $2t_o$, $4t_o$ and $6t_o$

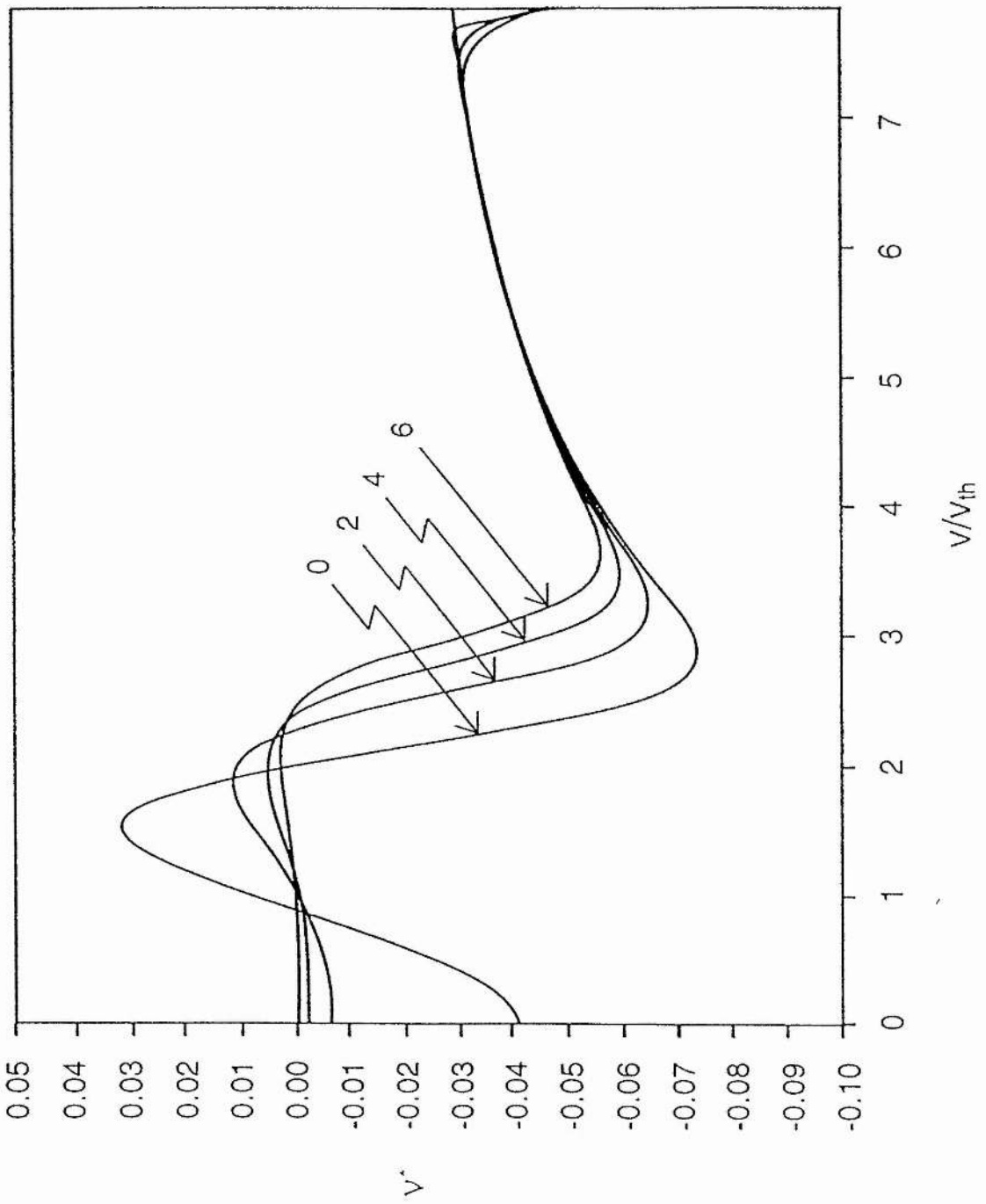

Figure 6.12: TEMPORAL EVOLUTION OF THE EFFECTIVE COLLISION FREQUENCY FOR A KAPPA DISTRIBUTION (K = 10) at t = 0, $2t_o$, $4t_o$ and $6t_o$

6.5 The Isotropic Two - Temperature Distribution

The isotropic two-temperature distribution is defined as:

$$f_e(v) = \frac{n_c}{\pi^{3/2} T_c^{3/2}} \exp\left[-\left(\frac{v^2}{v_c^2}\right)\right] + \frac{n_h}{\pi^{3/2} T_h^{3/2}} \exp\left[-\left(\frac{v^2}{v_h^2}\right)\right]$$

- eqn (6.5.1)

where n_c and n_h are the fraction of cold and hot particles respectively and T_c and T_h are the temperatures of the cold and hot particles. Such plasmas are created in the laboratory in heating processes and occur naturally in space plasmas where the two-temperature distribution may be used as an alternative to the kappa distribution to describe the presence of beams of high energy particles in a cooler plasma background.

To conserve density and energy it is necessary that:

$$n_c + n_h = 1 \quad \textit{and} \quad n_c T_c + n_h T_h = T$$

where T is the temperature of a Maxwellian distribution with the same energy.

The Fokker-Planck equation was solved with the same parameters as those in section 6.3 except that the last velocity mesh was moved out to 10 v_{th}.

For this simulation, we chose a two-temperature distribution with n_c = 0.9, T_c = 0.8 T, n_h = 0.1 and T_h = 2.8 T. In most experiments where an isotropic two-temperature distribution occurs, the values for n_h and T_h are much smaller and much larger respectively than the values used here. However, if a more realistic n_h and T_h had been used then the simulation would have either become computationally prohibitive, due to the large number of mesh points required, or very inaccurate due to a coarse velocity mesh.

Figure 6.13 shows the temporal evolution of the distribution at t = 0.0 t_0, 2.0 t_0, 4.0 t_0 and 6.0 t_0 as a function of the square of the velocity. It can be seen that the temperature of the hot and the cold components remain approximately constant during the simulation. It is the number of particles in each part of the distribution that varies during the relaxation process.

It is possible to explain this result if we assume that the two-temperature relaxation process is represented by a three-temperature distribution where the third component is the temperature of the final equilibrium distribution ie:

$$f(v,t) = \frac{n_c(t)}{\pi^{3/2}T_c^{3/2}}\exp\left(\frac{-v^2}{T_c}\right) + \frac{n_h(t)}{\pi^{3/2}T_h^{3/2}}\exp\left(\frac{-v^2}{T_h}\right) + \frac{n(t)}{\pi^{3/2}T^{3/2}}\exp\left(-\frac{v^2}{T}\right)$$

- eqn(6.5.2)

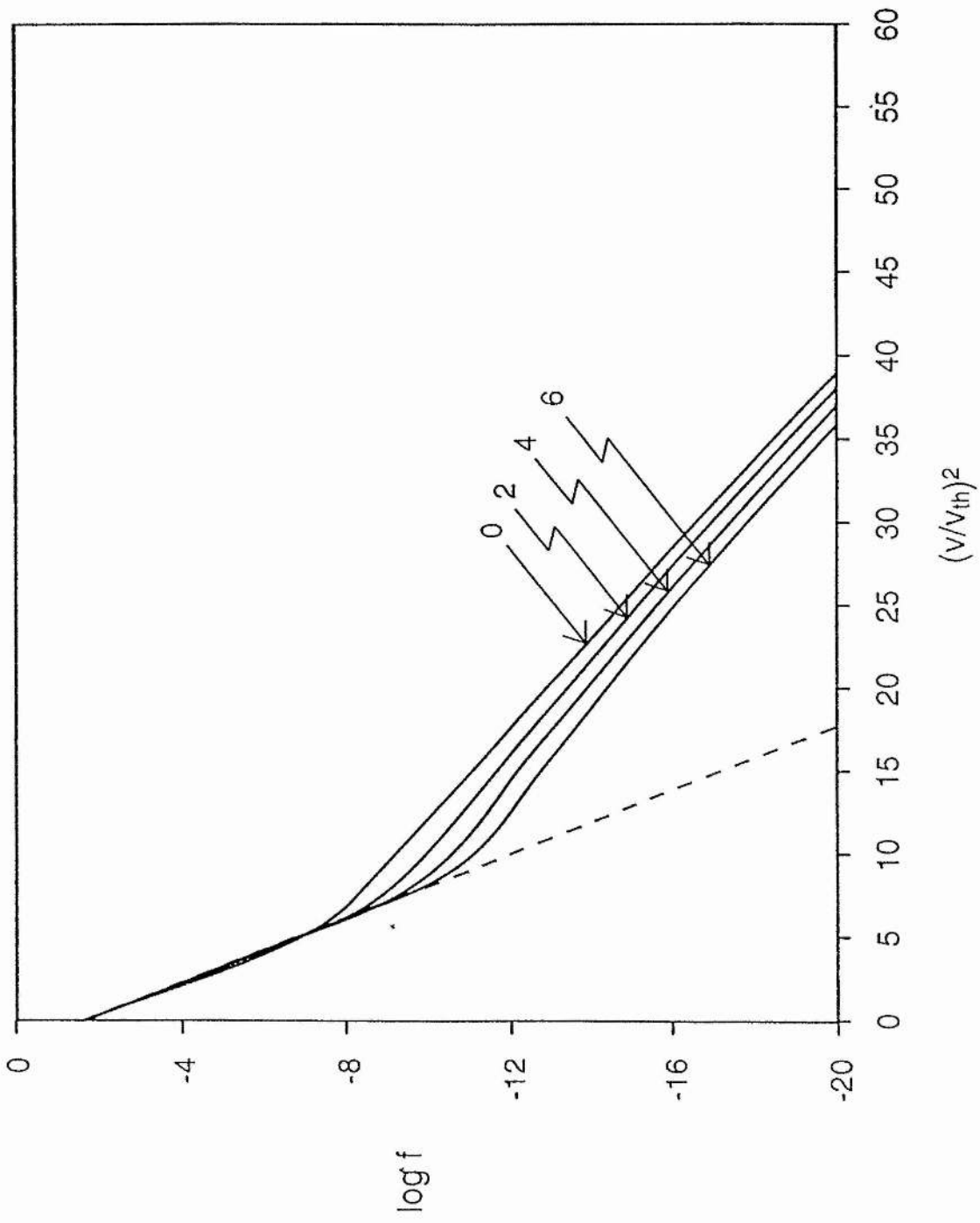

Figure 6.13: TEMPORAL EVOLUTION OF A TWO TEMPERATURE DISTRIBUTION (nc = 0.9, Tc = 0.8) at t = 0, $2t_o$, $4t_o$ and $6t_o$

It is assumed that the temperatures of all three components remain constant during the relaxation process but the number of particles varies with time. In other words, it is assumed that $n_c(t)$ and $n_h(t)$ decrease with time while n(t) increases from zero initial value until all the particles are in the equilibrium distribution and $n_c(t)$ and $n_h(t)$ are zero. Now for this distribution to conserve energy and density it is necessary that:

$$1 = n_c(t) + n_h(t) + n(t)$$

- eqn (6.5.3)

and

$$T = n_c(t)\,T_c + n_h(t)\,T_h + n(t)\,T$$

- eqn (6.5.4)

Eliminating n(t) from these two equations it follows that

$$n_h(t) = n_c(t)\,\frac{(T-T_c)}{(T_h-T)} = \lambda n_c(t)$$

$$T_c = \delta T_h$$

- eqn (6.5.5)

where λ and δ are constants and we can re-write the distribution as:

$$f(v,t) = \frac{n_c(t)}{\pi^{3/2}T_c^{3/2}}\exp\left(\frac{-v^2}{\delta T_h}\right) + \frac{\lambda n_c(t)\,\delta^{3/2}}{\pi^{3/2}T_c^{3/2}}\exp\left(\frac{-v^2}{T_h}\right) + \frac{n(t)}{\pi^{3/2}T^{3/2}}\exp\left(\frac{-1\,(1+\lambda)\,v^2}{(\lambda+\delta)\,T_h}\right)$$

- eqn (6.5.6)

If we assume that λ and δ are << 1, then T_c is approximately T and there are two distinct velocity regions to the relaxation process.

When $v^2 < \delta T_h$ then the distribution is approximately the first and third terms in equation (6.5.6) and the loss of particles from $n_c(t)$ is more than compensated by the gain in n(t). This can be seen by differentiating equation (6.5.3) with respect to time to obtain:

$$\frac{dn}{dt} = -\frac{dn_c}{dt} - \frac{dn_h}{dt} = -(1+\lambda)\frac{dn_c}{dt}$$

- eqn (6.5.7)

For $\delta T_h << v^2$ the distribution is approximately given by the second term in equation (6.5.6) giving:

$$\ln f(v^2,t) = \ln\left(\frac{n_h(t)}{\pi^{3/2}T_h^{3/2}}\right) - \frac{v^2}{T_h}$$

- eqn (6.5.8)

showing precisely the behaviour, observed in figure 6.13, of constant slope and slowly decreasing ordinate.

It is also possible to use the three temperature distribution model to predict what happens to the distribution at v = 0. If we set v = 0 in equation (6.5.6) and use the conservation relations then the distribution becomes:

$$f(v=0,t) = \pi^{-3/2} T_h^{-3/2} \left[\frac{n_c}{\delta^{3/2}} + n_h + \frac{(1-n_c-n_h)(1+\delta)^{3/2}}{(\delta+\lambda)^{3/2}} \right]$$

- eqn (6.5.9)

Now if we assume that $\delta << 1$ and $\lambda <= 1$, then around v=0 it can be shown that:

$$\log f(v=0,t) \cong \log\left(\frac{(1+\lambda)^{3/2}}{T_c^{3/2}} \right) + \frac{\lambda^{3/2} n_c(t)}{\delta^{3/2}(1+\lambda)^{3/2}}$$

- eqn (6.5.10)

So the model predicts that the point of intersection will fall until $n_c(t) = 0$ at which point it will have reached the equilibrium value. Figure 6.14 shows the relaxation of a distribution with $n_c = n_h = 0.5$, $v_c^2 = 0.1$ T and $v_h^2 = 2$ T at t = 0.0 t_0, 0.0125 t_0, . . ., 0.25 t_0 where the log of f is plotted against the square of the velocity. It can be seen that the point of intersection does decrease during relaxation.

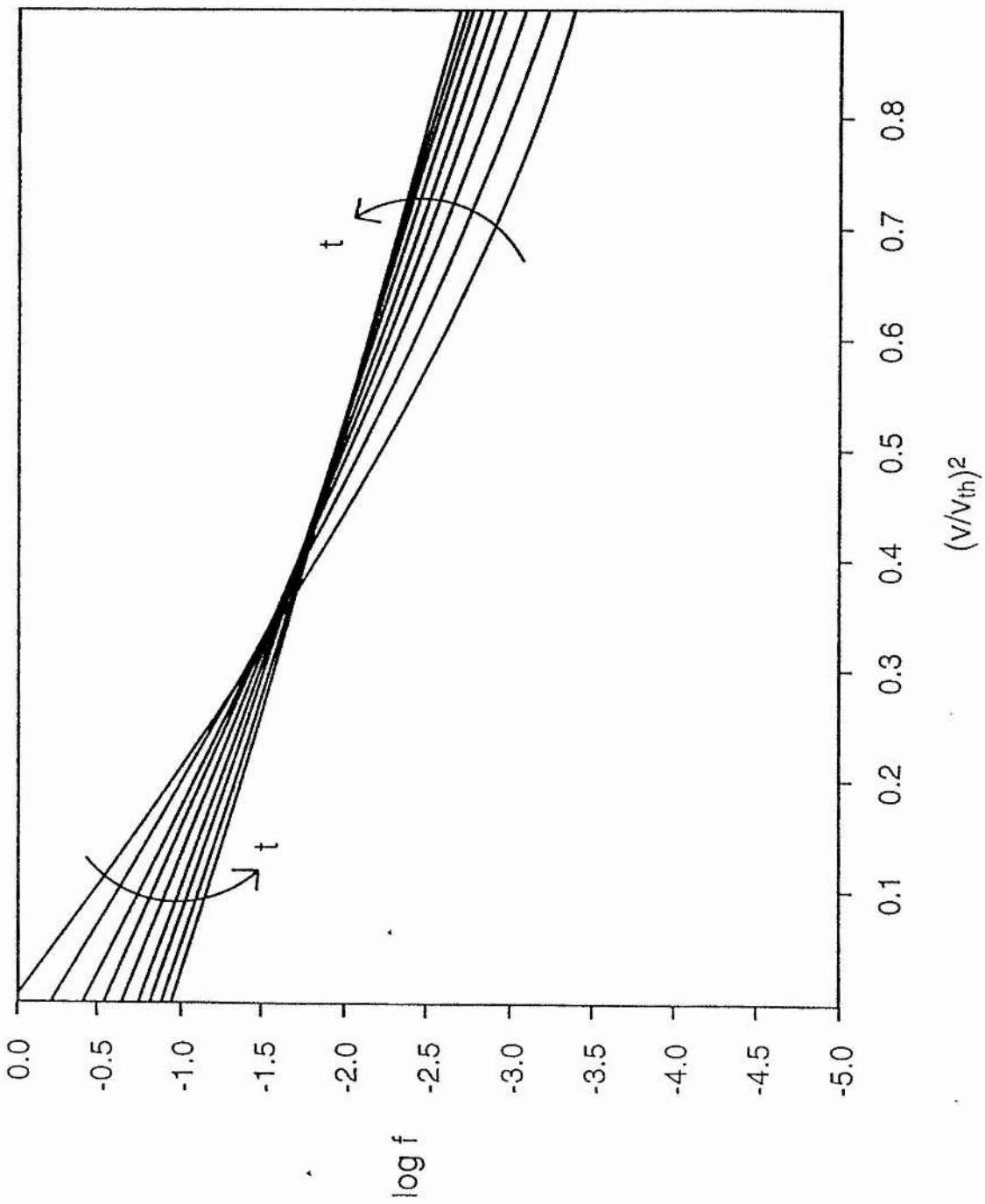

Figure 6.14: **TEMPORAL EVOLUTION OF A TWO TEMPERATURE DISTRIBUTION (nc = 0.5, Tc = 0.1T) at t = 0, $0.0125t_0$, $0.025t_0$.... and $0.25t_0$**

This model does appear to qualitatively describe the relaxation of the two-temperature distribution. However, it is not able to tell us how quickly n_h and n_c vary with time. It is possible to obtain some insight into how n_h and n_c vary with time by considering the effective collision frequency.

Figure 6.15 shows the effective collision frequency, as defined in equation (6.3.4) against normalised velocity for the same time sequence and initial conditions as in figure 6.13. The effective collision frequency reduces to zero within 2 t_0 for the particles below 2 v_{th}. However, the collision frequency of the high velocity part of the distribution remains relatively unaffected on account of the velocity dependence of the collisional interactions. It is only much later that the hot part of the distribution is thermalised. This implies that $n_c(t)$ decreases a lot faster than $n_h(t)$ during the relaxation process.

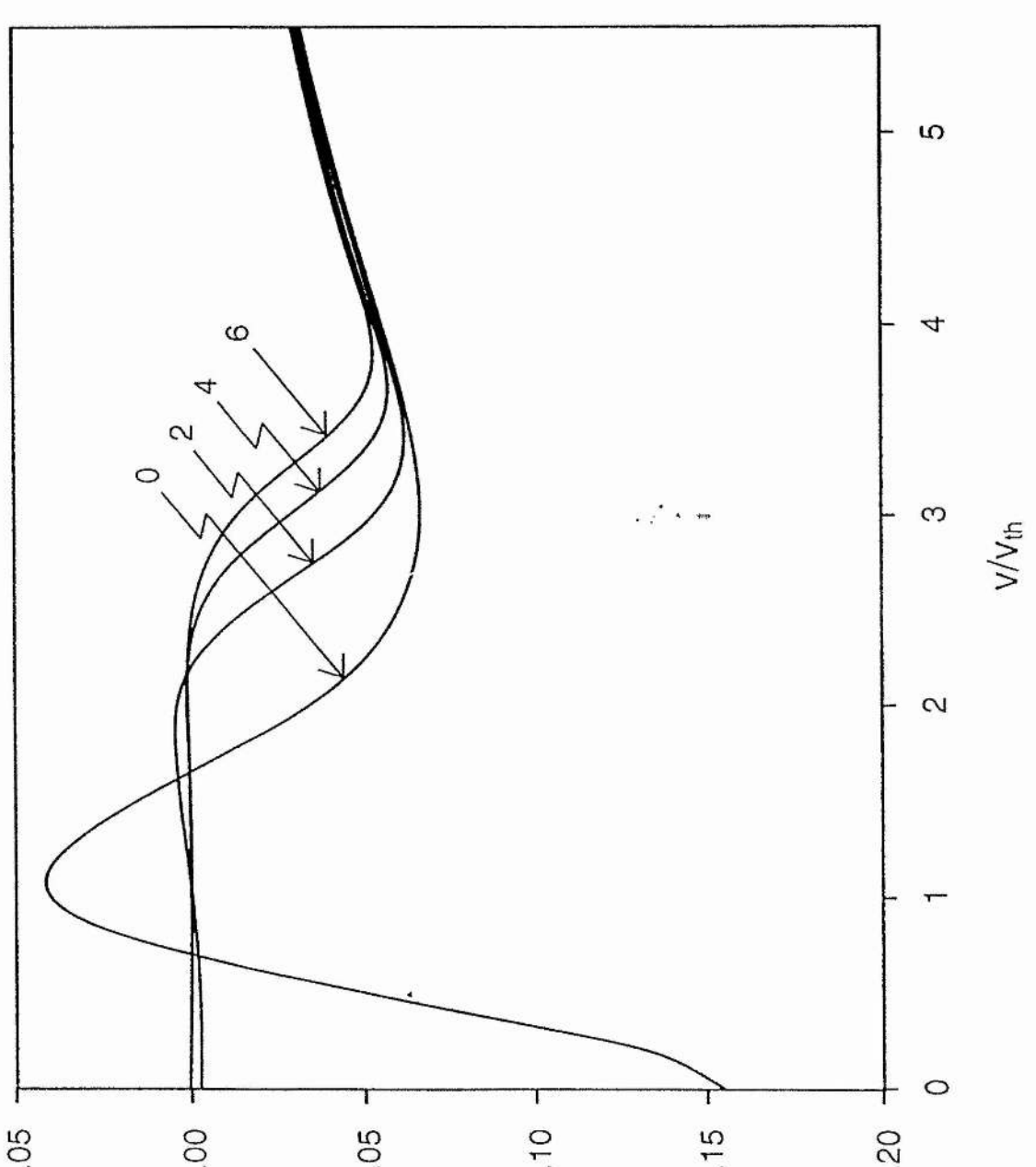

Figure 6.15: **TEMPORAL EVOLUTION OF THE EFFECTIVE COLLISION FREQUENCY FOR A TWO TEMPERATURE DISTRIBUTION at t = 0, $2t_o$, $4t_o$ and $6t_o$**

6.6 Conclusion

In this chapter, we have considered the collisional relaxation of a number of model distributions. We examined the relaxation of the bi-Maxwellian distribution and found that Schamel's bi-Maxwellian model was much better than the earlier version of the code predicted. The bi-Maxwellian model predicts $\epsilon(t)$ very accurately in the $\epsilon > 1$ case but overestimates $\epsilon(t)$ slightly for $\epsilon < 1$. The distribution is not exactly a bi-Maxwellian distribution during the relaxation but the difference is small.

The Isotropic code was used to follow the relaxation of self-similar and kappa distributions. The effective collision frequency for each distribution was calculated during the relaxation process and compared with Marsch and Livi's analytic expression for the effective collision frequency. It was shown that neither of the two distributions remains within their own class of distribution during the relaxation process.

Finally, we considered the relaxation of an isotropic two-temperature distribution. It was shown that when the number of hot particles was small, the temperature of the hot distribution remained approximately constant. This was explained by assuming that the relaxation process could be modelled by a three-temperature distribution made up of the hot and cold distributions and the equilibrium distribution in which the temperatures remained constant but the number of particles in each distribution varied. Calculation of the effective collision frequency gives an estimation of the thermalisation time for the hot and cold components of the plasma.

CHAPTER 7: CONCLUSION

The Fokker-Planck equation has been solved numerically in order to study thermal conduction in a laser produced plasma and the relaxation of several model distribution functions.

Initially, the Fokker-Planck equation was solved numerically using a code developed by Jorna and Wood. Jorna and Wood had solved the Fokker-Planck equation in spherical geometry with the full anisotropic collision term. Jorna and Wood had shown with the code that in a uniform plasma, the heat flow can be larger by a factor of 2 when the anisotropic portion of the collision term is included as compared to only including the isotropic part of the collision term. The original aim of this thesis was to extend the work of Jorna and Wood to non-uniform plasmas and to obtain a better understanding of how the anisotropic collision term affects the heat flow.

However, as described in Chapter 3, the original code was unable to simulate thermal conduction in a non-uniform plasma. The original code did not preserve neutrality which caused the plasma to become unstable. The code was unable to preserve neutrality because of the method used to calculate the electric field and because of the artificial way that it conserved particles. The time dilation method of calculating the electric field is unable to resist the electron pressure down the density gradient while the artificial method used to correct particle loss introduces artificial gradients to the plasma.

As a result of these problems, the original code was re-developed, as described in Chapter 4, in such a way that both the particle and energy conservation was greatly improved. Also, the anisotropic code collision term was no longer calculated directly but by representing the Rosenbluth potentials as a truncated expansion of Legendre polynomials in the angular variable. This increased the speed of the Fokker-Planck code two fold over the direct method used by Jorna and Wood.

In Chapter 5, the improved version of the Fokker-Planck code was applied to Jorna and Wood's original problem. It was shown that it is possible to estimate the effect of curvature on heat flow from geometrical arguments. In addition, the discrete ordinate method of solving the angular equation was compared with the Legendre polynomial method. It was shown that the Legendre polynomial method is a satisfactory method provided that enough terms in the expansion are retained. In the weakly collisional example that we have considered here, it was found that four terms in the expansion were adequate to describe the heat flow. Finally, we considered how the anisotropic component of the collision term affected thermal conduction. The analysis showed, in contradiction with the earlier version of the code, that including the anisotropic component of the collision term has a minimal effect on the heat flow. The modification of the heat flow when the anisotropic components is included is due to the anisotropic collision terms allowing the return current to travel through the plasma more easily which increases the flux at the outer boundary more quickly. This results in more hot particles being added earlier with the resulting modification to the heat flow profiles.

As the results with the anisotropic code were different from those found with the original version of the code, it was decided to repeat Jorna and Wood's work on the relaxation of a bi-Maxwellian distribution.

In Chapter 6, the new version of the anisotropic code was used to study the collisional relaxation of the anisotropic bi-Maxwellian distribution. The results were compared with an analytic equation developed by Schamel which described the development of $\epsilon = T_{par} / T_{perp}$. It was found that the analytic equation gave very reliable results when $T_{par} < T_{perp}$. However, for $T_{par} > T_{perp}$ the analytic equation gave less dependable results as the distribution was found to deviate more significantly from the bi-Maxwellian form.

These results were qualitatively similar to those of Jorna and Wood. However, the old anisotropic code predicted a faster relaxation in both the prolate and oblate case than was found with the new code. In addition, the old code predicted a much larger deviation from bi-maxwellian than was found in the new code and unlike the new code showed no sign of returning to the Maxwellian form. It is thought that the old code showed no sign of returning to the Maxwellian form because the old code was consistently adding particles throughout the plasma to counter-act the particle loss due to the particle loss caused by the method used to difference the velocity equation.

Finally, the isotropic version of the Fokker-Planck code was used to study the collisional relaxation of the self-similar, kappa and isotropic two temperature distributions. It was shown that the self-similar and kappa distributions do not remain self-similar during

collisional relaxation even though the final state, the Maxwellian, is a special case of both these classes of distribution. Subsequently, the analytic expression for the effective collision frequency for such distribution functions are invalid for t>0. After about two self-collision times the distribution is Maxwellian out to about 2 v_{th} but the relaxation is progressively slower beyond that. It should not be a surprise that in highly non-thermal plasmas the relaxation rates should depend strongly on the structure of the distribution functions.

Section 7.2: FURTHER WORK

In this final section, we shall discuss ways in which the re-developed code can be employed to extend the work presented in Chapters 5 and 6. In addition, an idea for a completely new Fokker-Planck code will be presented.

Section 7.2.1: Thermal Conduction in laser-produced plasmas

In Chapter 5, it was shown that the inclusion of the anisotropic collision coefficients had a small effect on the heat flow profiles. The modification of the heat flow profiles was due to the return current distorting the distribution at low velocities. The magnitude of the return current is directly related to the current carried by the hot electrons. Therefore, if the temperature of the hot boundary is increased, then the inclusion of the anisotropic collision coefficients should have a larger effect on the heat profiles. It would be of interest to see how the heat flow profiles are affected when simulations are performed with T_h / T_c = 10 or 100.

However, adding hotter distributions will introduce certain problems for the code. The velocity range that the code would have to simulate would be much larger and would either require many more velocity mesh points or non-linear mesh which had more points at low velocities.

The plasma that was considered in Chapter 5 was a weakly collisional one in which the mean free path of a thermal velocity electron was comparable to the width of the plasma. The plasma was considered so that the new code could be compared with Jorna and Wood's code. It would be of interest to re-examine all topics covered in Chapter 5 with a much more collisional plasma. It would be expected that if the discrete ordinate method is compared to the Legendre polynomial method, it would be discovered that the number of polynomials required would reduce. In addition, it is anticipated that the effect of the anisotropic coefficients would become smaller as the collisionality increased.

Section 7.2.2: Collisional Relaxation

When studying the collisional relaxation of a bi-Maxwellian distribution, in chapter 6 section 1, collisions between electrons and ions were ignored. Schamel has investigated the effect of unlike particle collisions within the restrictions of the bi-Maxwellian model by combining the equation for the evolution of ϵ, equation (6.2.1), with a test-particle approach in which the collision operator is modified to use isotropic Maxwellians rather than the "real" bi-Maxwellian when calculating the Rosenbluth potentials. In this way it was possible to derive 3 equations for the evolution of T_{par}, T_{perp} and T which describe how a bi-Maxwellian distribution relaxes under the influence of self and unlike particle collisions respectively. It was shown that in a single ion species plasma the temperature relaxation of the electrons is affected by unlike particle collisions, whereas only self interactions account for the isotropisation of ions.

However, as Schamel had only been able to investigate unlike particle collisions within the bi-Maxwellian model, there are certain important questions still to be answered.

For example, it was shown in Chapter 6 that there was a discrepancy between the oblate and prolate distributions when the temperature relaxation predicted by the bi-Maxwellian model was compared with the temperature relaxation predicted by the Fokker-Planck code. In addition, it was discovered that the relaxation process was insensitive to the truncation of the collision operator beyond $l_{max} = 2$. It would be of interest to see how a background ion distribution affected the relaxation process. As the ionic charge increases it would be

expected that the discrepancy between the oblate and prolate distributions would decrease as the electron-ion collisions began to dominate the electron-electron collisions. For the same reason, it would be expected that as the ionic charge increased the electron collisions could be truncated to $l_{max} = 0$ or even ignored altogether. However, exactly how this takes place requires the application of the Fokker-Planck code to the problem.

Finally, the new code could be used to consider the case when an anisotropic ion distribution relaxes back under the influence of self collisions and an isotropic ion distribution of a different ionic charge. Schamel was unable to say much about this case other than the isotropic distribution would be affect the relaxation. With the Fokker-Planck code it would be possible to vary the ionic charge of the anisotropic and isotropic distributions and determine when it was possible to only include self-collisions and when not. It would also be possible to verify how accurately Schamel's three equations predicted the temperature relaxation.

In Chapter 6 section 4, a model was proposed for the relaxation of an isotropic two temperature distribution. It was shown that the model predicted the initial evolution of the distribution. However, it would be interesting to see if the model was valid until the distribution relaxed back to equilibrium. By fitting the "true" distribution to the three temperature distribution it would be possible to determine the relative weights of the three distributions.

Another model distribution that could be analyzed with the re-developed Fokker-Planck code is the counter-streaming half-Maxwellian distribution which is defined by

$$f(v,\mu,t) = H(\mu)\frac{n_h}{\pi^{3/2}v_h^3}e^{-\frac{v^2}{v_h^2}} + H(-\mu)\frac{n_c}{\pi^{3/2}v_c^3}e^{-\frac{v^2}{v_c^2}}$$

-eqn (7.2.1)

where n_c and n_h are the fraction of cold and hot particles respectively and v_c and v_h are the thermal velocities of the cold and hot particles respectively.

To conserve density, energy and momentum it is necessary that

$$n_c + n_h = 1$$

$$n_c v_c^2 + n_h v_h^2 = v_{th}^2$$

$$n_c v_c = n_h v_h$$

From these conservation laws, it is possible to eliminate n_c and n_h from eqn (7.2.1) to give

$$f(v,\mu,t) = H(\mu)\frac{v_c}{\pi^{3/2}v_h^3(v_c+v_h)}e^{-\frac{v^2}{v_h^2}} + H(-\mu)\frac{v_h}{\pi^{3/2}v_c^3(v_c+v_h)}e^{-\frac{v^2}{v_c^2}}$$

-eqn (7.2.2)

However, this distribution would pose certain difficulties because of the discontinuity. It may be necessary to allow for a non-uniform angular mesh and to have a very fine mesh at the discontinuity. Alternatively, the discontinuity could be smoothed out slightly by joining the two distribution by linear ramp.

However, rather than studying the collisional relaxation of the distribution using the code, it may be possible to analyze the distribution by adopting the same approximation adopted by Schamel ie assume that the distribution relaxes back within its own class of functions. If we define the hot and cold temperatures as

$$T_h = \int_0^\infty \int_0^1 f v^4 d\mu dv \ , \ T_c = \int_0^\infty \int_{-1}^0 f v^4 d\mu dv$$

and the same moments are taken over the Fokker-Planck equation then it may be possible to derive an equation for the evolution of T_c and T_h.

Section 7.2.3: Collisional Absorption

Finally, we discuss an idea for a new Fokker-Planck code that could be used to study collisional absorption. The collisional absorption of laser light in a laser produced plasma and the evolution of the distribution from thermal equilibrium has been re-examined by several authors in recent years (Langdon (1980), Jones (1982) and Balescu (1982)). These authors have shown that in a high Z plasma when $Zv_o^2/v_e^2 >> 1$ and $v_o^2/v_e^2 < 1$, where v_o is the laser quiver velocity and v_e is the thermal velocity, that the electron-electron collisions are not strong enough to stop the modification of the distribution function produced by the interaction of the laser light and the electron-ion collisions. The effect of this distortion to the plasma is to reduce the number of low velocity electrons which reduces the effectiveness of collisional absorption. When electron-electron collisions have been completely neglected, it has been shown that the distribution evolves as a self-similar distribution.

However, the situation where $Zv_o^2/v_e^2 >> 1$ and $v_o^2/v_e^2 > 1$ has not been examined thoroughly. Jones examined this situation but simplified the problem by ignoring the anisotropic part of the distribution. In addition, nobody has analyzed how different polarisations may affect the evolution of the distribution.

To investigate this situation, it is proposed that it would be of interest to solve the Fokker-Planck equation in cartesian velocity-space, using the Landau form of the collision integral, in a laser field. If electron-electron collisions are ignored then the equation to solve is

$$\frac{\partial f}{\partial t} + a_x \frac{\partial f}{\partial v_x} + a_y \frac{\partial f}{\partial v_y} = \frac{\Gamma n_i}{m_e} \frac{\partial}{\partial v_\alpha} \left[V_{\alpha\beta} \frac{\partial f}{\partial v_\beta} \right]$$

where

$$V_{\alpha\beta} = \frac{v^2 \delta_{\alpha\beta} - v_\alpha v_\beta}{v^3}$$

$$a_\alpha = \frac{eE_\alpha}{m_e} \cos(wt)$$

This equation could be solved by splitting the equation into four equations. The first equation would be the left hand side of the equation which describes the motion of the plasma in the laser field. This equation could be solved by the method of characteristics after fitting the distribution to a two dimensional spline. The next three equations would describe how the ions would scatter the momentum imparted to the electrons by the ions. These equations could be solved using the same method as the velocity and angular equations are solved in the existing Fokker-Planck code except that the mixed terms could be differenced implicitly using the same method as Lindemuth (1973).

This new code could then be used to investigate the

evolution of the distribution for $v_o^2/v_e^2 > 1$. Unlike Jones earlier work, it would be possible to determine if the distribution developed any significant anisotropy. Also, as the plasma heated up, it would be so determine how long it would take the plasma to evolve to the $v_o^2/v_e^2 < 1$ scenario and ultimately to the self-similar distribution.

It may also be possible to add a spatial dimension to the code. This would enable the code to simulate how a laser field interacted with a plasma to produce the steep temperature gradients. In doing this, it would be the first code to accurately model the coupling between laser absorption and thermal conduction in a laser produced plasma.

REFERENCES

Albritton J.R, Phys. Rev. Lett. 50, 2078 (1983)

Balescu R, J Plasma Physics 27, 553 (1982)

Bell A.R., Evans R.G., Nicholas D.J., Phys. Rev. Lett., 46, 248, (1981)

Bell A.R., Phys. Fluids, 284, 2007, (1985)

Bing G., Roberts J.E., Phys. Fluids, 4, 1039, (1961)

Book D.L., "NRL Plasma Formulary", NRL, Washigton DC, (1987)

Chang J.S., Cooper G., Journal of Comp. Phys., 6, 1, (1970)

Delettrez J., "Workshop on Physics of Laser Fusion ", Vancouver, Canada, (1985)

Dreicer H., Phys. Rev., 117, 329, (1960)

Dolinsky, Phys. Fluids, 8, 436, (1965)

Dum C.T., Phys. Fluids, 21, 956, (1978)

Epperlein E., Rickard G., Bell A.R., Commput. Phys. Comms. (submitted for publication)

Feldman W.C., Anderson R.C., Journal Geophys. Res., 88, 96, (1983)

Fuch V., Cairns R.A., Lashmore - Davies C.N ., Phys. Fluids, 29, 2931, (1986)

Harvey R.W., Marx K.D., McCoy M.G., Nuclear Fusion, 21, 153, (1981)

Jones R., Lee K., Phys Fluids 25, 2307, (1982)

Jorna S., Wood L., Journal of Plasma. Phys., 38, 317, (1987)

Jorna S., Wood L., Phys. Rev.A, 36, 397, (1987b)

Kho T.H., Proceedings of 1983 Centre Europen de Calc Atomique et Moleculaire Workshop on Transport, Interations and Instabilities in Laser Plasmas (Universitie Paris Sud, France 1983) p31

Killeen J., Heckrotte W., Boer G., Nuclear Fusion, 1, 183, (1962)

Killeen J., Futch A.H., Journal of Comp. Phys., 1, 236, (1968)

Killeen J., Mirin A., Fourth Conference on Numerical Solution of Plasmas, NRL, 685, (1970)

Killeen J., Mirin A., McCoy C., Comput. Phys. Commun., 24, 37, (1980)

Kogan V.I., Plasma Physics and the Problem of Controlled Thermonuclear Reactions (Pergammon, New York, 1961), 1, 153

Langdon A.B., Phys. Rev. Lett., 44, 575, (1980)

Langdon A.B., Proceedings of 1981 Centre Europen de Calc Atomique et Moleculaire Workshop on the Flux Limiter and Heat Flux Instablities in Laser Fusion (Universitie Paris Sud, France 1981) p69

Marsch E., Livi S., Phys. Fluids, 28, 1836, (1985)

Matte J.P, Virmont J., Phys. Rev. Lett., 49, 1936, (1982)

Matte J.P., Johnston T.W., Delettrez J., McCrory R.L., Phys. Rev. Lett., 53, 1461, (1984)

McGowan A.D, Sanderson J.J, Proceedings of 18th Annual Conference on Plasma Physics IOP, 3-5 July, Colchester, pp9-12, (1991)

McGowan A.D, Sanderson J.J, Proceedings of 18th Annual Conference on Plasma Physics IOP, 3-5 July, Colchester, pp13-16, (1991)

McGowan A.D, Sanderson J.J, J. Plasma Physics, in press (1992)

Nicholson D.R., "Intro to Plasma Theory", Chapters 3 - 5, Wiley, 1987

O'Brien M.R., Cox M., Start D.F.H., Comp. Phys. Comm., 40, 123, (1986)

Roberts J.E, Carr M.L., "End - Losses from Mirror Machines", Report UCRL-5651, (1960)

Rosenbluth M.N., MacDonald W.M., Judd D.L., Phys. Rev., 107, 1, (1957)

Schamel H., Hammen H., Duchs D.F., Stringer T.E., O'Brien M.R., Phys. Fluids B, 1, 76, (1989)

Shkarofsky P., Johnston T.W., Brachynsky M.A., "The Particle Kinetics of Plasmas " (Addison - Wesley, London 1966) Chapter 7

Appendix A

Shvartz D., Delettrez J., McCrory R.L., Verdon R.L., Phys. Rev. Lett., 47, 247, (1981)

Spitzer L., Harm R., Phys. Rev., 89, 977, (1953)

Wiley J.C. Duk-In Choi, Horton W., Phys. Fluids, 23, 2198, (1980)